AN ASSESSMENT OF COMPUTERIZED TOMOGRAPHY PARAMETERS IN SPINAL BONE MINERALIZATION DETERMINATION

by

JAMES STEPHEN DAVIS

A DISSERTATION PRESENTED TO THE GRADUATE SCHOOL
OF THE UNIVERSITY OF FLORIDA IN PARTIAL FULFILLMENT
OF THE REQUIREMENTS FOR THE DEGREE OF
DOCTOR OF PHILOSOPHY

UNIVERSITY OF FLORIDA

1988

U OF F LIBRARIES

ACKNOWLEDGMENTS

I would like to recognize the Department of Radiology at Shands hospital for their assistance and support. Their efforts in providing office space, computer support, the purchase of a research phantom, access to the CT scanner, and other necessary equipment have in large part made this research possible.

I would also like to thank the members of my committee whose kind support, gentle encouragement, and sound advice enabled me to complete this research effort within the time frame available. I especially wish to acknowledge Thurman Gillespy, III, M.D., for his clinical advice and direction, Walter Mauderli, D.Sc., for his guidance and gentle humor, and Emmett Bolch, Ph.D., to whom I owe far more than can be expressed in this limited space. I also wish to thank Libby Brateman, Ph.D., who served as an ex-officio member of my committee, providing technical advice and critical review.

I especially want to thank my family for their understanding and patience. To my wife I wish to give special thanks for making all the day to day sacrifices that enabled me to pursue this degree. Finally, to my daughter, Amanda, and almost four year old son, Christopher, who innocently asks, "Daddy, do you live at school?" I dedicate this effort.

TABLE OF CONTENTS

PAGE

ACKNOWLEDGMENTS ii

TABLE OF CONTENTS iii

LIST OF TABLES vii

LIST OF FIGURES xi

ABBREVIATIONS xv

ABSTRACT xvii

CHAPTERS

I. INTRODUCTION 1

- Osteoporosis 2
- Diagnostic Aids 6
  - Radiogrammetry 7
  - Photodensitometry 8
  - Single Photon Absorptiometry 9
  - Dual Photon Absorptiometry 11
  - Quantitative Dual Energy Projection Radiography 11
  - Quantitative Computed Tomography 12
- Objectives of Study 20
  - Field Nonuniformity Effects 22
  - Patient Geometry 23
  - Patient Size Effects 23
  - Air Gap Effects 24
  - Longitudinal Off-Set 24
  - Gantry Angular Positioning 25
  - Aortic Calcifications 26
  - Simulated Bowel Gas 27
  - Reproducibility Study 27
  - Dose Assessment 29
  - Dose Reduction Effects on Accuracy 31
  - Accuracy and Precision of Single Slice Scanning 31
  - Optimization of Parameters 32
  - Summary of Objectives 33

CHAPTER PAGE

II. METHODS AND MATERIALS 36

- Materials 36
  - G.E. 9800 37
    - X-ray production 37
    - Data acquisition 39
    - Data processing 40
    - Image display 40
  - Phantoms 41
    - CIRS Phantom 41
    - Solid Water Phantoms 43
    - Rando Phantom 51
    - Cann-Genant Phantom 53
- Methods 55
  - Quality Assurance 55
    - GE 9800 55
    - Phantoms 56
      - CIRS phantom 56
      - Solid Water^{TM} phantoms 69
      - Rando phantom 70
      - Cann-Genant phantom 70
  - Experimental Methods 72
    - Field nonuniformity effects 72
      - Vertical decentering 73
      - Lateral decentering 76
    - Patient geometry 78
    - Patient size effects 80
    - Air gap effects 81
    - Effects of longitudinal off-set 85
    - Effects of gantry angulation 87
    - Effects of aortic calcifications 90
    - Simulated bowel gas 91
    - Reproducibility study 95
  - Dose assessment 100
    - Dose to skin and bone 101
    - Gonadal dose 107
    - Dosimetry calculations 111
  - Dose Reduction Effects on Accuracy 118
  - Accuracy and precision of single slice scanning 119

III. RESULTS 120

- Field Nonuniformity Effects 120
  - Vertical Decentering 120
  - Lateral Decentering 122
- Patient Geometry 123
- Patient Size Effects 124
- Air Gap Effects 125
- Longitudinal Slice Off-Set 126

CHAPTER PAGE

III. Gantry Angular Positioning 127
Aortic Calcification Effects 128
Simulated Bowel Gas 129
Reproducibility Study 132
Dose Assessment 135
    Dose to Skin and Bone 135
        Dose from direct axial scanning 136
        Dose from axial scattering 137
        Dose from lateral scouts 137
        Total dose 138
    Gonadal Dose 140
Dose Reduction Effects on Accuracy 141
Accuracy and Precision of Single Slice Scanning 142

IV. DISCUSSION 144

Field Nonuniformity Effects 144
    Vertical Decentering 144
    Lateral Decentering 148
Patient Geometry 150
Patient Size Effects 153
Air Gap Effects 155
Longitudinal Slice Off-Set 158
Gantry Angular Positioning 159
Aortic Calcifications 159
Simulated Bowel Gas 162
Reproducibility Study 163
Dose Assessment 170
    Dose to Skin and Bone 171
        Dose from direct axial scanning 171
        Dose from axial scattering 172
        Dose from lateral scouts 172
        Total dose 174
    Gonadal Dose 176
    Health Implications 178
        Risks 178
        Benefits 194
Dose Reduction Effects on Accuracy 201
Accuracy and Precision of Single
    Slice Scanning 206

V. CONCLUSIONS 215

Field Nonuniformity Effects 215
    Vertical Decentering 215
    Lateral Decentering 216
Patient Geometry 217
Patient Size Effects 218
Air Gap Effects 219
Longitudinal Slice Off-Set 219
Gantry Angular Positioning 220
Aortic Calcification Effects 220

Simulated Bowel Gas Effects 221
Reproducibility Study 222
Dose Assessment 223
Dose to Skin and Bone 223
Dose from direct axial scanning 223
Dose from axial scattering 224
Dose from lateral scouts 224
Total dose 225
Gonadal Dose 225
Health Implications 225
Dose Reduction Effects on Accuracy 226
Accuracy and Precision of Single Slice Scanning 227
Optimization of Parameters and Recommendations 228

APPENDICES

A DOSIMETRIC SYSTEMS 231
B RESEARCH PROPOSAL 282

REFERENCES 294

BIOGRAPHICAL SKETCH 297

LIST OF TABLES

TABLE PAGE

1-1 Normal QCT spinal BMD protocol 19

1-2 Summary of research objectives and methodologies 34

2-1 Ratio of characteristics of SOLID WATER^{TM} to water 45

2-2 Comparison of scattering effects from CIRS phantom with and without SOLID WATER^{TM} 59

2-3 Scattering effects from CIRS phantom 61

2-4 Analysis of amount of SOLID WATER^{TM} required to account for scattering effects 63

2-5 Pair-wise analysis on amount of SOLID WATER^{TM} required to account for scattering effects 66

2-6 Uniformity of vertebral bone mineral insert 68

2-7 Technique factors used to assess air gap effects 85

2-8 QCT scanning protocol used to assess the effects of small changes in longitudinal slice position and gantry angulation on the precision of QCT measurements 86

2-9 Reproducibility as a function of confidence level and number of measurements obtained 95

2-10 Percent dose enhancement to bone marrow and endosteal tissues from secondary electrons 117

2-11 Percent dose enhancement to bone marrow and endosteal tissue as a function of effective beam energy 117

2-12 Technique factors used for dose reduction study 118

3-1 BMD and percent change as a function of vertical decentering 121

TABLE PAGE

3-2 BMD and percent change as a function of phantom vertical decentering 122

3-3 BMD and percent change as a function of phantom lateral decentering 123

3-4 Statistics for patient geometric effects 124

3-5 Statistics for patient size effects 125

3-6 Percent change in measured BMD as a function of air gap size and radiographic technique 126

3-7 Percent change in BMD as a function of longitudinal slice position 127

3-8 Effect of gantry angulation on QCT precision 128

3-9 BMD values (mg/cc) measured with and without aortic calcifications 129

3-10 The effects on measured BMD of a constant volume of bowel gas at varying distances 130

3-11 Analysis of variance on constant volume bowel gas effects 130

3-12 Effects of varying volumes of bowel gas on measured BMD at a constant distance 131

3-13 Analysis of variance for effects of varying volumes of bowel gas at constant distance on measured BMD 131

3-14 Statistics for the effects on measured BMD of bowel gas in the transverse colon 132

3-15 Regression output by QCT analyst 135

3-16 Dose from single axial scan to skin, mineralized bone, bone marrow, endosteum, and soft tissue 136

3-17 Dose contribution from axial scattering 137

3-18 Dose contribution from lateral scouts 138

3-19 Total dose from QCT examination 139

3-20 Percent of total dose from direct axial scans, axial scattering, and lateral scouts at various locations 140

TABLE PAGE

3-21 Gonadal dose contribution from two lateral scout exams 141

3-22 Average patient BMD (mg/cc) at various imaging technique factors 142

3-23 Standard errors of vertebral BMD values regressed against overall patient BMD 143

3-24 Reproducibility of vertebra for exam one regressed against exam two 143

4-1 Analysis of variance for patient geometric effects 151

4-2 Pair-wise comparisons of the means for the geometric phantom configurations 151

4-3 Analysis of variance for patient size effects data 154

4-4 Comparison of variances of BMD measurements for different phantom sizes (circumferences) 154

4-5 Dose equivalent to radiosensitive tissues 178

4-6 Risk of fatal leukemias per QCT procedure 182

4-7 Risk of fatal bone cancers per QCT procedure 185

4-8 Risk of fatal skin cancers per QCT procedure 187

4-9 Average BMD and standard deviation at various mA settings for 80 kVp 202

4-10 Paired t-test comparisons at 80 kVp and various tube current settings. 203

4-11 BMD differences (mg/cc) from values measured at technique settings of 80 kVp and 40 mA. 205

4-12 Accuracy data for individual vertebrae and vertebral combinations 209

4-13 Reproducibility data for individual vertebra and vertebral combinations 213

A-1 Properties of some commercially available TLDs 235

A-2 CT HVL Measurements 245

TABLE PAGE

A-3 Matching of CT and Diagnostic unit HVLs 252

A-4 TLD frequency distribution 261

A-5 TLD response as a function of energy 267

A-6 Dark current readings at 650 volts 271

A-7 Light current readings at 650 volts 274

A-8 Signal to noise ratio as a function of voltage 275

A-9 Output of TLD reader on first and second chip readings 278

A-10 Linearity of TLD reader at one energy 280

LIST OF FIGURES

FIGURE		PAGE
1-1	Lateral scout exam showing postings for axial scans	18
1-2	Axial scan showing placement of ROI	21
1-3	Axial scan showing a) aortic calcification ring and b) gas within the bowel	28
2-1	Schematic of G.E 9800 CT scanner system	38
2-2	C.I.R.S. lumbar phantom	42
2-3	Geometric phantom showing: a) circular geometry b) elliptical ratio of 1.3:1, c) elliptical ratio of 1.6:1	46
2-4	Simulated Bowel gas-aortic calcification phantom	49
2-5	Rando phantom (exterior view)	52
2-6	Cann-Genant reference phantom	54
2-7	Change and percent change in measured BMD as a function of amount of Solid Water™ used as a scattering medium	65
2-8	Axial scans of phantom configurations used to assess changes in measured BMD as a function of vertical position within scan field	75
2-9	Axial scans of phantom configurations used to assess changes in measured BMD as a function of lateral decentering within the scan field	77
2-10	Axial images of C I.R.S phantom used to assess patient size effects on measured BMD values	82
2-11	Axial scans of phantoms configurations used to assess air gap effects on measured BMD	84
2-12	Lateral scout image showing postings for axial scans used to study the effects of small changes in longitudinal slice position on BMD	88

FIGURE PAGE

2-13 Lateral scout image showing postings for axial scans used to study the effects of small changes in gantry angulation on measured BMD 89

2-14 Section 25 of Rando phantom indicating sites used for direct axial scanning dosimetry measurements 102

2-15 Section 25 of Rando phantom indicating sites used for axial scattering dosimetry measurements 105

2-16 Section 25 of Rando phantom indicating sites used for lateral scout dosimetry measurements 108

2-17 Section 31 of the Rando phantom indicating sites used for gonadal measurements 109

2-18 F-factor as a function of photon energy for water, muscle, and bone 112

2-19 HVL as a function of effective x-ray beam energy 113

2-20 HVL versus peak tube potential 115

3-1 Age matched bone mineral density values for females 133

4-1 Change in measured BMD as a function of vertical table position within the scan field 145

4-2 Percent change in measured BMD at a constant table height as a function of vertical decentering above isocenter 147

4-3 Percent change in measured BMD as a function of lateral decentering at a constant table height 149

4-4 Percent change in measured BMD as a function of air gap size with a 2 s at various kVp and mA values 156

4-5 Percent change in BMD relative to the midplane as a function of longitudinal slice position for cadaver one 160

4-6 Percent change in BMD relative to the midplane as a function of longitudinal slice position for cadaver two 161

4-7 Regression of average patient BMD for exam one regressed against the average patient BMD for exam two (data analyzed by CT tech one) 165

FIGURE PAGE

4-8 Regression of average patient BMD for exam one regressed against the average patient BMD for exam two (data analyzed by CT tech two) 166

4-9 Regression of average patient BMD for exam one regressed against the average patient BMD for exam two (data analyzed by author) 167

4-10 Dose from direct axial scanning to radiosensitive tissues 173

4-11 Soft tissue dose distribution as a function of depth (cm) from phantom surface 175

4-12 Dose and percent dose contribution from axial scanning to total patient dose 177

4-13 Risk of developing a fatal leukemia as a result of one QCT examination 183

4-14 Risk of developing a fatal bone cancer as a result of one QCT examination 186

4-15 Risk of developing a fatal skin cancer as a result of one QCT examination 189

4-16 Risk of developing a fatal cancer by type at various QCT technique factors as a result of one QCT examination 190

4-17 Total fatal cancer risk as a result of one QCT examination 191

4-18 Comparison of QCT fatality risk with other common risks 193

4-19 Average patient BMD as a function of radiographic technique used for QCT examination 204

4-20 Individual vertebral BMDs plotted against average patient BMD 207

4-21 Vertebral pair BMDs plotted against average patient BMD 208

4-22 Measured BMD of individual vertebra for exam one plotted against the measured BMD of individual vertebra for exam two 211

4-23 Measured BMD of vertebral pairs for exam one plotted against measured BMD of vertebral pairs for exam two 212

A-1 Typical glow curve for Lithium Flouride TLD-100 . 234

A-2 Normalized CT HVL determination at technique settings of 120 and 80 kVp measured at isocenter 247

A-3 Normalized CT HVL determination at technique settings of 120 and 80 kVp 14 cm laterally decentered from isocenter 248

A-4 Experimental apparatus used to determine diagnostic unit HVLs, sensitivity matching, and calibration of TLD chips 250

A-5 Normalized diagnostic unit HVL determination at technique settings of 80 and 110 kVp 253

A-6 Normalized diagnostic unit HVL determination at technique settings of 100 and 130 kVp 254

A-7 Comparison of HVL of diagnostic unit and CT scanner measured at the isocenter 256

A-8 Comparison of HVL of diagnostic unit and CT scanner measured at the decentered location 257

A-9 Frequency distributions of TLD readings 262

A-10 Sensitivity of TL phosphors as a function of photon energy 265

A-11 TLD-100 response as a function of beam HVL 268

A-12 Harshaw 2000 TLD system reader signal to noise ratio as a function of PM tube potential ... 276

A-13 Harshaw 2000 system TLD reader TLD calibration curve 281

ABBREVIATIONS

ANOVA, analysis of variance

BMC, bone mineral content

BMD, bone mineral density

cfs, cubic feet per second

CIRS, Computerized Imaging Reference System, Inc.

CT, computed topography

DAS, CT data acquisition system

DPA, dual photon absorptiometry

FOV, field of view

G.E., General Electric, Inc.

HVL, half-value layer

IA, Image Analysis, Inc.

I.V., intra-venous

keV, kiloelectron volts

kVp, kilovoltage potential

NaI, sodium iodide

NRI-TL, Non-radiation induced thermoluminescence

pixel, picture element

PM, preventive maintenance (or photomultiplier)

post, mark vertebrae for location and angle of axial scan

QCT, quantitative computed tomography

R, roentgen

RAD, radiation absorbed dose

RMI, Radiation Measurements, Inc.

ROI, region of interest

SPA, single photon absorptiometry

TLD, thermoluminescent dosimeter

voxel, volume element

Z, effective atomic number

Abstract of Dissertation Presented to the
Graduate School of the University of Florida in Partial
the Requirements for the Degree of
Doctor of Philosophy

AN ASSESSMENT OF COMPUTERIZED TOMOGRAPHY PARAMETERS
IN SPINAL BONE MINERALIZATION DETERMINATION

By

James S. Davis

December, 1988

Chairman: W. Emmett Bolch
Major Department: Environmental Engineering Sciences

This research investigates the effects of changes in clinical parameters on measured bone density values using Quantitative Computed Tomography (QCT). These parameters include changes in patient size, geometry, internal anatomic conditions such as aortic calcifications and bowel gas, gantry slice position and angulation, spine-water bolus air gap distance, and field uniformity effects. It also assesses the reproducibility of the QCT technique on the G.E. 9800 CT scanner as well as the dose to radiosensitive tissues. The CIRS torso phantom was used in each of three size configurations to assess size effects. Mean bone mineral density (BMD) did not significantly vary with phantom size. Variations in patient cross-sectional geometry at constant volume were assessed using a custom manufactured body phantom constructed with three elliptical ratios: 1:1 (round), 1.3:1, and 1.6:1. Measured BMD values of a 50 mg/cc mineral plug

decreased significantly (59.03, 58.12, 56.95 mg/cc) with increasing elliptical ratio. Bowel gas effects were simulated by drilling holes into the body phantom. No significant differences in BMD were noted with a constant volume of air (3.14 cm^3) at varying distances from the mineral plug nor were any significant differences in BMD noted with varying volumes of air at a constant distance from the mineral plug. A simulated aortic calcification similarly caused no significant difference in measured BMD. A spine-water bolus air gap distance as small as 0.5 cm increased measured BMD by approximately 5%. QCT measurements were also sensitive to changes in table height, as well as vertical and lateral patient decentering. To assess the effects of small changes in longitudinal slice position and gantry angulation on BMD, 35 vertebrae from 9 cadavers were imaged. Within 4 mm of the midplane 64% of the vertebrae varied in density by less than 4% of the midplane value. The effects of gantry angulation were less pronounced. Reproducibility, using patient volunteers, was found to be in the range of 1 to 3% and heavily dependent on the size of the ROI selected.

CHAPTER 1
INTRODUCTION

Quantitative Computed Tomography (QCT) is a computational tomographic technique that measures the density of body tissues. QCT is most commonly used in the evaluation of osteopenia and osteoporosis. In the treatment of osteoporosis, the rate of bone loss is important in evaluating the patient's response to therapy. In order to determine the rate of bone loss, patients may have several spinal QCT analyses, resulting in repeated exposures to ionizing radiation. This, along with QCT's potential for widespread use in screening asymptomatic individuals, makes QCT of particular concern to the health physicist.

Since spinal QCT examination imparts a large patient dose (100-300 mrad) compared to other methods of bone mineral analysis (5-15 mrad), the radiological health risk from longitudinal QCT studies must be considered (Peck et al., 1987). Additionally, clinical procedures should be evaluated in terms of dose delivered and diagnostic information obtained. Without sacrificing diagnostic information, the dose should be reduced wherever possible to minimize the likelihood of adverse health consequences

Various clinical variables are known to potentially affect the accuracy and precision of QCT. Clinicians may challenge the validity of QCT measurements obtained when changes in gantry angulation, longitudinal slice position, air gap distance, patient position in the scan field, aortic calcifications, or bowel gas are present. The clinical question that must be answered is, "Do these conditions degrade the precision or accuracy of BMD measurements enough to warrant repeating the procedure, thereby doubling the patient dose?" To date, little research has been done to assist the clinician in answering this question.

This study quantifies the impact of clinical variables on the accuracy and precision of QCT measurements, enabling the clinician to decide, based on empirical data, if a repeated QCT examination is warranted. Additionally, the study examines the health consequences of QCT examination, provides a health risk versus benefit analysis, and explores ways to minimize patient dose through changes in the standard QCT protocol.

Osteoporosis

Osteoporosis is the excessive and prolonged loss of bone to the point where microscopic or obvious fractures occur. This loss of bone may occur in both dense (cortical) and cancellous (trabecular) bone.

While the entire skeleton is approximately 80% cortical and 20% trabecular bone, this ratio is not evenly distributed throughout the skeleton. Long bones of the appendicular skeleton are primarily cortical bone, while areas of the axial skeleton such as vertebrae may contain up to 65% trabecular bone. Due to the high surface to volume ratio of trabecular bone, it is nearly eight times more metabolically active than cortical bone (Frost, 1964). As a result of this increased metabolic activity, loss of bone mineral is usually first seen in skeletal regions containing a high percentage of trabecular bone, such as the vertebral spine and femoral neck.

In the vertebrae and femoral neck, osteoporosis so thins and weakens the bone that it is no longer able to support normal body weight. The immediate medical consequences of osteoporosis include pain, postural disfigurement, and fracture of the wrist, spine, and hip.

Osteoporosis may affect both men and women, but its effects are usually more pronounced and consequences more severe for women. For both men and women, age related bone loss begins before or during the third decade of life (Buchanan et al., 1988). Although a postmenopausal woman will normally lose bone at a rate twice that of a man, during the first five to six years postmenopause, the rate may be six times that of a man. By age 60, a woman may lose almost three times (47%) as much bone as a man (14%). These differences relate to the greater decrease in estrogen levels in postmenopausal women than in men of comparable age (Peck et al., 1987).

Osteoporosis is more common in older women than heart attack, stroke, diabetes, rheumatoid arthritis, or breast cancer. Twenty-five percent of naturally postmenopausal women are osteoporotic. For women who undergo surgical menopause (removal of the uterus and ovaries) without hormone replacement therapy, the outlook is worse. Up to 50% of surgically menopausal women develop osteoporosis.

In terms of quality and length of life, osteoporosis presents the greatest health risk to a woman's older years (Notelovitz and Ware, 1982). Two hundred thousand osteoporotic American women over age 45 fracture one or more of their bones each year. Of these women, 40,000 die as a direct result of complications following their injuries.

The most life threatening consequence of osteoporosis is hip fracture. Fifteen percent of osteoporotic women who fracture their hip die shortly after injury and 30% die within a year after injury. Deaths are usually caused by blood clots, fat embolism (from bone marrow fat trapped in the lung), and complications from supportive care such as pneumonia. A hip fracture has been estimated to reduce a woman's life span by 12% (Notelovitz and Ware, 1982).

While the mortality associated with osteoporosis is substantial, osteoporosis more frequently causes significant morbidity. Fewer than half the women who suffer hip fracture regain normal function. If the blood supply to the head of the femur is disrupted, avascular necrosis, resulting in the need for hip replacement surgery, may occur. Additionally, the health care costs involved in hip fracture may represent a severe financial burden. The first nine days following a hip fracture are estimated to cost an average of $10,000. Nationally, over one billion dollars each year is spent on osteoporotic related medical treatment and care.

Less quantifiable is the pain associated with spinal fractures resulting from osteoporosis. In the acute phase, which lasts up to a month post-fracture, intense pain results from bone collapse, damage to the surrounding tissues, and muscular spasms. Chronic pain may last anywhere from one to six months. The pain during the chronic phase is less intense and results from muscle and ligamentous strain. After six months post-fracture, remission of pain occurs as the body adapts to the new spinal condition.

Diagnostic Aids

Due to the severe consequences of osteoporosis, wide scale efforts have been made to diagnose its precursor, osteopenia. The early diagnosis and treatment of osteopenia can reduce the severity of later bone loss. For example, long term estrogen use reduces the risk of hip and vertebral fractures by approximately 50% (Weiss et al., 1980). However, since estrogen therapy cannot restore lost bone mass, the early detection and treatment of osteoporosis is critical.

Many methods of bone mineral analysis are now in use to assess osteopenia. These include radiogrammetry, photodensitometry, single and dual photon absorptiometry, dual energy projection radiography, and quantitative computed tomography. Proponents of each method abound, frequently advocating their procedure while denouncing competing ones. Accuracy and precision of the various methods may be biased by citing a tightly controlled experimentally determined value for one method and a less rigorous clinically determined value for a competing method. Patient dose comparisons frequently fail to cite the location at which the dose is being specified, leaving the reader to wonder if exposure, skin dose, soft tissue or bone doses are being cited. To put each method in a more objective perspective, a brief discussion of each technique along with its advantages and disadvantages will be presented.

Radiogrammetry

Radiogrammetry uses a fine grain non-screen industrial film to obtain a high quality xray of a circular bone in the appendicular skeleton. The most common site for measurement is the second metacarpal of either hand (Cohn, 1981). One method measures the midshaft on the diaphysis of the second metacarpal, taking two measurements. The first measurement is made laterally across the shaft of the bone from periosteal border to periosteal border. The second measurement is made laterally across the medullary cavity. The subtraction of these two measurements indicates the combined cortical diameter of the bone. Other measurements may also be made in similar fashion to obtain cortical area and percent cortical to bone width diameters.

This method has several advantages. Among them are low cost, good correlation with mineral content of the hand, high precision, and high reproducibility when using multiple metacarpal measurements. For measurements made by the same individual, the reported precision ranges from 1.5

to 3%. Increased precision is possible, however, by obtaining measurements of the second, third, and fourth metacarpals. Additionally, the radiation dose from radiogrammetry is on the order of 100 mrad. Since the hand is relatively insensitive to radiation, the adverse health consequences from radiogrammetry are minimal. Age versus normal ranges have also been well established for this technique.

Unfortunately, metacarpal measurements of bone weight in women do not correlate well with vertebral weights (Cohn, 1981). This makes radiogrammetry a poor indicator of spinal bone mass. Further, since this method measures cortical bone and not the more metabolically active trabecular bone, radiogrammetry's usefulness as a sensitive indicator of bone change is very limited. Radiogrammetry can detect a minimal bone loss of 25% to 60%, although detectable bone losses as low as 10% have been reported.

Photodensitometry

Photodensitometry uses a non-screen film to image the hand, similar to radiogrammetry. The primary difference between the two methods is the manner in which the radiograph is analyzed. In photodensitometry, a computer controlled densitometer scans a reference wedge along with the phalanges, incrementally moving laterally across the digits. A comparison of the optical densities of each picture element (pixel) of the bone with pixels of the reference wedge (for which the true density is known) yields the density of the phalanxes.

The advantages of this procedure include a patient dose of approximately 100 mrad, ease in repositioning on longitudinal scans, and low expense. Precision is approximately 2% to 3%. Further, the measurements are not very dependent on x-ray machine used, tube potential, or reference wedge so that inter-hospital readings show high consistency.

Disadvantages include inaccuracies when measuring bones surrounded by large amounts of soft tissue and poor correlation with spinal bone mineral as measured by QCT (Rosenthall, 1987).

Single Photon Absorptiometry (SPA)

In SPA, a beam of photons from a radioactive source passes through an area of the appendicular skeleton, normally the radius and ulna, and is intercepted by a sodium iodine crystal detector. The beam consists of low energy photons from ^{125}I (half-life = 60 days, gamma = 27.4 keV) or ^{241}Am (half-life = 458 years, gamma = 60 keV). The photons emitted are readily absorbed due to the strong photoelectric effect predominating at these low energies. Since the probability of a photoelectric interaction is proportional to $Z^{3.5}E^{-3}$, at low keV, gamma interactions are strongly influenced by small changes in atomic number (Z). Since the degree of beam attenuation relates to the amount of high Z material (bone) in the path of the beam, the intensity of the beam at the detector is an indication of the amount of bone mineral present. A measure of the bone mineral content (BMC) is obtained by summing all the points along a transverse scan. To compensate for differences in bone size, most investigators divide the BMC by the area of interest and report their findings in terms of bone mineral density (BMD) as grams x cm^{-2}.

The advantages of single photon absorptiometry include high precision, ranging from 1 to 2%, and an extremely low dose, ranging from 2 to 5 mrad. Accuracy from this procedure is reported to be approximately 3%.

Unfortunately, to yield a constant tissue thickness, the site of measurement must be surrounded by a tissue equivalent material. This makes SPA suitable only for measurement of the long bones of the appendicular skeleton. SPA is not, therefore, appropriate for spinal measurement or measurement at other common fracture sites such as the hip. Further, SPA measurements of the appendicular skeleton are not highly correlated with spinal bone mineral content. SPA also suffers from repositioning errors which may degrade an otherwise high precision. More modern SPA instruments, however, use the radial-ulnar distance for repositioning, which greatly reduces repositioning errors, Dual Photon Absorptiometry (DPA)

This method is very similar to single photon absorptiometry but uses a radionuclide with dual energy gamma emissions as the radiation source. ^{153}Gd (which emits two gammas of different energies) is commonly used. By using two gammas of different energies, the need to surround the region of interest (ROI) in a tissue equivalent material is eliminated, allowing any region of the body to be scanned. Additionally, the patient dose is small, in the range of 5 to 15 mrad. Precision is approximately 1.5 to 3%.

Since DPA gives a measure of the total bone mineral through which the beam travels, inaccuracies due to the presence of fat and arterial calcium deposits surrounding the vertebrae may occur. Further, DPA is incapable of isolating trabecular bone, which, because of its much higher metabolic turnover, is a more sensitive indicator of bone loss.

Quantitative Dual Energy Projection Radiography (QDR)

QDR, like DPA, can measure bone mineral in both the axial and appendicular skeletons. QDR has several advantages over DPA, however. QDR uses an x-ray tube as a radiation source. Compared to the typical one curie ^{153}Gd source used in DPA, the x-ray tube provides 500 to 1000 times more photon flux (Sartoris, 1988). The increased photon flux results in higher image resolution and shorter scan times (five minutes) with QDR than with DPA (20 minutes). Additionally, QDR is more precise (1%) when compared to DPA (3%). The patient dose from QDR is on the order of 3 mrad and accuracy is reported to be as high as 1%.

Unfortunately, QDR is unable to selectively measure cancellous bone. This makes QDR less sensitive than QCT to small changes in bone mineralization.

Quantitative Computed Tomography (QCT)

In Computed Tomography (CT) scanning, an x-ray tube, pre-patient, and post-patient collimators define a narrow beam of polychromatic photons passing transversely through the patient. A detector assembly, consisting of numerous gas filled proportional chambers, intercepts the photon beam. The source-detector assembly is normally rotated a full 360° around the patient. The detector assembly accurately measures the attenuation of the beam passing through the patient.

Like DPA, CT does not need a constant tissue thickness, and may be used to image any portion of the body. BMD values are obtained by simultaneously scanning the patient and a reference phantom. The patient BMD values are normally obtained from the trabecular region of the vertebral bodies in the lumbar spine.

The advantages of QCT are significant. QCT permits determination of trabecular bone mineralization separate from that of the cortex. Since QCT can directly measure the metabolically active trabecular bone, QCT measurements sensitively indicate changes in bone mineralization.

In single energy mode (SEQCT), the precision is high, about 1%. It is, therefore, appropriate for serial measurements of a single patient. SEQCT BMD values are lowered by fat in the marrow and show an accuracy of 5% to 10%.

In the dual energy mode (DEQCT), one can compensate for fat in the marrow to obtain an accuracy of about 6% (Hangartner, 1986). The dual energy mode is most appropriate to quantify bone mineral, differentiating the BMD of an individual from that of a normal population.

Disadvantages of QCT include a high patient dose, in the range of 100 to 300 mrad, high cost of the CT scanner to the treatment facility, and a concomitantly higher cost to the patient.

QCT Theory and Practices

The primary computational problem with which a CT scanner must contend is to determine the degree of attenuation occurring in each pixel. For a narrow beam monoenergetic source, the attenuation coefficient relates to the degree of photon attenuation by

$$\mu = -[\ln(I/I_0)]/x$$

For a photon penetrating several layers of material of varying attenuation, the total attenuation is equal to the sum of the individual attenuation coefficients:

$$\mu_t = (\mu_1+\mu_2+\mu_3+..\mu_n) = -[\ln(I/I_0)]/x$$

Since there are many unknowns in this equation, it cannot be solved without a corresponding number of similar equations. By taking multiple projections through the tissue slice, equations of this form may be solved simultaneously. Modern CT scanners may require the solution of 250,000 or more simultaneous equations. Since this procedure requires vast amounts of computing power and time, most image reconstruction is not performed by solution of simultaneous equations.

Image reconstruction algorithms replace the need to solve such large numbers of equations, considerably increasing the speed with which images are reconstructed and displayed. The result of reconstruction is a CT value which corresponds to the attenuation of each pixel element. This information, when reconstructed, yields images of and values for bone mineralization in any ROI desired.

The reconstructed image of the scan can be thought of as a three dimensional matrix of picture elements (pixels) and volume elements (voxels). Modern scanners use a 512 by 512 pixel display yielding a total of 262,144 pixels. Each pixel is assigned a CT number proportional to the attenuation occurring in that picture element. The CT number is calculated from

$$\text{CT}\ \# = \text{K}\ (\mu_p - \mu_{H2O})/\mu_{H2O}$$

where K is the scaling factor (usually 1000), μ_p is the linear attenuation coefficient of the pixel, and μ_{H2O} is the linear attenuation coefficient for water.

Procedures for QCT scanning vary from institution to institution. The procedure currently in use at Shands Teaching Hospital, Gainesville, Florida, is described below

Before patient scanning, the CT gantry table is lowered 130 mm from isocenter so that the spine of the patient will locate at the approximate isocenter of the scan field, accounting for the combined thicknesses of an external reference phantom, water bolus, and the patient posterior paraspinous tissue. Image Analysis, Inc. manufactures the exterior reference phantom (Cann-Genant phantom) used in this study. The Cann-Genant phantom consists of a crescent shaped plastic housing containing tubes filled with serial dilutions of K_2HPO_4. Since K_2HPO_4 closely approximates the photon absorption characteristics of bone mineral, the serial dilutions of K_2HPO_4 provide a range of bone equivalent density reference values.

Removing the curved table-top liner from the CT table, foam cushions are placed on top of the table along with the Cann-Genant phantom. This allows the patient to recline on a flat even surface. A bolus bag filled with water is placed length-wise over the Cann-Genant phantom. Lying supine atop the cushions, Cann-Genant phantom, and bolus bag, the patient is centered on the table with feet toward the gantry. The anterior iliac crest is aligned with the base of the Cann-Genant phantom. A knee pad is used to elevate the patient's knees. This reduces air gaps between the patient's back and water bolus by lessening the natural curvature of the lumbar spine. The patient's arms are raised above the head to avoid including them within the scan field.

Once properly positioned, the patient is translated into the scan field to roughly the level of the tenth thoracic vertebra. The x-ray tube head is locked into position at 90° relative to the patient. The gantry table translates the patient through the scan field, stopping at the level of the iliac crest.

The image obtained in this manner is called a lateral scout (see Figure 1-1). The lateral scout image is used to determine exact locations for axial scanning. CT software allows the CT technician to determine these locations by positioning a cursor (consisting of a straight line) linearly and angularly over the lateral scout image. This process of selecting the exact location for axial scans is called posting.

During posting, the technician aligns a linear cursor through each vertebra midway between and perpendicular to the vertebral end plates (see Figure 1-1). The cursor location and angulation are then recorded.

Normal vertebrae from the 12th thoracic vertebra to the fourth lumbar vertebra are marked for scanning. Any vertebrae having wedge or crush fractures are excluded. Vertebrae above the level of T-12 and below L-4 are not used since this would require scanning through portions of

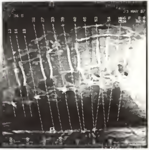

Figure [illegible]. Lateral scout exam [illegible] the lung and the pelvic girdle respectively. Such scans would involve large field nonuniformities which could adversely affect QCT accuracy.

Once the location and angulation for the axial scans are obtained, the patient is translated into the scan field and four axial scans are made. The normal technique factors for the axial scans are indicated in Table 1-1, "Normal QCT Protocol". At these technique factors, an axial scan is reported to deliver a peak skin exposure in the range of 150-350 mR (Image Analysis, 1987). The scan and display fields of view are normally set to large (48 cm). The reconstruction matrix is set to 512 x 512. Other scanning technique factors normally used for these images are also shown in Table 1-1.

Table 1-1. Normal QCT protocol.

Table Height	130 mm
Patient Position	Supine
Scan Field of View (FOV)	48 cm
Display FOV	48 cm
Scan Type	Normal
Recon Resolution	Standard
Matrix Size	512
Slice Thickness	10 mm
Tube Current	40 mA
Tube Potential	80 kVp
Scan Time	2 s

After obtaining the axial scans, they are analyzed to determine vertebral BMD. During this analysis a computer generated elliptical cursor is placed within a vertebral ROI. The ROI is positioned entirely within the trabecular portion of the vertebrae. Its location specifically excludes the cortical rim of the vertebrae and the basivertebral complex (see Figure 1-2).

The IA QCT software automatically computes ROIs for each of the mineralization tubes within the Cann-Genant phantom, obtaining the average CT number for each tube and the operator specified vertebral ROI. The IA software performs a linear regression of the average CT number from each of the mineralization tubes within the Cann-Genant phantom and the bone mineral equivalent densities of the mineral tubes. This regression curve associates the average CT number from the vertebral ROI with its equivalent bone mineral density. This procedure is repeated for each vertebra imaged. The overall patient BMD value is determined by averaging the BMD measurements for each of the vertebrae imaged.

Objectives of Study

While the scanning protocol as outlined in Table 1-1 is well delineated, many clinical variables associated with QCT spinal bone mineral analysis are not routinely noted. These include such variables as patient waist size, patient

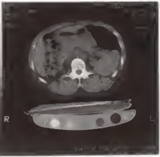

Figure 2.6 Both bone marrow placement of ROI

geometry, internal anatomical conditions such as extra-osseous calcifications and bowel gas, table-top height, and the amount of air gap between the water bolus and patient dorsal surface. Cann (1988) warns of inaccuracy and imprecision as a consequence of change in these clinical variables. Little effort, however, has been made to quantify the magnitude or assess the clinical impact of these variables. Without quantifiable data, the clinician must rely on intuitive judgment to decide if these variables degrade precision and accuracy enough to warrant repeating the examination in light of the potential health risks to the patient. In order help the clinician better interpret the results of QCT measurements, this research looks at the following clinical variables and evaluates their impact on QCT spinal bone mineral measurement

Field Nonuniformity Effects

As indicated previously, during normal QCT examination, the patient is positioned isocentrically within the scan field. This is accomplished by first centering the patient along the longitudinal axis of the gantry table and then raising the table so that the patient is located vertically at the scan field isocenter. Although alignment lights provide a visual reference, exact repositioning of the patient on repeat scans is seldom attained. This research objective assesses the impact of both vertical and lateral decentering on the accuracy of QCT measurements.

Patient Cross-sectional Geometry

QCT is frequently used to follow a patient's bone mineral status over the course of many years. During this time, the patient geometry (shape) may change dramatically due to diet or disease. Changes in body geometry may result from spinal fractures, with resultant kyphosis, associated with osteoporosis. Additionally, patient geometry typically changes over the region of the torso encompassing vertebrae T-12 through L-4 which is normally imaged during QCT.

The reconstruction algorithms used in CT assume the object being irradiated possesses a circular geometry. The ability of CT to mitigate the effects of such changes in geometric shape is uncertain. This research objective investigates the impact of changes in patient shape on the accuracy of QCT BMD analysis as measured by the GE 9800 CT scanner presently used at this institution

Patient Size Effects

The patient circumference and cross-sectional area can be expected to change over the course of a long term study. The effect of changes in patient circumference and cross-sectional area has not been fully investigated. This research assesses the impact changes in patient cross-sectional size have on the accuracy of QCT BMD measurements.

Air Gap Effects

A water bolus is used during routine QCT to provide a uniform tissue-like material between the patient and the reference phantom. The presence of air between the water bolus and the dorsal surface of the patient is known to degrade QCT BMD accuracy. Due to the lordotic nature of the lower spine, complete elimination of these air gaps is extremely difficult. Further, the amount of air gap present may change upon repeat examination due to changes in patient size, shape, spinal condition, positioning, and type of water bolus used. The amount of inaccuracy introduced by these changes in air gap size is unknown. This research assesses the magnitude of change introduced as a result of varying air gap distances.

Longitudinal Slice Off-Set

According to Zamanhoff (1987), at the 95% confidence level, the minimum detectable change in bone mineral density on any two sequential scans equals 2.83 times the reproducibility of the procedure. Therefore, high reproducibility (precision) with QCT is required to detect small changes in bone mineral density.

Small changes in axial slice position are known to worsen QCT reproducibility. To determine patient movement, a pre-scout and post-scout image is obtained during each QCT examination. These images tell the clinician the amount of change in axial slice position that occurred during the examination. If the patient has moved, the QCT scanning procedure is usually repeated. This doubles the patient dose and slows patient throughput. To aid the clinician in better determining when conditions warrant repeating the QCT procedure, this research objective assesses the impact of small changes in longitudinal slice position on measured QCT BMD values.

Gantry Angular Positioning

Another clinical factor which adversely affects QCT reproducibility is small changes in gantry angulation. During the course of a QCT examination, the muscles of the lower back may relax, allowing the curvature of the spine to decrease. When this occurs, the angle of the vertebrae change. If a change in vertebral angle occurs after the axial images are posted but prior to making the axial scans, the axial scans will not occur perpendicular to the vertebral endplates as anticipated. Further, the gantry angle selected during one examination may not be exactly matched on subsequent examination. To help the clinician better understand BMD results and determine when conditions warrant repeating the QCT procedure, this research objective assesses the impact of small changes in gantry angulation on measured QCT BMD values.

Aortic Calcifications

CT reconstruction algorithms assume the objects being irradiated are homogeneous in composition and then attempt to overcome inhomogeneities through various reconstruction techniques. Inhomogeneities involving large differences in tissue density result in streak artifacts and errors associated with volume averaging and beam hardening.

Figure 1-3 shows a CT axial image of a patient with a ring of calcification located within the aorta proximal to the vertebrae. Clinical experience indicates that this is a relatively common occurrence. The commonplace nature of such extra-osseous calcifications, coupled with the fact that high density materials near a ROI have been shown to cause various artifacts, warrant an investigation into the impact of aortic calcifications on spinal BMD measurements

Simulated Bowel Gas

Figure 1-3 is an axial CT image of the mid-torso showing the presence of bowel gas within the large intestine. This is a rather common condition encountered during QCT examination. Variations in the amount of gas contained within the bowel could potentially affect the accuracy and reproducibility of QCT measurements by introducing large variations in density within the scan field. This research investigates the effect of varying quantities of simulated bowel gas on the accuracy of QCT BMD measurements.

Reproducibility Study

The reproducibility study was undertaken to determine the in-vivo reproducibility of spinal bone mineral determination using QCT and the GE 9800 CT scanner currently in use at Shands Teaching Hospital, University of Florida.

This information is important for several reasons. First, the literature often cites reproducibility without explicitly stating whether clinical, in-vivo, or in-vitro reproducibility is being reported. Also, the reproducibility estimates cited when comparing QCT with competing methods of bone mineral assessment are often those obtained under tightly controlled experimental

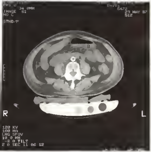
34 0MM
IMAGE 61
NO C
STND/P
5472
23 MAY 87
512
B
R
L
120 KV
100 MA
LRG SFOV
10 0 MM
-2 0 TILT
2 0 SEC 11 06 12

[illegible]

conditions. To make the reproducibility issue more clinically relevant, it is necessary to

1. Obtain an estimate of reproducibility under normal clinical conditions using state of the art equipment (GE 9800);

2. Obtain a baseline from which corrections for various clinical variables found to influence QCT measurement could be applied to improve the reproducibility from normal scanning procedures, and

3. Determine the minimum change in bone mineral detectable by QCT in order to assess the frequency of examinations during a longitudinal study.

Dose Assessment

To mitigate the effects of the preceding variables, the clinician may decide to repeat a QCT examination. Such a decision must consider the health consequences of the examination, both in terms of benefit to the patient and risk from increased exposure to ionizing radiation. Unfortunately, the clinician is provided with little empirical data upon which to base this decision. Recognizing this fact and the potential for increased use of QCT in routine evaluation of osteoporosis, a study was undertaken to assess the radiation dose from the QCT procedure.

The literature cites numerous estimates of radiation dose from QCT but is seriously lacking in specificity and clarity. Genant et al. (1987) cite the radiation exposure for single energy QCT to be in the range of 100-300 mrem. The use of dose equivalent units to express exposure calls into question what quantity was actually measured. Other citations give estimates of dose from QCT using correct units but fail to specify the type of CT scanner, technique factors used, location on or within the body where the dose is measured, type of the dosimeter, or specifics regarding conversion of units of exposure to those of dose equivalent. The dose estimates in the literature are, therefore, extremely varied. This fact permits proponents of competing bone mineral assessment techniques to cite dose estimate which best suit their purpose, regardless of the reasonableness of such estimate.

This research objective assesses the patient dose from the QCT procedure and CT scanner (GE 9800) used at this institution. This research determines the dose from normal clinical technique factors to the most radiosensitive organs of the body as well as various other sites within the body.

A further objective of this study is to assist in the development of protocols to provide adequate diagnostic information with minimal patient dose. This requires the evaluation of various clinical parameters and their dose related effects on accuracy and precision to determine where dose sparing measures might best be utilized. Specifically, assessments include:

1. The impact of reducing patient dose on the accuracy of bone mineralization determination and

2. the impact of single slice CT scanning on accuracy and precision as a means to reduce patient exposure.

Dose Reduction Effects on Accuracy

The normal QCT technique uses a series of four axial images, each at a tube potential of 80 kVp and a tube current of 40 mA with a 2 s scan time. This has widely been accepted as the lowest practical technique, below which the radiographic image appears grainy and mottled due to photon quantum effects. Cann (1987) postulated that the dose for QCT may be reduced without loss of accuracy despite a visually degraded radiographic image. A cadaveric study was conducted to test this hypothesis and to assess the extent of dose reduction achievable without a sacrifice in QCT accuracy.

Accuracy and Precision of Single Slice Scanning

It is hypothesized that a substantial portion of the patient dose from the QCT procedure is attributable to axial scanning If true, the elimination of some axial scans would result in a substantial dose sparing

Prior to implementing such dose sparing measures it will be necessary to determine

1. How accurately and confidently can the patient BMD be predicted using fewer than normal vertebral images per exam?

2. How few vertebrae can be imaged without significantly degrading the reproducibility of the procedure?

The data obtained from the reproducibility study are analyzed in an effort to answer such questions and to more fully investigate what effect reducing the number of imaged would have on accuracy and precision.

Optimization of Parameters

The assessment of the clinical variables discussed up to this point was undertaken to determine which variables have little clinical significance and which require tight control to insure QCT accuracy and reproducibility Based on these determinations, necessary modifications to the normal QCT protocol are proposed Such recommendations are contained in Chapter V, Conclusions and Recommendations.

Summary of Objectives

The preceding sub-sections have outlined both the problems and potential solutions to many unanswered questions regarding the use of QCT in bone mineral determination. Table 1-2 summarizes the study objectives and briefly outlines the overall methodologies necessary to obtain solutions.

Table 1-2. Summary of research objectives and methodologies.

Research Objective	Parameter	Methodology
Patient Decentering		
Vertical	Accuracy	Vary vertical position of CIRS phantom
Lateral	Accuracy	Vary lateral position of CIRS phantom
Changes in Patient Size	Accuracy	Vary size of CIRS phantom
Changes in Patient Geometry	Accuracy	Vary shape of geometric phantom
Spine-water Bolus Air Gaps	Accuracy	Vary air gap distance between CIRS phantom and water bolus
Changes in Longitudinal Position	Accuracy	Vary slice position along vertebral body (cadavaric study)
Changes in Gantry Angulation	Accuracy	Vary gantry angulation through the midpoint of vertebral bodies (cadavaric study)
Aortic Calcifications	Accuracy	Multiple measurements of calcification phantom with and without calcifications
Bowel Gas	Accuracy	Multiple measurements of bowel gas phantom with and without bowel gas
QCT Reproducibility	Precision/Minimum detectable change	Patient study, sequential measurements of vertebra

Table 1-2. Continued.

Research Objective	Parameter	Methodology
Dose Assessment	Health risk	Rando Phantom TLD measurements
Dose Reduction factors	Accuracy	Measurements at various technique (cadaveric study)
Single Slice Scanning	Minimize dose	Analyze fewer than normal axial scans using patient data from reproducibility study
Optimization of Parameters	Maximize accuracy and minimize dose	Assess research and make recommendations

CHAPTER II
MATERIALS AND METHODS

The Department of Radiology and the Department of Radiation Therapy at Shands Teaching Hospital provided or purchased all materials cited in this chapter. The CT section of the Department of Radiology provided all staff support used during the reproducibility study. Experimental procedures were usually performed after clinic hours or on weekends and holidays to avoid conflicts with patient treatment times.

Materials

Of the various materials used in the study, three deserve detailed discussion: the CT scanner, the phantoms, and the dosimetry system. The following sections cover the first two systems since they are unique and relevant to the central theme. The dosimetry system, though obviously relevant, is not unique to this research. The dosimetry system description, calibration, and use is, therefore, contained in Appendix A. The cadavers and patients used were also important to the study objectives and will be discussed as necessary.

GE 9800 "Quick"

To insure consistency of results, the same CT scanner, a third generation General Electric (GE) 9800, was used in all portions of this study. This series scanner has four basic systems: x-ray production, data acquisition, data processing, and image display (see Figure 2-1).

X-ray production

The GE 9800 uses a rotating x-ray tube of conventional design for x-ray production. It is capable of handling exposures from 1.3 s to 8 s in duration. The x-ray tube has a 0.9 x 0.7 mm focal spot size. A high voltage transformer provides for three tube potential selections (80, 120, and 140 kVp) and 12 tube current selections ranging from 10 to 300 mA. A bow-tie filter provides varying levels of filtration for more uniform beam intensity at the detector elements. A four aperture collimator restricts the x-ray fan beam to a 49° angle with beam widths of 1.5, 3, 5, and 10 mm.

The x-ray tube is located within a doughnut-shaped gantry. The gantry opening is 70 cm in diameter. The gantry supports variable tilting from vertical through a range of ± 20° in 0.5° increments. The gantry has two laser beams which assist in patient positioning

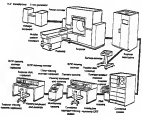

Figure 2-1. Schematic of G.E. 9800 CT scanner system (courtesy of Picker International).

A table capable of supporting a 300 lb patient translates horizontally and vertically within the gantry. The table may be adjusted in increments of 1 mm either horizontally or vertically and has a one meter horizontal range.

Data acquisition

The detector acquisition system consists of a large metallic chamber sectioned by baffles located at 1 mm intervals. This forms an array of 742 individual detector elements consisting of a set of tungsten plates filled with pressurized xenon gas. Xenon is used as an inert fill gas because of its high atomic number (54) which enhances photon interaction in the photoelectric energy range. The amount of ionization of the gas in each detector element is proportional to the radiation incident on the chamber. During scanning, some detector elements are not directly irradiated by the fan shaped beam and serve as reference calibration cells. The number of reference cells varies according to FOV selected during scanning. During the largest FOV, 730 detector elements are active, with the remaining 12 used for reference.

The data acquisition system (DAS) samples each detector element 984 times per second. For a typical QCT axial scan of two second duration, the number of samples obtained is 1,968. If a large FOV (48 cm) is selected, each of the 730 non-reference detector elements will contribute 1,968 samples per second for a total of over 1.4 million measurements per scan

Data processing

The measurements undergo over a dozen mathematical filtering processes. The filtered measurements are back projected onto matrix of picture elements (pixels), each representing a cube of anatomy irradiated (voxel). By calculating the CT number for each voxel, a shade of gray corresponding to the CT number may be assigned and displayed. In this manner, tissue density differences of less than 1% can be distinguished.

Image display

The image display system consists of the operator's console, physician's console, and multi-format camera. The consoles can display the image with varying degrees of contrast. The range of CT values (window) displayed can be varied from 2 to 4000 while the center value of the window width (level) can be varied from -1024 to +3071. Depending upon the type of reconstruction algorithm chosen, the GE 9800 can resolve objects as small as 0.5 mm.

Phantoms

This study used commercially available phantoms and phantoms specially fabricated for this research. The commercially available phantoms include the Computerized Imaging Reference Systems, Inc., (CIRS) phantom, the Cann-Genant reference phantom, and the Kando phantom. Phantoms specially fabricated for this study include the geometric, aortic calcification, and bowel gas phantoms.

CIRS phantom

The CIRS phantom is a resin based lumbar reference phantom. It represents an average section of the anatomy from approximately the second to the fourth lumbar regions. Within the range of diagnostic energies it interacts with xrays in a manner identical to the human body. The phantom simulates areas of fat, muscle, and bone within the body. As shown in Figure 2-2, the CIRS phantom consists of four parts. These are the phantom itself, two large fat equivalent rings that fit around the phantom, and vertebral mineral plugs. The fat rings simulate medium and large size patients while the vertebral inserts simulate vertebrae of varying fat and mineral content.

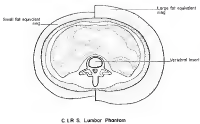

Figure 2-2. C.I.R.S. lumbar phantom.

The phantom itself is 3 cm thick with a circumference of 80 cm. The addition of one fat ring increases the phantom circumference to 94 cm. With both fat rings added, the total phantom circumference becomes 106 cm. The mineral content of the vertebral inserts range from 50 through 150 mg/cm^3 of calcium hydroxyapatite, the major mineral component of bone. A velcro covered support board and lucite stand provide support and vertical alignment within the scan field.

Since the CIRS phantom is widely sold to institutions for QCT, it is important that the phantom accurately models the patient under actual scanning conditions. One unresearched area in the use of this phantom is the extent to which the phantom thickness fully accounts for all scattering effects. Before using the CIRS phantom for research, its ability to account fully for photon scattering effects at diagnostic energies was investigated.

Solid Water^{TM} phantoms

To assess the effects on measured QCT values introduced by changes in patient geometry, internal bowel gas, and aortic calcifications, it was necessary to construct phantoms which would allow for alterations in geometry, internal air spaces, and increased density. Two phantoms were constructed out of a 30 x 30 x 3 cm block of Solid Water^{TM}.

Solid Water^{TM} is an epoxy resin based material manufactured and marketed by Radiation Measurements, Inc. (RMI) of Middleton, Wisconsin. Its formulation is based upon the work done by Contantiou et al. (1982).

Four basic components comprise Solid Water^{TM}: an epoxy resin base, polyethylene, calcium carbonate, and phenolic microspheres. Their composition by weight is 80.48, 10.00, 5.77 and 3.75% respectively. Two components, Araldite (Ciba-Geigy Corporation) and Jeffamine T-403 (Jefferson Chemical Company of Houston, Texas) comprise the resin base. This resin base material constitutes the largest component of Solid Water^{TM}.

The other materials provide enhanced structural and radiographic properties. The addition of the phenolic microspheres reduces the specific gravity of the material to 1.015 ± 0.002 gr/cm^3. This compares favorably to the specific gravity of distilled water at 22° centigrade of 0.997 g/cm^3. The elemental composition of Solid Water^{TM} is 8.09% hydrogen, 67.22% carbon, 2.40% nitrogen, 19.84% oxygen, 2.32% calcium and 0.13% chlorine.

Table 2-1. Ratio of characteristics of Solid Water^{TM} to water.

Solid Water^{TM}/Water Radiation Characteristics				
		ENERGY (KeV)		
RADIATION QUALITY	MATERIAL	10	100	1000
Mass attenuation coefficient ratio	Solid Water^{TM}	1.05	0.97	0.97
	Polystyrene	0.41	0.95	0.97
	Lucite	0.64	0.96	0.97
Mass energy absorption ratio	Solid Water^{TM}	1.10	1.00	0.97
	Polystyrene	0.37	0.90	0.97
	Lucite	0.60	0.93	0.97
Electron mass stopping power	Solid Water^{TM}	0.97	0.97	0.97
	Polystyrene	0.98	0.97	0.97
	Lucite	0.97	0.97	0.97

Table 2-1 compares the radiation characteristics of Solid Water^{TM} with those of polystyrene and lucite in the range of diagnostic energies. As shown, in the diagnostic energy range, Solid Water^{TM} very closely approximates the radiographic properties of water. Its use as a soft tissue model, therefore, is appropriate.

Figure 2-3 shows the Solid Water^{TM} phantom used in determining geometric effects. It consists of a 30 x 30 x 3 cm block of Solid Water^{TM} machined into seven sections. Each section was machined so that when assembled, no detectable air gaps would be present. The phantom is capable of modeling three different patient geometries.

By assembling the sections labelled A_3, A_2B_2, and $A_1B_3C_3$, a circular geometry is obtained. If one places a rectangular co-ordinate system over an ellipse so that the

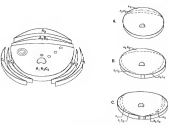

Figure 2-3. Geometric phantom showing: a) circular geometry b) elliptical ratio of 1.3:1, c) elliptical ratio of 1.6:1.

x-axis extends through both foci and the y-axis is midway between the foci, an elliptical ratio may be obtained by using the ratio of the distances from the origin to the perimeter of the ellipse along the x and y-axes respectively. In this circular geometry, the elliptical ratio is one to one. This configuration forms a cylinder with cross-sectional area of 452 cm^2 and circumference of 75.4 cm. The circumference closely matches the average circumference of 75.6 cm obtained from the nine cadavers used in the study of longitudinal and angular repositioning.

By assembling phantom sections C_1, B_1C_2, $A_1B_2C_3$, B_4C_4, and C_5, a geometry with the same circumference and cross-sectional area but with an elliptical ratio of 1.6:1 is obtained. This elliptical ratio is equivalent to the average elliptical ratio of the subjects used in the cadaveric study.

By assembling phantom sections B_1C_2, A_2B_2, $A_2B_3C_3$, and B_4C_4, an intermediate geometry with the same circumference and cross-sectional area is obtained. This intermediate geometry with an elliptical ratio of 1.3:1 approximates the ratio of 1.22:1 found by the Navy Clothing and Textile Research Center among 1331 females in the military (Navy Clothing and Textile Research Center, 1979).

At a distance of 7.5 cm from the dorsal surface of the phantom, a core accommodates a vertebral mineral insert of the type used for the CIRS phantom. The position of the core compared with the dorsal surface of the phantom is constant for all three geometries.

Figure 2-4 shows the Solid Water^{TM} phantom utilized to assess bowel gas and aortic calcification effects. It was fabricated using the three sections from the geometric phantom forming the circular geometry. At a distance of 0.3 cm above the location of the vertebral insert, a hole of 2 cm diameter has been cut to simulate the aorta. The hole is filled by two rings of 100 mg/cc density bone mineral material cut from a CIRS vertebral insert. The central 1 cm solid core is made from Solid Water^{TM}. Each ring is 2 mm thick with interior diameters of 12 and 16 mm respectively. The rings and central Solid Water^{TM} core are machined to fit together with no measurable air gap. The design closely simulates the aortic calcification "rings" (Figure 1-3) seen during the cadaveric and reproducibility studies. Two rings of bone density material were used to allow flexibility in simulating the degree of calcification within the aorta.

The phantom was further modified to allow for the assessment of bowel gas effects. Beginning 1 cm from the vertebral mineral insert and extending at a 45° angle, a series of three holes of 2 cm diameter were cored. Each

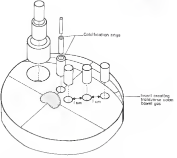

Figure 2-4. Simulated Bowel gas-aortic calcification phantom

hole was separated from the other by a distance of 1 cm so that their centers were located 2, 5, and 8 cm respectively from the vertebral insert. Each hole had a removeable Solid Water^{TM} core which, when placed within the hole, showed no detectable air gap. This series of holes was used to assess the effects from the same volume of bowel gas located at varying distances from a vertebra.

Additionally, a circular hole of 5 cm diameter was made at a distance of 6.5 cm and an angle of 135° from the vertebral insert. This hole was filled with two rings and one cylindrical core made from Solid Water^{TM}. The rings were constructed with interior diameters of 3.54 and 2.50 cm. The diameter of the central core was 2.50 cm. By removing the core and various rings, air gap volumes of 4.91, 9.82, and 19.63 cm^3 could be simulated. This series of holes was used to determine the effects of varying volumes of bowel gas at approximately the same location within the body.

By removing section A_2B_2 of the phantom and replacing it with two small inserts as shown in Figure 2-4, the phantom can also be used to simulate a much larger volume of bowel gas. This configuration simulates gas within the transverse colon

Rando phantom

The Rando phantom (Alderson Research Laboratories, Connecticut) was utilized for all dosimetric studies. According to Alderson Research Laboratories (1969) the phantom is molded around a natural human skeleton and consists of thermosetting synthetic material modified to an effective atomic number (Z) of 7.30 ± 0.5% with a mass density is 0.985 g/cm^3 ± 1.25%. This atomic number is slightly less than the effective atomic number for muscle (7.64) in order to allow for randomly distributed fat (Z = 6.46) occurring within the human body. Rando man is designed to correspond to a person who is 5'8" tall and weighs 162 lbs.

Figure 2-5 is an sketch of the Rando phantom used during the dosimetry study. The phantom is sectioned axially into twenty-five 2.5 cm thick sections beginning at the top of the cranium and extending downward to the level of the upper femur. The sections are aligned with each other by means of two plastic pins, 0.63 cm in diameter. Each individual section is drilled to produce a 3 x 3 cm grid of holes, each hole having a 0.5 cm diameter. The holes are of sufficient size to accommodate, without modification, the thermoluminescent dosimetry (TLD) chips used during the course of this study.

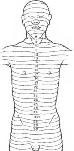

Figure 2-5. Rando phantom (exterior view).

Cann-Genant phantom

During CT scanning, a number of factors may introduce variability in the CT numbers obtained. These include beam hardening, variations in x-ray energy, and scattered radiation as well as many others. In order to mitigate these factors, a bone mineral reference phantom is usually scanned simultaneously with the patient.

The Cann-Genant phantom produced by Image Analysis, Inc. of Irvine, Ca., and shown in Figure 2-6 is one of the most widely used reference calibration phantoms for QCT. It was used as a reference calibration phantom for all research objectives in this study. The phantom consists of a curved plastic housing 45 cm in length, 26 cm wide, and 4 cm thick at the midplane. The housing contains five tubes filled with serial dilutions of dipotassium hydrogen phosphate, water, and glycerol. These solutions closely approximate the x-ray attenuation properties of bone mineral (calcium hydroxyapatite), soft tissue, and fat within the body. The five tubes are calibrated to 200, 100, 50, and zero mg/cc of bone mineral equivalent with the fifth tube serving as a fat calibration.

Also included in the Cann-Genant phantom are two small rods of high density material which serve as alignment pins for QCT software analysis programs. These index alignment

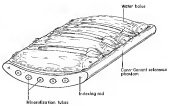

Figure 2-6. Cann-Genant reference phantom.

pins are used to locate and position circular regions of interest in each of the five reference calibration tubes. Improper alignment of the regions of interest will result in the software sampling inappropriate regions of the reference phantom resulting in an erroneous calibration curve. These alignment pins are normally indexed by the bone mineral analysis software program automatically.

Methods

The methods employed in this research are of two types. The first type are methods used to provide quality assurance and investigate properties of the materials used during the course of this study. The second type consists of the experimental methods used to investigate the research objectives. Each will be described in detail below.

Quality Assurance

Prior to experimentation, the materials used in this study were evaluated to insure they performed adequately and were suitable for their intended purpose.

GE 9800

Since the GE 9800 requires continuing calibration in order to yield high quality and accurate images, preventive maintenance (PM) was performed by the GE service technician on the scanner monthly throughout the period of this study. These PM checks included calibrations with air, water, and polyethylene phantoms. These calibrations were performed at every tube potential, scan thickness, and scan FOV used for these studies.

Phantoms

The properties of the phantoms used during the course of this research were generally well known. In those cases where clinical utility had not previously been obtained, the phantoms were evaluated prior to use in this study.

CIRS phantom

Although the CIRS is a commercially manufactured lumbar reference phantom in use at a number of institutions, its clinical utility had not been experimentally verified at Shands hospital. In particular, the ability of the CIRS phantom to adequately simulate a patient by fully accounting for photon scattering effects was undetermined. Additionally, the uniformity of the bone mineral insert provided with the phantom was unknown. To insure the clinical relevancy of study findings, it was necessary to assess the adequacy of the CIRS phantom in these regards

Scattering effects. In order to investigate the ability of the CIRS phantom to completely account for scattering effects, the CIRS phantom was used in conjunction with two 30 x 30 x 4 cm blocks of Solid Water^{TM}. Solid Water^{TM} has the same photon attenuation and absorption properties as water at diagnostic energies. It is, therefore, a good model for human soft tissue, the major component of which is water.

The CIRS phantom was used with one surrounding tissue ring to model the average torso in the region of L-3. In this configuration, the phantom has a circumference of 96 cm. Using measurements made on the nine cadavers used for longitudinal and angular offset research, the average circumference at the level of L-3 was found to be 75.6 cm One criteria used in the initial selection of these cadavers was that they should be "elderly white petite females". As such, they represent the elderly female osteoporotic population. Another population on which QCT is routinely performed for bone mineral determination is the adult renal patient. These patients tend to be very rotund. Although no normative data was obtained on the average girth of the renal patients, the phantom circumference of 96 cm was felt to be approximately midway between that of the petite female (75.6 cm) and the more rotund renal patient. The CIRS phantom with one fat ring was considered a good compromise representation of these two patient populations.

The CIRS phantom with a 50 mg/cc mineral insert was placed between two blocks of Solid Water^{TM} and mounted on the lucite support provided with the CIRS phantom. Each block of Solid Water^{TM} was 30 cm on a side with a thickness of 4 cm. The lucite support maintained the phantom perpendicular to the table-top. The support, Solid Water^{TM} blocks and phantom were held together with three strips of cloth tape. Since patients are routinely imaged while clothed, it was felt that cloth tape would not interfere with the clinical accuracy of BMD measurements. The outside edge of the CIRS phantom was marked to provide a reference for alignment with the CT laser beam. In this manner, the precise location on the CIRS phantom could be repositioned for scanning after movement.

The CIRS phantom-Solid Water^{TM}-lucite support apparatus was placed on water bags secured to the Cann-Genant reference phantom. The CIRS phantom was positioned so that the CT laser alignment beams indexed on the reference marks along the edge of the CIRS phantom. The gantry table height was set to 130 mm. Scan parameters were 80 kVp tube potential, 100 mA tube current, 2 s scan time, zero air gap, and a slice thickness of 10 mm. Twelve scans were made under these conditions. The CIRS phantom-Solid Water^{TM}-lucite support apparatus was then modified by removing both of the blocks of Solid Water^{TM} surrounding the CIRS phantom. The CIRS phantom was then remounted on the lucite support, placed on the water bags and Cann-Genant reference phantom, and repositioned so that the CT laser alignment light corresponded to the external reference marks on the edge of the CIRS phantom. The apparatus was then rescanned twelve times using the same CT settings as before.

The scans from both procedures were analyzed using the IA QCT software program. In each case the software default ROI was used to insure that the ROI was the same size and shape for each measurement. Since the maximum number of images that can be analyzed without repositioning the ROI is six, each procedure required that the ROI be positioned one time during each analysis. The results of the bone mineral density measurements are shown in Table 2-2.

Table 2-2. Comparison of Scattering effects from CIRS phantom with and without Solid Water^{TM}.

		Bone Mineral	
Amount of Solid Water^{TM}	Number of Scans	Mean (mg/cc)	Standard Deviation (mg/cc)
Two Blocks	12	57.79	0.87
None	12	53.10	0.99

It is clear from Table 2-2 that the BMD for the CIRS phantom surrounded by two blocks of Solid Water^{TM} as a scattering medium was higher than for the same phantom without the surrounding Solid Water^{TM}. To test the significance of this difference, a paired t-test was used. A t-score of 11.7 was obtained, representing a significant difference (probability $< 10^{-6}$) between these two measurement sets. If the CIRS phantom alone had adequately accounted for scattering effects, no significant difference should have been detected. Clearly, the addition and removal of the blocks of Solid Water^{TM} have an effect on measured BMD.

Since errors are unavoidably introduced whenever experimental conditions are changed even slightly, it was thought that perhaps the repositioning of the CIRS phantom after removal of the Solid Water^{TM} might have caused the difference in measured BMD. To test for this possibility a second procedure was conducted.

In this second procedure, the same CIRS phantom-Solid Water^{TM}-lucite support apparatus was again used. The CIRS phantom was placed between two blocks of Solid Water^{TM} and aligned with the CT scanner laser lights and external reference marks as before. All previous scanning conditions were maintained as during the first procedure with one exception. Since the first procedure used a tube current of 100 mA with a 2 s scan time to reduce variability from quantum effects, it was thought that the scattering effects seen at this technique might not be significant if the standard QCT scanning protocol was used. The mA was therefore decreased to 40 mA with a 2 s scan time to reduce the number of photons equivalent to those found during normal QCT scanning conditions. To compensate for the increased variability in the data from quantum effects, the number of scans made during this second trial was increased to 25.

After the first 25 scans were obtained, one block of Solid Water^{TM} was removed without moving the CIRS phantom-Solid Water^{TM}-lucite support apparatus. This alleviated any possible errors associated with repositioning of the apparatus that may have occurred during the first trial. Twenty five additional scans were then made of the CIRS phantom together with the remaining block of Solid Water^{TM} BMD analyses were made using the same procedure described in the first trial.

Table 2-3. Scattering effects from CIRS phantom.

		Bone Mineral	
Amount of Solid Water^{TM}	Number of Scans	Mean (mg/cc)	Std Deviation (mg/cc)
One Block	25	55.12	1.53
Two Blocks	25	58.59	1.49

As indicated in Table 2-3, at standard QCT technique, the BMD for the CIRS phantom surrounded by two blocks of Solid Water^{TM} was higher than for the same phantom with only one block of Solid Water^{TM}. The difference was compared with a paired t-test and a score of 7.7 was obtained, representing a significant difference (probability < 10-4) between the two measurement sets.

It is clear from these results that some additional material is necessary to account for the effects of photon scattering during bone density measurements An effort was made to determine the amount of Solid Water^{TM} required to completely account for scattering effects at 80 kVp and 40 mA and 2 seconds (normal spinal QCT scanning protocol). To do this, the CIRS phantom with one fat equivalent ring and the 50 mg/cc bone mineralization insert was utilized without Solid Water^{TM}. As before, the CIRS phantom was placed on the Cann-Genant phantom and water bag bolus and positioned so that no air gap was present between the water bolus and CIRS phantom. The lucite support and laser alignment beams insured proper positioning within the scan field The table height was set to 130 mm. Scan parameters were 80 kVp, 40 mA, 2 s, with a 10 mm slice thickness. Eighteen axial scans were then made using this configuration

The apparatus was then changed to allow the addition of a 30 x 30 x 2 cm block of Solid Water^{TM} to be placed on each side of the CIRS phantom. The phantom was then realigned with the laser light and axially rescanned eighteen times. The configuration was again changed by adding an additional 30 x 30 x 2 cm block of Solid Water^{TM} on each side of the CIRS phantom to provide a total thickness of 4 cm of Solid Water^{TM} on each side of the CIRS phantom. Eighteen axial scans were made in this configuration. Finally, additional blocks of Solid Water^{TM} were added to form a thickness of 6 cm of Solid Water^{TM} on each side of the CIRS phantom. Again, 18 axial scans were made in this configuration.

All axial scans were analyzed using the Image Analysis, Inc. QCT software. The ROI was chosen within the trabecular portion of the spinal mineral insert and the computer generated 2.6 cm^2 elliptical ROI was utilized.

Table 2-4. Analysis on amount of Solid Water^{TM} required to account for scattering effects.

		Bone Mineral	
Thickness of Solid Water^{TM} (cm)	Number of Scans	Mean (mg/cc)	Standard Deviation (mg/cc)
0	18	52.609	1.39
2	18	59.27	1.37
4	18	60.05	1.23
6	18	60.44	1.29

The results of this analysis are shown in Table 2-4. Again it is evident that the presence of Solid Water^{TM} results in an increase in the measured bone mineral density. Figure 2-7 shows a graphic illustration of the change in measured BMD as a function of the amount of Solid Water^{TM} used as a scattering medium. As shown, the most pronounced change occurs between the phantom without Solid Water^{TM} and the phantom with 2 cm of Solid Water^{TM} on each side. Additional thicknesses of Solid Water^{TM}, while increasing the total amount of change, do so at a less dramatic rate.

To evaluate the significance of this effect, an analysis of variance (ANOVA) was performed on the data. The ANOVA yielded an F-value of 140.8 (3,68 degrees of freedom). If the means of these distributions were the same, the probability of obtaining an F-value as high as 140.8 is less than 1×10^{-6}.

The ANOVA indicates a significant difference exists in the mean value obtained with the four phantom configurations It does not indicate between which configurations the significant difference may be found To determine this, a series of paired t-tests were used The results of these pair-wise comparisons are shown in Table 2-5.

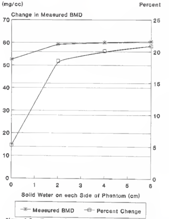

Figure 2-7. Change and percent change in measured BMD as a function of amount of Solid Water^{TM} used as a scattering medium.

Table 2-5. Pair-wise analysis on amount of Solid Water^{TM} required to account for scattering effects.

<- compared to ->				
Solid Water^{TM}	Solid Water^{TM}	T	Probability>T	Significant
0 cm	2 cm	13.5	10^{-6}	YES
0 cm	4 cm	19.04	10^{-6}	YES
0 cm	6 cm	14.92	10^{-6}	YES
2 cm	4 cm	1.95	0.068	NO
2 cm	6 cm	3.08	0.007	YES
4 cm	6 cm	0.97	0.350	NO

As indicated, a significant difference in measured BMD exists between the CIRS phantom when used alone and when used in conjunction with thicknesses of Solid Water^{TM}, 2 cm or above. No significant difference exists when increasing the amount of scattering material from 2 to 4 cm, nor when increasing the amount from 4 to 6 cm of material.

Since the CIRS phantom is widely used to measure BMD as a stand alone package without additional scattering material, the results were both surprising and clinically significant. Clearly, the CIRS phantom does not model clinical conditions since it fails to fully account for scattering effects and yields significantly differing results when used alone and in conjunction with Solid Water^{TM}. This makes the use of the CIRS phantom alone as a calibration standard for QCT bone mineral determination suspect. It is apparent that a minimum thickness of 2 cm of Solid Water^{TM} is needed on each side of CIRS phantom to account for the majority (94%) of photon scattering effects. Based on these findings, all research using the CIRS phantom was conducted with a minimum thickness of 2 cm of Solid Water^{TM} on each side of the phantom.

Mineral insert uniformity. Prior to using the CIRS phantom for research, the uniformity of the 50 mg/cc vertebral insert was assessed. This was done by placing the CIRS phantom with the 50 mg/cc vertebral insert between two 30 x 30 x 2 cm blocks of Solid Water^{TM}. The phantom was then centered on the CT gantry table on top of the Cann-Genant phantom and water bolus combination. An image using technique factors of 80 kVp, 100 mA, and 2 s was obtained and displayed on the operator's console.

A 2.6 cm^2 elliptical ROI was positioned within the region of the vertebral mineral insert. The ROI was then moved incrementally downward, one pixel at a time, vertically through the vertebral mineral insert. The average CT number at each pixel location was recorded. This process was then repeated while moving the ROI laterally across the width of the vertebral insert.

The results of the vertebral insert uniformity analysis using the average CT number at each pixel location are shown in Table 2-6.

Table 2-6. Uniformity of vertebral bone mineral insert.

Statistic	Vertical Uniformity	Lateral Uniformity
Mean	113.67	113.29
Standard Deviation	1.43	0.75
Maximum	115.57	114.80
Minimum	110.59	113.29
Range	4.98	1.51

As indicated in the table, CT numbers obtained vertically through the vertebral insert showed a higher variability than those obtained laterally. Although the range of CT numbers in the vertical direction was larger than anticipated, the uniformity of the vertebral insert was considered acceptable since the research related positioning of the ROI would not vary over the entire range of 13 pixels used in this analysis. It was anticipated that the ROI placement within the vertebral ROI could be accomplished with a variation of only one or two pixels.

To test this hypothesis, the author used the same phantom configuration and scanning conditions to re-image the phantom. Displaying the image of the phantom on the console, a 2.6 cm^2 ROI was positioned within the region of the vertebral insert. The x and y coordinates of the ROI were recorded. The image was cleared and then redisplayed on the console. The same 2.6 cm^2 ROI was repositioned in approximately the same location within the vertebral insert. This process was repeated through 30 iterations.

The results showed that the pixel location of the center of the ROI did not vary by more than one pixel in either the vertical or horizontal direction. The standard deviation of the measurements was 0.25 pixels horizontally and 0.42 pixels vertically. Intra-operator errors in repositioning the ROI within the vertebral body are thus seen to be minimal. Therefore, even though the mineral insert showed some variability in CT numbers over its entire breadth, the variability of CT numbers associated with an ROI repositioning error of one pixel was considered clinically inconsequential.

Solid Water^{TM} phantoms

The radiological properties of Solid Water^{TM} are well known. The fabrication of the geometric, aortic calcification, and bowel gas phantoms from Solid Water^{TM} would not likely alter these properties. The performance of quality assurance tests on these phantoms was considered unnecessary.

Rando phantom

Like Solid Water^{TM}, the properties of the Rando phantom have been extensively investigated. No quality assurance tests were deemed necessary to further evaluate the suitability of the Rando phantom for this research.

Cann-Genant phantom

The Cann-Genant phantom is normally scanned simultaneously with the patient. By concurrently obtaining CT numbers for the ROI within the patient and for each of the reference calibration tubes within the Cann-Genant phantom, a linear regression of CT number versus actual bone mineral density may be obtained. In this manner, the equivalent bone mineral density for the ROI within the patient may be determined. This approach requires that the ROI for each of the reference calibration tubes within the phantom be entirely contained within the margins of the tube. This is normally accomplished automatically by the QCT software. It is not uncommon, however, for the software program to "miss" the alignment pins, requiring the CT technologist to manually position the indexing cursors over the rods

Since variability introduced by manually positioning the cursors over the alignment pins in the Cann-Genant reference phantom will result in measurement inaccuracies and degraded precision, the magnitude of this effect required evaluation prior to the Cann-Genant phantom's use in this research.

Two sets of six identical axial images were used to investigate intra-operator alignment errors. Each scan was displayed on the console while the software generated vertebral ROI was maintained in a fixed location within the vertebral body. Since the maximum number of images that may be analyzed by the QCT software package without repositioning the ROI is six, two sets of six scans were analyzed individually. After each image was displayed on the screen, manual alignment of index marks was accomplished. The average CT numbers for each mineral tube within the reference phantom as well as the average CT number for the vertebral mineral insert was obtained. Additionally, the measured BMD for the vertebral mineral insert was noted.

Except for very minor variations in the first BMD measurement in each set, all BMD measurements were identical, even though index mark alignments varied. From the above, it may be concluded that small variations introduced through the manual alignment of cursors over the indexing rods in the Cann-Genant phantom do not significantly degrade measurement accuracy or precision of QCT measurements.

Experimental Methods

This section describes the experimental methodology used to accomplish the various research objectives. It includes a description of the experimental configuration as well as the procedures used to perform the experiments. The research objectives will be presented in the same order as in the previous chapter. Their sequence does not indicate relative importance. Unless otherwise noted, all axial scans were analyzed with a 2.6 cm^2 ROI using the Image Analysis QCT software analysis program.

Field nonuniformity effects

Due to changes in beam energy and intensity across the scan field, it was expected that QCT BMD measurements of an object made at one location would differ from those of the same object made at a different location within the scan field. In order to investigate this phenomenon, BMD measurements made with the CIRS phantom and its 50 mg/cc vertebral insert were analyzed, incrementally off-setting the phantom in both the vertical and horizontal directions.

Vertical decentering

To investigate the effects of vertical decentering on measured BMD values, the CIRS phantom configured with one fat equivalent ring and the 50 mg/cc vertebral bone mineral insert was used. The phantom was placed between two 30 x 30 x 4 cm blocks of Solid Water^{TM} and mounted atop the Cann-Genant reference phantom and water bolus. The Solid Water^{TM} was used to more fully account for photon scattering effects. The CIRS phantom, Cann-Genant phantom, and water bolus, was placed on the CT gantry table and located to a height of 130 mm, consistent with the standard QCT protocol. A series of four axial images was obtained at this table height using technique factors of 80 kVp and 100 mA with a 2 s scan time. A 10 mm slice thickness was used for all axial scans. These technique factors remained the same throughout the investigation. The table was then decentered vertically in 10 mm increments. Four images were obtained at each 10 mm vertical off-set distance through the range of table heights from 70 through 190 mm yielding a total of 52 axial scans. All axial images were analyzed using the largest ROI possible.

Since Shand's QCT protocol specifies a table height of 130 mm for all QCT examinations, a more clinically relevant measure of scan field nonuniformity would be obtained by varying the phantom height within the scan field while holding the Cann-Genant phantom and table height constant This would serve to approximate the types of changes in vertebral position which occur during routine QCT examinations due to differences in patient dorsal thickness and spinal curvature.

To accomplish this, the experimental procedure used above was modified by taking measurements only at a table height of 130 mm. The CIRS phantom, configured as above, was vertically decentered by increasing and decreasing the amount of water within the water bolus This was accomplished by using a syringe to add or remove varying amounts of sterile saline from the water bags. Sufficient pressure was maintained on the water bolus to prevent the formation of air gaps between the water bolus and the CIRS phantom. Figure 2-8 shows some of the variations in the experimental configuration used for this study. Since the vertical position of the CIRS phantom was controlled by a varying the amount of solution within the water bags, the overall shape of the scanned area (CIRS phantom, water bolus, and Cann-Genant phantom) was not constant. Possible confounding effects of changes in geometry are recognized as a limitation of the study.

A series of six scans were made at each vertical offset using a technique factor of 80 kVp, 100 mA, and 2 s. Vertical off-set distances ranged from zero through

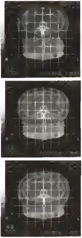

Figure 2-8 [illegible] tions used to assess changes in measured [illegible] tical position within scan field

7.59 cm above the scan field isocenter and from 8.71 through 16.59 cm measured from the base of the vertebral insert to the top of the Cann-Genant phantom. A total of 60 axial images were obtained and analyzed using the largest ROI that could be inscribed within the vertebral insert. The results were tabulated and plotted as percent change in measured BMD as a function of vertical position above scan field isocenter.

Lateral decentering

To investigate the effects of lateral decentering, the CIRS phantom was used as configured in "vertical decentering" above. All scan parameters previously used were retained and the table height remained constant at a height of 130 mm. The only procedural difference was in the direction of the decentering. In this case, the CIRS phantom was decentered laterally. The lateral decentering was accomplished in approximately 1.5 cm increments ranging from 5 cm to the left of isocenter to 5.15 cm to the right of isocenter. Efforts were made to insure that fluctuations in vertical distance did not occur during the process of decentering the phantom. Sufficient pressure on the CIRS phantom was obtained to eliminate all air gaps. The experimental configurations used during the lateral decentering study are shown in Figure 2-9.

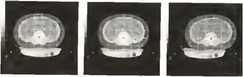

Figure [illegible] Typical scan of phantom configuration used to assess changes in measured BMD as a function of lateral decentering within the scan field

A total of 54 axial images were obtained, six at each decentered location, and analyzed using the largest ROI that could be inscribed within the vertebral insert. The results were tabulated and plotted as percent change in measured BMD as a function of lateral position within scan field.

Patient geometry

In order to investigate the effects of changes in patient geometry on the accuracy of spinal QCT bone mineral determination, the geometric phantom as previously described was used in conjunction with the 50 mg/cc bone mineral insert. The geometric phantom in its circular geometry was mounted on the lucite support and placed on top of the Cann-Genant reference phantom. Between the geometric phantom and the Cann-Genant reference phantom, was placed a water bolus consisting of intra-venous (i.v.) bags filled with distilled water. The purpose of the water bolus was to eliminate air gaps which have been shown to perturb scan accuracy. Two 30 x 30 x 4 cm blocks of Solid Water^{TM} were placed, one on each side of the geometric phantom to more adequately account for photon scattering effects and provide more clinically relevant data. The geometric phantom was adjusted so that there were no air gaps present between it and the water bolus - Cann-Genant phantom combination. The entire apparatus was then centered on the gantry table and raised to a height of 130 mm, in agreement with the standard QCT scanning protocol. The technique factors were 80 kVp, 40 mA, and 2 s. A total of 25 scans were made in this configuration.

The geometric phantom was then reconfigured to its elliptical ratio of 1.3:1. The geometric phantom, water bolus, and Cann-Genant reference phantom were readjusted to eliminate any air gaps. No other scan parameters were modified. Twenty five scans were made using this configuration.

Upon completion of these scans, the geometric phantom was reconfigured to its elliptical ratio of 1.6:1. After insuring the absence of any air gaps between the geometric phantom and Cann-Genant reference phantom and using the same scan parameters as previously described, 25 more scans were taken. Care was taken to insure the vertebral insert remained at the same position within the scan field in each phantom configuration. The location of the vertebral insert was visually confirmed on the operator's console prior to scanning. The scan data was analyzed to assess the vertebral bone mineral equivalent content of the 50 mg/cc bone mineral insert within the phantom.

Patient size effects

In order to investigate the effects of changes in patient size on the accuracy of QCT, the CIRS phantom was used in conjunction with the 50 mg/cc vertebral insert. The CIRS phantom, with no external fat rings, was mounted on the lucite support and placed atop of the Cann-Genant reference phantom and water bolus combination. Two 30 x 30 x 4 cm blocks of Solid Water^{TM} were placed, one on each side of the CIRS phantom to more fully account for photon scattering effects. The CIRS phantom was adjusted so that no air gaps were present between the CIRS phantom and water bolus. The entire apparatus was then centered on the gantry table and raised to a height of 130 mm. The standard QCT technique factors of 80 kVp, 40 mA, and 2 s were used for imaging. A total of 24 scans were made using these conditions. The scan data was analyzed with I.A. QCT software using the computer generated 2.6 cm^2 ROI.

One fat equivalent ring was then added to reconfigure the phantom to its intermediate size. The CIRS phantom, water bolus, and Cann-Genant reference phantom were readjusted to eliminate any air gaps. The position of the vertebral insert was maintained by withdrawing water from the water bolus to compensate for the added thickness of the fat equivalent ring. No other scan parameters were modified. Twenty four scans were made with this configuration.

Upon completion of these scans, the CIRS phantom was again reconfigured by placing it within the second fat equivalent ring, bringing it to its largest cross-sectional area. The absence of air gaps between the CIRS phantom and Cann-Genant reference phantom was assured and the position of the vertebral insert within the scan field was maintained. Using the same scan parameters as previously described, twenty four scans were taken in this configuration. Figure 2-10 shows the CIRS phantom configured in each of its three sizes.

The scan data was analyzed to assess the vertebral bone mineral equivalent content of the 50 mg/cc bone mineral insert within the phantom. During the course of analyzing the CIRS phantom in each configuration, the ROI was repositioned four times.

Air gap effects

Variations in air gap size between the dorsal surface of the patient and the water bolus during repeat scans was assessed by using the CIRS lumbar spine phantom. The phantom with one tissue ring and a 50 mg/cc bone mineralization vertebral insert was positioned between two blocks of Solid Water^{TM}. Each block of Solid Water^{TM} had

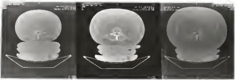

Figure 2-10. Axial images of C.I.R.S. phantom used to assess patient size effects on measured BMD values.

dimensions of 30 x 30 x 4 cm and was used to account for photon scattering effects.

The Solid Water^{TM}-C.I.R.S. spine phantom combination was placed over a water bolus resting upon the Cann-Genant reference phantom. Axial scan alignment was assured by marking the phantom medially along its circumference and matching these scorings with the CT scan laser alignment beams. The water bolus consisted of a series of partially filled 1,000 cc normal saline bags taped to the Cann-Genant reference phantom. Various air gaps were obtained by withdrawing water from the water bolus while maintaining the same vertical and horizontal phantom position within the scan field. Figure 2-11 shows the variations in phantom arrangement used in determining the effects of air gaps on QCT accuracy.

All images in this study were analyzed using the largest elliptical ROI that could be inscribed within the trabecular portion of the vertebral insert without encroaching on the cortical rim. Two axial images were obtained at each the following air gap distances: 0, 0.6, 1.1, 2.3, 3.1, 4.2, and 5.7 cm for each technique factor used. Air gap distance was measured from the top of the water bolus to the base of the CIRS phantom. Technique factors used are shown in Table 2-7.

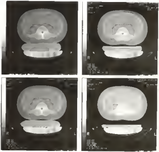

Figure [illegible]-11 Axial scans of phantom configurations used to assess air gap effects on measured BMD values.

Table 2-7. Technique factors used to assess air gap effects.

Tube Potential (kVp)	Time (s)	Tube Current (mA)					
80	2	120	100	70	40	20	10
120	2	120	100	70	40		
140	2	120	100	70	40		

Effects of longitudinal off-set

In order to detect small changes in bone mineral density, high reproducibility (precision) with QCT is required. One clinical factor which is known to worsen QCT reproducibility is small changes in axial slice position. This research objective assesses the impact from small changes in longitudinal slice position on measured QCT BMD values.

In order to study the effect of small changes in longitudinal slice off-set on the precision of QCT BMD measurements, 35 vertebrae in nine cadavers were imaged. All cadavers selected were petite females who had died of cardiovascular disease and ranged from 56 to 86 years of age at time of death. The average age at time of death was 76 years.

Cadavers were placed supine on the CT scanning table with arms restrained above the head. The lower spine was positioned over a Cann-Genant reference phantom and water bolus. A lateral scout scan was made from the region of T-11 through the top of the iliac crest. Once obtained, the lateral scout view was posted for axial scanning of vertebrae T-12 through L-4 with the imaging protocol shown in Table 28.

Table 2-8. QCT scanning protocol used to assess the effects of small changes in longitudinal slice off-set and gantry angulation on the precision of QCT measurements.

Table Height	130 mm
Patient Position	Supine
Scan FOV	48 cm
Display FOV	48 cm
Scan Type	Normal
Recon Resolution	Standard
Matrix Size	512
Slice Thickness	10 mm
Tube Current	100 mA
Scan Time	2 seconds
Tube Potential	120/80 kVp*

* Ten vertebrae were imaged at 120 kVp and 9 vertebrae were imaged at 80 kVp.

The images were reviewed for any abnormality that might affect the QCT results and sixteen vertebrae were excluded, five for air in the aorta, three for air within the vertebral body, four for severe scoliosis and four due to the presence of an arm within the scan field. Of the remaining seven cadavers and 19 vertebrae, the effect of small changes in longitudinal slice position was assessed by making axial images beginning at the vertebral endplate and off-setting that position in 2 mm increments from endplate to endplate (see Figure 2-12). The ROI used within the trabecular portion of the vertebra was the largest ellipse possible without encroaching on the cortical rim or the basivertebral complex.

Effects of gantry angulation

In order to study the effect of gantry angulation on QCT precision, the same nine cadavers used in the study of longitudinal off-set were imaged. Cadavers were placed supine on the CT scanning table with arms restrained above the head. The lower spine was positioned over a Cann-Genant reference phantom and water bolus. The GE 9800 "Quick" CT scanner was utilized to image vertebrae T-12 through L-4 with the imaging protocol shown in Table 2-8.

The images were reviewed for abnormality and the same vertebrae excluded from the longitudinal off-set study were excluded here as well. Of the remaining seven cadavers and 19 vertebrae, the effect of small changes in gantry angulation was assessed by making axial images beginning at the vertebral midplane and off-setting the midplane angle in 2° increments from -10° to +10° (see Figure 2-13). Due to limitations in gantry angle movement, not all vertebrae

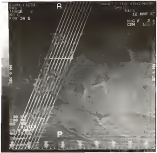

Figure [illegible]-12 Lateral scout image showing postings for axial scans used to study the effects of small changes in longitudinal slice position on BMD.

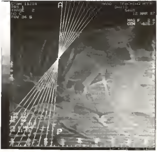

Figure 2-13. Lateral scout image showing postings for axial scans used to study the effects of small changes in gantry angulation on measured BMD.

were imaged a full 10° from the midplane angle. The ROI used within the trabecular portion of the vertebra was the largest ellipse possible without encroaching on the cortical rim or the basivertebral complex.

Effects of aortic calcifications

CT is known to be adversely affected by streak artifacts caused by very dense materials. In an effort to determine the sensitivity of QCT to aortic calcifications, the aortic calcification-bowel gas phantom (Figure 2-4) was utilized.

The aortic calcification phantom was placed on the CT gantry table, resting on the Cann-Genant phantom and water bolus. All portions of the phantom were assembled to form a circular geometry. All holes were filled with Solid Water^{TM} cores with the exception of the vertebral mineral insert. The vertebral mineral insert used consisted of 50 mg/cc bone mineral equivalent material. To eliminate any variability that might be introduced by air gaps, the calcification phantom was adjusted so that no air gaps were present between the it and the water bolus. Additionally, the seams between adjacent parts of the phantom were coated with surgical lubricant to replace any minute air filled areas with a water equivalent material. To fully account for the effects of beam scattering, one 30 x 30 x 4 cm block of solid water was placed on each side of the calcification phantom. This allowed for a total of 5 cm of solid water on each side of the 1 cm beam. The table height was set to a height of 130 mm which placed the center of the phantom at the approximate isocenter of the scan field. Using the CT laser alignment light, the horizontal location of the calcification phantom was adjusted so that the x-ray beam would intersect axially through its midplane.

Using standard QCT imaging parameters of 80 kVp, 40 mA, 2 s, and a 1 cm beam width, a series of 24 axial scans were made of the phantom in this configuration. The phantom was then reconfigured by removing the Solid Water^{TM} core at the location of the aorta and replacing it with the two 100 mg/cc aortic calcification rings. A second series of 24 axial scans was made of the phantom in this "calcified" configuration.

Simulated bowel gas

The effects of simulated bowel gas within the patient were examined with the use of a specially fabricated phantom made from Solid Water^{TM}. This phantom was fabricated from a 30 x 30 x 4 cm slab of Solid Water^{TM} with various cores removed as described in the materials section above.

In order to assess bowel gas effects, the modified Solid Water^{TM} phantom in circular geometry was placed on a water bolus resting on the Cann-Genant phantom. The phantom was adjusted so that no air gap existed between the Cann-Genant phantom and the Solid Water^{TM} phantom. This was done to eliminate any confounding effects from external air gaps. One 30 x 30 x 4 cm block of Solid Water^{TM} was placed on each side of the phantom. The entire apparatus was held securely against a lucite support apparatus. Beam alignment through the center of the phantom was insured by scoring the edge of the phantom and positioning the CT laser alignment lights to coincide with the scorings. In order to insure clinical relevancy, normal QCT scanning protocol settings as specified in Table 1-1 were used. A 50 mg/cc bone mineralization insert was used for all scans.

In order to assess both the effects of a constant volume of bowel gas at varying distances from the vertebral bone mineral insert and to assess the effect of varying amounts of bowel gas at approximately the same distance from the vertebral bone mineral insert, the Solid Water^{TM} phantom was first imaged without any of the internal cores removed. This series of 24 scans served as the control or "ideal" patient configuration.

To assess the effects of the same volume of bowel gas at varying distances, the Solid Water^{TM} phantom underwent three additional series of scans. Each series consisted of

24 images at a particular simulated bowel gas core distance. In the first series of 24 images, a 2 cm diameter core located a distance of 8 cm from the vertebral mineral insert (measured at a 45° angle from the edge of the vertebral mineral insert to center of the circular bowel gas core) was removed. This created a 3.14 cm^3 volume of air within but near the periphery of the phantom for imaging.

It was suspected that small volumes of bowel gas at large distances from the vertebral mineral insert would perturb the BMD measurements to some degree; the effect becoming greater as the vertebral bone mineral insert - bowel gas distance became less. In order to test this assumption, another series of 24 images were taken with the outermost simulated bowel gas core reinserted into the phantom and an identical simulated bowel gas core located at a distance of 5 cm (measured as before) removed. The last series of 24 images were made with only one simulated bowel gas core located a distance of 3 cm from the vertebral bone mineral insert removed.

An analogous configuration was used to assess the effects of varying amounts of bowel gas at approximately the same distance from the vertebral mineral insert. Three simulated bowel gas core shells were utilized. The shells provided three simulated bowel gas volumes, 4.91 cm^3, 9.82 cm^3, and 19.63 cm^3. Each shell was centered at a distance of 6.5 cm on a 45° diagonal from the vertebral bone mineral insert.

The series of images taken from the control or "ideal" patient configuration used to assess the effects of the same volume of bowel gas at varying distances from the vertebral mineral insert, were also used as the control images in this procedure. Three additional series consisting of 24 images each were then made. Each series was made with a different bowel gas core volume. By serially removing simulated bowel gas shells, 24 scans were taken at each simulated bowel gas volume of 4.91 cm^3, 9.82 cm^3, and 19.63 cm^3.

Additionally, a "worst case" bowel gas configuration was measured against the control or "ideal" patient configuration as discussed above. This worst case scenario would be an image taken at the level of the transverse colon, the transverse colon being heavily distended with bowel gas. This condition was simulated by removing the "A_2B_2" crescent from the geometric phantom and replacing it with two small wedges of Solid Water^{TM}. This created a large simulated bowel gas volume at the approximate location of the transverse colon. Twenty-four images were obtained using the same procedures and parameters as for the other bowel gas studies.

Reproducibility study

Table 2-9 extracted from Cummings and Black (1986) indicates the confidence interval as a function of degree of reproducibility and number of examinations. As indicated, the degree of confidence placed in measurement values is closely related to the reproducibility obtained. For example, if two sequential measurements made with a scanner having a 2% reproducibility show a average 10% loss in bone mineral, the 95% confidence interval for bone loss would be 10% ± 5.5%. This would represent an actual bone loss within the range of 4.5% to 15.5%.

Table 2-9. Reproducibility as a function of confidence level and number of measurements obtained.

Confidence Level	Number of Measurements	Reproducibility			
		1%	2%	3%	4%
95%	2	±2.8	±5.5	±8.3	±11.1
	3	±1.4	±2.8	±4.2	±5.5
	4	±0.9	±1.8	±2.6	±3.5
90%	2	±2.3	±4.7	±7.0	±9.3
	3	±1.2	±2.3	±3.5	±4.7
	4	±0.7	±1.5	±2.2	±2.9

If the clinician would like to measure the loss in bone mineral using two sequential studies with 95% confidence, the minimal change that he can confidently measure is approximately 2.77 times the reproducibility of the procedure. This fact can be demonstrated by using the confidence interval for a paired t-test which is:

$$\text{Confidence Interval} = \pm\ t_{(a/2)} \times \text{sigma}(\sqrt{(1/n_1+1/n_2)})$$

where $t_{(a/2)}$ is the t-value for 0.025 (95% confidence for a two tailed test), sigma is the sample standard deviation, and n_1 and n_2 are the number of examinations in each sample. If the reproducibility of the technique is assumed to be well established based on many prior measurements so that the DOF is essentially infinite, $t_{(a/2)}$ is 1.96. For two consecutive measurements, n_1 equals 1 and n_2 equals 1.

For the purposes of illustration, assume a 2% reproducibility. In such a case the confidence interval is

$$\pm\ 1.96 \times 2\% \times \sqrt{(1+1)}$$

or

$$\pm\ 1.96 \times 2\% \times 1.414$$

or

$$\pm\ 2.77 \times 2\%$$

which equals 5.5%. Five and a half percent, then, is the minimal change in bone mineral detectable with a QCT technique having a 2% reproducibility.

This places an effective limit on the frequency of sequential examinations. If, for example, the clinician anticipated a maximal bone loss of 5% in one year for a particular patient, it would make little sense to perform a QCT examination on that patient at intervals more frequent than one year since the technique could at best detect only a 5.5% change in bone mineralization. In order to measure more subtle changes without increased dose to the patient, the reproducibility of the technique would need to be improved.

In order to assess the clinical reproducibility of QCT and to determine the minimal detectable change in BMD from two sequential scans, an in-vivo reproducibility study was undertaken. All accredited medical institutions require approval from an institutional review board prior to undertaking any studies involving the use of human subjects. In order to obtain this approval, a research protocol was prepared and submitted. As a first step in developing the research protocol, an estimation of the health risks to the subjects was made. Appendix B contains the research proposal submitted to the Institutional Review Board for approval. The appendix also contains initial dose estimates for the QCT examination as well as a brief description of the procedure.

Subjects for this study were volunteers selected from the Gainesville community. All were postmenopausal or surgically menopausal Caucasian females ranging from 40 to 68 years of age with a mean age of 55.8 years. A total of 21 volunteers were obtained. Each volunteer was informed in writing and counseled verbally as to the purpose, procedures, potential risks, potential benefits, and alternative procedures available for this study (see Appendix B). A consent form for this study was obtained from each participant. Patients were assigned unique study numbers in order to protect the confidentiality of their results.

Each individual was placed in a supine position on the gantry table and scanned using standard procedures for QCT spinal bone mineral determination. The Cann-Genant reference phantom and water bolus was centered under the lower spine of each patient. The patient's knees were elevated to reduce spinal curvature. The sagittal plane of the body was aligned with the center of the scan field by using the laser alignment lights. In each case, a lateral scout scan, encompassing the region of the torso from just below the lungs to the top of the hips (vertebrae T-12 through S-1), was obtained.

Based on the lateral scout images, specific locations for the axial scans were determined. In each case, a total of four axial x-ray scans was taken, each from a different vertebrae in the small of the back. The vertebrae selected ranged from T-12 through L-4. Radiographic technique factors for these scans were designed to minimize radiation exposure. A radiographic technique of 80 kVp, 40 mA, 2 s, and 10 mm slice thickness was utilized whenever possible. In those cases where, in the opinion of the CT technician, the size of the patient required higher technique factors, a technique of 80 kVp, 100 mA, and 2 s was used. Upon completion of the four axial scans, a second lateral scout was obtained in order to verify that the patient had not moved during the course of the study.

Upon completion of the first examination, the patient was allowed to get off the scanning table. After a few moments, the CT technician assisted in repositioning the patient on the scanning table. The scanning protocol was then repeated, using the same procedure as indicated above.

In order to expedite patient handling, two CT technicians were used for this study. The first technician was used solely to position patients on the CT table, the second technician was utilized solely for scanning. Although this trade off was necessary due to time and financial constraints, it was not considered to be significantly different from normal clinical routine since one CT technician will frequently assist another in patient positioning. Further, since a pre-exam lateral scout was performed, the final determination for patient placement rested with the CT technician who would be doing the actual scanning.

Each axial scan as well as the lateral scouts were filmed and stored on tape for archival purposes. Each axial image was analyzed by both CT technicians as well as the author.

Dose assessment

The assessment of patient dose from the QCT procedure involved numerous steps to insure the proper functioning of the dosimetry system and the appropriate calibration of TLD's. Appendix A contains a detailed explanation of the procedures used to insure reliability and accuracy of the dosimetry measurements made during this study.

Soft tissue exposures were converted to units of dose by using the f-factor for water at the appropriate effective beam energies. The dose to mineralized bone was similarly computed. The dose to the red marrow and endosteal tissues were obtained by first converting to dose the measured exposure at the location of trabecular bone using the f-factor for muscle, then applying dose enhancement factors (King and Spiers, 1985) to account for the effects of secondary electrons emitted from the surrounding bone.

Dose to skin and bone

Sections 23 through 33 of Rando Phantom number 145 were utilized for dosimetry measurements. This region encompasses the torso from vertebrae T-11 through the symphysis pubis.

The Rando phantom was placed supine upon the Cann-Genant phantom water bolus combination at a table height of 130 cm. This locates the vertebral body at the center of the scan field and matches the standard QCT protocol. Section 25 of the Rando phantom, which corresponds to vertebra L-1, was used for non-gonadal dosimetry measurements. This section has a circumference of 85 cm, adequately approximating the 75.6 cm average circumference measurement obtained during the cadaveric study at the level of L-1. Section 25 measures 20 cm anteriorly to posteriorly and 27 cm laterally. It has an elliptical ratio of 1.3:1 which suitably approximates the 1.6:1 elliptical ratio of the cadavers used during the study of small changes in longitudinal and angular repositioning.

All TLD chips used were matched in groups of six, each group of six consisting of three sensitivity matched pairs. Each group of chips was wrapped in polyethylene and tagged for identification. One group of six chips was placed in each of four dosimetry sites within section 25 of the Rando phantom (see Figure 2-14). These sites were located

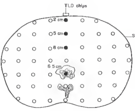

Figure 2-14. Section 25 of Rando phantom indicating sites used for direct axial scanning dosimetry measurements.

anteriorly to posteriorly along the midplane of the phantom torso. The sites were located 2, 5, 8, and 14 cm posterior to the ventral surface of the phantom. The 14 cm location was within the trabecular portion of vertebrae L-1. On the ventral surface of phantom, one matched pair of TLD chips was positioned along the midplane in order to determine skin dose. The pairs of chips used for measurement of skin doses were wrapped in polyethylene and covered by two thicknesses of label paper to prevent non-radiation induced thermoluminescence (NRI-TL) from the fluorescent lighting.

Section 25 of the Rando phantom was positioned on the CT table along with contiguous phantom sections 23 through 33 This provided a minimum of 5 cm of material on each side of section to fully account for scattering effects. The laser alignment beams were used to position the phantom along the midline of section 25, encompassing the surface TLD chips. An axial scan was then taken with technique factors of 140 kVp, 40 mA, 2 s, and a 10 mm slice thickness.

The four groups of six each TLD chips were then removed from the phantom and replaced with four other groups of sensitivity matched chips. The axial scans were repeated at technique factors of 120 kVp and 40 mA for 2 s, 80 kVp and 40 mA for 2 s, and at 80 kVp and 10 mA for 2 s.

The last axial scan was done as a linearity check and as a measure of the lowest technique factor selectable on the GE 9800

From Axial scatter. The measured dose from an axial scan will include the dose received by direct irradiation from the primary beam as well as scattered radiation from adjacent axial scans. The dose contribution from an adjacent axial scan was determined by placing sets of six each sensitivity matched pairs of chips within Rando phantom section 26. These sets of chips were placed at depths of 0 cm, 2 cm, 8 cm, and within the trabecular bone along the vertical midline of the phantom section (see Figure 2-15). All sections of the phantom from 23 through 33 were then reassembled. Section 25, which corresponds to the level of L-1, was irradiated using an axial scan aligned along the midplane of the section with technique factors of 80 kVp, 40 mA, for 2 s and a slice thickness of 10 mm. The TLD chips were removed from the adjacent phantom section (26) and read following the standard pre-anneal and second read post-anneal procedure discussed previously. This procedure was then repeated at technique factors of 140 and 120 kVp, each at 40 mA and 2 s

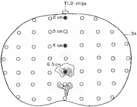

Figure 2-15. Section 25 of Rando phantom indicating sites used for axial scattering dosimetry measurements.

During the standard QCT protocol, the two most extreme vertebrae would receive scattered radiation from the axial scans on only one side. The two most medial vertebrae would, however, receive scattered radiation from axial scans made on both sides. In order to obtain a "worst case" dose estimate, it was assumed that all vertebrae received scattering from both sides. Consequently, the dose contribution from axial scattering was doubled and added to the measured dose of each axial scan directly irradiated.

From Lateral Scouts. Up to this point, the magnitude of measured radiation has not been representative of the QCT procedure since it does not account for the effects of the two lateral scans which are routinely taken. The first lateral scout is used clinically to localize the vertebrae and select positions for axial scanning. The second lateral scan indicates any patient movement occurring during the procedure. Both lateral scout scans are made with technique factors of 120 kVp and 40 mA.

To assess the dose contribution from the lateral scouts, sections 23 through 33 of the Rando phantom were utilized. Here sensitivity matched pairs of chips were used as a two chip set rather than as a six chip set as before. This was possible since, duribg the lateral scout, a large portion of the torso is irradiated uniformly and the effective beam width is not constrained to act only over a 1 cm width of tissue. Consequently, the interception of the x-ray beam by each TLD chip was assured.

One pair of chips was placed at each depth of 2, 5, and 8 cm along the vertical axis of section 25 of the Rando phantom. One pair of chips was placed a depth of 5 cm measured laterally from the phantom surface on the side closest to the x-ray tube head. One pair of chips was placed at a depth of 4.5 cm measured laterally from the phantom surface on the side farthest away from the x-ray tube head. Additionally, pairs of chips were placed at the location of the trabecular bone within the spinal vertebra, on the ventral surface of the phantom and on both lateral surfaces (see Figure 2-16).

Since two lateral scans are routinely performed during the QCT procedure, the dose obtained from the lateral scout scan was doubled. This dose was then added to that of the direct axial scans and axial scattering to get a total dose estimate.

Gonadal dose

To measure the gonadal dose, section 31 of the Rando phantom was used (see Figure 2-17). This section represents a distance approximately midway between the top of the iliac crest and the symphysis pubis. This location has been cited by Properzio (1975) as the anatomic site for

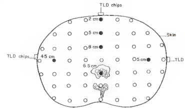

Figure 2-16. Section 25 of Rando phantom indicating sites used for lateral scout dosimetry measurements.

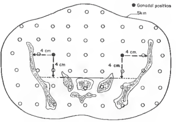

Figure 2-17. Section 31 of the Rando phantom indicating sites used for gonadal measurements

the ovaries. The exact location of the ovaries within this area was chosen based on clinical judgment. The two bilateral locations selected were 4 cm anterior to the sacrum and 4 cm medial to the ilium.

A set of six sensitivity matched TLD chips was placed at each of these two locations. Section 31 was positioned contiguously with all other sections of the phantom and secured to the CT table. To simulate the dose that the gonads would receive from a typical QCT procedure, a total of six scans were made. Two lateral scout scans were obtained with technique factors of 120 kVp and 40 mA. They encompassed the torso from approximately T-11 through all of L-5. This placed the site selected for the gonadal dose measurement approximately 2.5 cm from the ending location of the scout scans. The gonadal dosimetry site was not, therefore, directly irradiated by the scout scans.

To further simulate the QCT protocol, four axial scans were also made at sections of the phantom corresponding to vertebrae L-1 through L-4 (sections 25 through 28). The technique factors used for the axial scans were those used in a standard QCT protocol (see Table 1-1). Since the gonads are not directly irradiated during this procedure either, the dose to the ovaries represents only scattered radiation from other scans

After all scans were completed, the TLD chips were removed from the phantom and read. All chips were preannealed prior to reading in the same manner as discussed previously.

Dosimetry calculations

Since the readings obtained from the TLD chips were calibrated in terms of exposure, it was necessary to convert the TLD readings into units of absorbed dose. This was done by using f-factors, which are proportional to the ratio of the mass absorption coefficients of the medium of interest to that of air. This ratio is then multiplied by 0.00873 rad/R to obtain units of absorbed dose from the amount of exposure measured in roentgens. Once the proper f-factor is determined, the conversion of exposure to absorbed dose becomes a straight forward multiplication of exposure (R) by f-factor (rad/R) to obtain dose (rad) Figure 2-18, taken from Johns and Cunningham (1983), shows the wide variability of the f-factor with energy up to approximately 200 keV.

Since the f-factor varies as a function of effective beam energy over the energy range of interest, the selection of the correct f-factor depends upon the correct determination of the effective energy of the CT x-ray beam.

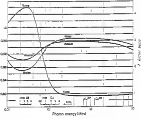

Figure 2-18. F-factor as a function of photon energy for water, muscle, and bone [Reprinted with permission from Charles C Thomas, from The Physics of Radiology, Johns and Cunningham, p 287, Illinois (1983)]

HALF VALUE LAYER AS A FUNCTION
OF EFFECTIVE X-RAY BEAM ENERGY

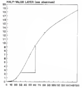

From Table A-4a of Johns and Cunningham

HALF VALUE LAYER AS A FUNCTION
OF EFFECTIVE X-RAY BEAM ENERGY

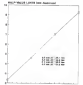

From Table A-4a of Johns and Cunningham

Figure 2-19. HVL as a function of effective x-ray beam energy.

Figure 2-19 is a graph of effective x-ray beam energy as a function of half-value layer. The graph was obtained from data from Table A-4e of Johns and Cunningham (1983).

The measured half-value layers for the CT scanner at a tube potential of 80 kVp ranged from 3.8 mm of aluminum at isocenter to 6 mm of aluminum measured 14 cm away from isocenter for an average HVL of 4.9 mm of aluminum. At 120 kVp the half-value layers ranged from 4.8 at isocenter to 8 mm of aluminum at the decentered position with an average HVL of 6.4 mm of aluminum. Although the HVL at 140 kVp was not measured, a reasonable approximation of the HVL at 140 kVp may be obtained using beam quality data from CFR 1020.30(M). Figure 2-20 taken from CFR 1020.30(M) along with extrapolated CT HVLs shows the change in HVL in millimeters of aluminum as a function of beam energy.

By plotting the HVLs measured at the isocenter for 80 kVp and 120 kVp, the curve is seen to parallel that obtained from CFR 1020.30(M). By extrapolating this isocentric curve parallel to the CFR 1020.30(M) curve to a tube potential of 140 kVp, a reasonable approximation of the CT HVL at 140 kVp is obtained. HVLs for the averaged and decentered values are similarly plotted.

Having obtained HVLs for all tube potentials used during this study, their corresponding effective energy was obtained by interpolation from Table A-4e of Johns and Cunningham (1983). The appropriate f-factor was obtained

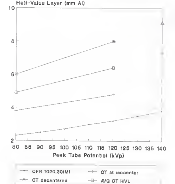

Data extracted from CFR 1020.30 (M)
Dashed lines are extrapolated values

Figure 2-20. HVL versus peak tube potential.

by interpolation from Table A-7 of Johns and Cunningham based on the effective energies for each tube potential. Since soft tissues of the body are composed mostly of water, it was chosen as the medium of interest for all soft tissue dose determinations. The f-factors listed for bone were used for mineralized bone dose determinations.

The application of these f-factors approximates the absorbed dose to the soft tissues of the body, including skin, as well as to bone mineral from the exposures measured at corresponding locations. They are, however, insufficient for assessing the health risks from such QCT exposures. In order to allow inferences to be made regarding health risks, doses to the radiosensitive regions within the bone, specifically the red bone marrow and osteogenic cells, must first be obtained.

The absorbed dose to the red bone marrow and endosteal cells of the bone are obtained using the f-factor for muscle measured at the location of the trabecular bone following the procedure of Wall et al. (1988). Studies by King and Spiers (1985) compared bone marrow doses measured with TLD material both with and without the effects of secondary electrons produced within the bone. Since the range of secondary electrons produced in the bone is extremely small, the polyethylene wrapped TLD chips used in this study were shielded from the secondary electrons and, therefore, do not reflect the actual dose to either red bone marrow or osteogenic cells. Table 2-10 below, taken from Wall et al. (1988) shows the percentage dose enhancement as a result of secondary electrons to bone marrow and to osteogenic tissues at various effective photon energies.

Table 2-10. Percent dose enhancement to bone marrow and endosteal tissues from secondary electrons.

Tissue	Photon Energy (keV) 40	50	60
Bone Marrow	7.0	9.5	8.0
Endosteal Tissue	109.0	130.0	98.0

The percent enhancement to the bone marrow and osteogenic tissues utilized for dosimetry were obtained by interpolation from Table 2-10 above for the effective energies of each technique factor used. These values are tabularized as follows:

Table 2-11. Percentage dose enhancement to bone marrow and endosteal tissues as a function of effective beam energy.

Technique (kVp/mA/s)	Eff. Energy (keV)	Percent Dose Enhancement Bone Marrow	 Endosteum
140/40/2	50.0	9.5	130.0
120/40/2	47.5	8.9	124.8
80/40/2	41.5	7.4	112.2
80/10/2	41.5	7.4	112.2

Dose measurements made at the location of the vertebral trabecular bone were increased by the percentages indicated in order to obtain a red bone marrow and an osteogenic dose. These values were subsequently applied to risk estimates for leukemia and bone cancer respectively.

Dose Reduction Effects on Accuracy

To determine the effects of reducing patient dose on the accuracy of QCT, 35 vertebrae from the nine cadavers used to study small changes in vertebral slice position were imaged. Of these nine cadavers, two were excluded due to vertebral abnormalities. Of the remaining seven cadavers, a series of axial scans were made through the midplane of vertebrae T-12 through L-4. Each vertebral midplane was imaged axially with a 10 mm slice thickness using the following technique factors.

Table 2-12. Technique factors used for dose reduction study

Tube Potential (kVp)	Tube Current (mA)					
140	120	100	70	40	20	
120	120	100	70	40	20	
80	120	100	70	40	20	10

All other scanning factors were identical to those listed in Table 1-1. The average BMD was then determined. The average BMD was taken to be the average BMD of all vertebrae imaged on a particular cadaver at a particular technique factor. The use of these technique factors allowed the assessment of bone mineral density of each vertebra at 16 different doses.

Accuracy and Precision of Single Slice Scanning

To assess the effect on accuracy from reducing the number of axial scans obtained per QCT examination, data from the reproducibility study was used. To obtain information on the ability of a reduced number of vertebrae to accurately predict the overall patient bone mineral density, only the data from the CT technician attaining the highest precision during the reproducibility study was used.

In a longitudinal study, reproducibility is usually of greater concern than overall accuracy. To determine if fewer vertebrae could be imaged during longitudinal studies without a sacrifice in reproducibility, the BMD for a single vertebra taken during the first examination in the reproducibility study was compared against the BMD measured during the second examination. Additionally, the averaged BMDs for the two most extreme and two most medial vertebrae for exam one were compared against their corresponding values for exam two

CHAPTER III
RESULTS

This chapter contains tabularizations of the data obtained for the experimental procedures used to investigate the research objectives listed at the end of Chapter I. Graphic presentations and interpretation of the data are contained in Chapter IV, Discussion.

Field Nonuniformity Effects

Field nonuniformities generate differences in measured BMD values. Changes in table height, patient spinal curvature, and dorsal thickness induce vertical decentering while positioning errors relative to the midline of the gantry table elicit lateral decentering.

Vertical Decentering

The measured BMD values obtained as a result of vertically decentering the CIRS phantom by raising and lowering the gantry table is shown in Table 3-1. Each BMD shown represents an average of four scans. The percent change is relative to 50 mg/cc. The BMD values range from 50 to 61 mg/cc (-1% to +22%).

Table 3-1. BMD and percent change as a function of vertical decentering.

Table Position (mm)	BMD (mg/cc)	Percent Change
190	61.23	22
180	62.32	25
170	62.51	25
160	61.19	22
150	60.19	20
140	59.79	20
130	58.35	17
120	56.66	13
110	55.52	11
100	54.38	9
90	54.71	9
80	51.71	3
70	49.56	-1

The results of vertical decentering the CIRS phantom obtained while maintaining a constant table height is shown in Table 3-2. The results are an average of six scans. The percent change is relative to the BMD value obtained with the vertebral insert positioned at the scan field isocenter. The BMD values range from 54 mg/cc at isocenter to 51 mg/cc (-5.7%) measured at a vertical off-set of 7.6 cm.

Table 3-2. BMD and percent change as a function of phantom vertical decentering.

Centimeters Decentered Vertically	BMD (mg/cc)	Percent Change
0.00	53.97	0.0
0.65	53.52	-0.1
1.31	53.96	0.0
2.06	53.58	-0.7
3.00	53.71	-0.4
3.84	53.63	-0.6
4.78	52.75	-2.2
5.90	51.57	-4.4
6.65	51.25	-5.0
7.59	50.88	-5.7

Lateral Decentering

The results of laterally decentering the CIRS phantom obtained while maintaining a constant table height is shown in Table 3-3. The results are an average of six scans. The percent change is relative to the BMD value obtained at the scan field isocenter. The BMD values range from 57.5 mg/cc at isocenter to 53.7 (-6.5%) when laterally decentered 5.2 cm.

Table 3-3. BMD and percent change as a function of phantom lateral decentering

Centimeters Decentered Laterally	BMD (mg/cc)	Percent Change
-5.00	54.48	-5.18
-4.12	55.17	-3.98
-3.37	55.35	-3.66
-1.87	57.37	-0.15
0.00	57.46	0.00
1.59	57.36	-0.16
3.09	57.11	-0.61
4.21	55.35	-3.67
5.15	53.72	-6.51

Patient Geometry

The results of the investigation into the effects of changes in patient geometry on QCT are shown in Table 3-4. As indicated, the average measured BMD decreases with increasing geometric ratio from 59.0 mg/cc at 1:1 to 57.0 mg/cc (-3.5%) at 1.6:1. The variability of the measurements also decreases with increasing geometric ratio with a standard deviation of 1.3 mg/cc at 1:1 to 0.65 mg/cc (-50%) at 1.6:1.

Table 3-4. Statistics for patient geometric effects.

	Elliptical Ratio		
	1:1	1.3:1	1.6:1
Number of Observations	25.00	25.00	25.00
Mean	59.03	58.12	56.96
Median	58.88	58.11	57.12
Standard Deviation	1.31	0.99	0.65
Variance	1.71	0.97	0.42
Maximum	61.56	60.69	58.14
Minimum	56.41	56.69	55.50
Range	5.15	4.00	2.64

Patient Size Effects

The results of the investigation into the effects of changes in patient size are shown in Table 3-5. The mean BMD values measured at each phantom circumference were well within one standard deviation of one another and varied less than 0.5 mg/cc (~0.8%) among circumferences ranging from 80 cm to 106 cm. Variability as indicated by the standard deviation, increases with increasing phantom size from a low of 0.97 mg/cc at 80 cm to a high of 1.66 mg/cc at 106 cm.

Table 3-5 Statistics for patient size effects.

	Circumference (cm)		
	80	96	106
Number of Observations	24.00	24.00	24.00
Mean	57.72	57.73	57.24
Standard Deviation	0.97	1.01	1.66
Variance	0.95	1.01	2.77
Maximum	59.59	59.90	60.69
Minimum	55.53	55.89	54.33
Range	4.06	4.01	6.36

Air Gap Effects

The results of varying air gaps on QCT precision are tabularized in Table 3-6 below. The results are an average of two scans and show the percent change in measured BMD relative to the BMD value obtained with no air gap. The measurements were made at a tube potential of 80 kVp with a 2 s scan time.

Table 3-6. Percent change in measured BMD as a function of air gap size and radiographic technique.

Percentage change in BMD from 0 air gap value at 80 kVp				
Air Gap Size (cm)	Technique Factor (mAs)			
	240	200	140	80
0.00	0.00	0.00	0.00	0.00
0.56	0.16	1.70	1.19	4.31
1.12	3.57	4.41	4.25	6.71
2.25	3.59	5.02	3.51	6.70
3.09	7.39	9.01	6.78	10.15
4.22	14.14	18.46	17.93	18.24
5.71	29.31	28.42	24.57	29.72

Longitudinal Slice Off-Set

The results obtained on the effects of small changes in slice vertebral off-set are shown in Table 3-7. The values are based on multiple axial scans of 19 vertebrae. The percent change is given relative to the BMD measured at the vertebral midplane. As indicated, the percentage of vertebrae showing a given amount of change in BMD relative to the midplane value decreases with increasing distance from the vertebral midplane. Within 2 mm of the midplane, nearly 74% of the vertebrae showed less than or equal to a 4% change, while 92% showed less than a 10% change in measured BMD. At ±4 mm, these percentages dropped to 50 and 76% respectively. At a longitudinal off-set of ±6 mm, the percentage of imaged vertebrae that showed an absolute percent change in measured BMD of ≤4% has decreased to approximately 40% and those showing ≤10% change decreased to 50%.

Table 3-7. Percent change in BMD as a function of longitudinal slice off-set.

Percent change in BMD compared to midplane BMD value	Percentage of scans that showed indicated amount of change		
	At ± 2 mm	At ± 4 mm	At ± 6 mm
0	2.6	0	0
≤2	57.9	31.6	15.8
≤3	65.8	47.4	36.8
≤4	73.7	50.0	39.5
≤5	81.6	52.6	44.7
≤6	81.6	65.8	47.4
≤7	84.2	71.1	47.4
≤8	89.5	76.3	50.0
≤9	89.5	76.3	50.0
≤10	92.1	76.3	50.0

Gantry Angular Positioning

The results obtained on the effects of small changes in slice vertebral angle are tabularized below. The values are based on multiple axial scans of 19 vertebrae. The percent change is given relative to the BMD measured at the vertebral midplane with angulation parallel to the vertebral endplates.

Within 2° of the midplane, nearly 92% of the vertebrae showed less than or equal to a 4% change, while all showed less than a 10% change in measured BMD. At ±4°, these percentages decreased to 83 and 94% respectively. At an angular off-set of ±6°, the percentage of imaged vertebrae that showed an absolute percent change in measured BMD of ≤4% has decreased to approximately 67% and those showing ≤10% change decreased to 81%.

Table 3-8. Effect of gantry angulation on QCT precision.

Percent change in BMD compared to midplane BMD value	Percentage of scans that showed indicated amount of change		
	±2 degrees	±4 degrees	±6 degrees
0	0.0	0.0	0.0
≤2	61.1	55.6	44.4
≤3	77.8	72.2	52.8
≤4	91.7	83.3	66.7
≤5	97.2	83.3	77.8
≤6	97.2	86.1	77.8
≤7	97.2	88.9	77.8
≤8	100.0	91.7	77.8
≤9	100.0	91.7	77.8
≤10	100.0	94.4	81.1

Aortic Calcification Effects

The measured BMD for the aortic calcification phantom as measured with and without the presence of aortic calcifications is tabulated in Table 3-9. The values are based on two sets of 24 measurements each. BMD values vary over a range of 4.9 mg/cc and 3.4 mg/cc respectively for the phantom configured without and with aortic calcifications. As indicated, the mean BMD for the two phantom configurations show very little difference, varying less than 0.3%.

Table 3-9. BMD values (mg/cc) measured with and without aortic calcifications

	Without Calcifications	With Calcifications
Number of Observations	24.00	24.00
Mean	58.18	58.33
Standard Deviation	1.17	0.93
Variance	1.37	0.87
Maximum	60.56	60.52
Minimum	55.68	57.13
Range	4.88	3.39

Simulated Bowel Gas

The effect on measured BMD values of a constant volume of simulated bowel gas at various distances from the vertebral mineralization insert are tabularized below. The values are based on a series of 24 scans at each phantom configuration. The mean BMD values varied from a low of 58.2 mg/cc with no simulated bowel gas to a high of 58.9 mg/cc (1.2%) with simulated bowel gas in the middle core.

Table 3-10. The effects on measured BMD of a constant volume of bowel gas at varying distances.

INSERT REMOVED	MEAN	STD. DEVIATION	NUMBER OF IMAGES
NONE	58.18	1.17	24
OUTERMOST	58.63	1.22	24
MIDDLE	58.91	1.09	24
INNERMOST	58.00	1.47	24

An analysis of variance indicates an F-value of 2.6. At a 95% confidence level, this reflects a non-significant difference among the mean BMD values.

Table 3-11. Analysis of variance on constant volume bowel gas effects.

EFFECT	SS	DOF	MS	F	PROBABILITY
BETWEEN	12.258	3	4.086	2.632	.054
WITHIN	142.804	92	1.552		

The results for the effect of varying volumes of simulated bowel gas at approximately the same distance from the vertebral mineralization insert are tabularized below. The values are based on a series of 24 scans at each phantom configuration. The mean BMD values varied from a low of 57.7 mg/cc with the middle and inner ring removed to a high of 58.3 mg/cc (-0.1%) with only the innermost ring removed.

Table 3-12 Effects of varying volumes of bowel gas on measured BMD at a constant distance.

RING REMOVED	MEAN	STD. DEVIATION	NUMBER OF IMAGES
NONE	58.1842	1.17198	24
INNERMOST	58.3054	1.08723	24
INNER+MIDDLE	57.7458	1.09408	24
ALL	57.9550	1.05106	24

An analysis of variance of the data shown in Table 3-15 indicates an F-value of 1.2. At a 95% confidence level, this reflects a non-significant difference among the mean BMD values.

Table 3-13. Analysis of variance for effects of varying volumes of bowel gas at constant distance on measured BMD.

EFFECT	SS	DOF	MS	F	PROBABILITY
BETWEEN	4.434	3	1.478	1.216	0.308
WITHIN	111.785	92	1.215		

The results for the effect of a large volume of simulated bowel gas at the approximate position of the transverse colon on measured BMD is shown in Table 3-14. The mean of two sets of 24 measurements varied from 58.2 mg/cc with no inserts removed to 58.5 mg/cc (-0.5%) with gas present in the simulated transverse colon. A paired t-test conducted on the transverse colon data had a t-value of -0.927 (36.65% probability) showing no significant difference between measurements made with or without simulated bowel gas present in the transverse colon.

Table 3-14. Statistics on the effects on measured BMD of simulated bowel gas in the transverse colon.

INSERT REMOVED	MEAN	STD. DEVIATION	NUMBER OF IMAGES
NONE	58.18	1.17	24
TRANSVERSE	58.47	1.29	24

Reproducibility Study

Of the 21 subjects volunteering for this study, two were excluded. One individual revealed upon questioning that she was peri-menopausal. Additionally, the lateral scout exam indicated moderate scoliosis of the spine. Her results were excluded on these bases. The other individual was so extremely obese that her size introduced ring artifacts even at higher than normal technique factors. These ladies were counseled regarding the limitations on the accuracy of their results and elected to have an examination. In these cases, only one examination was performed, the results of which were provided to the patient but not used for the purposes of this study.

The measured bone mineral densities obtained by the CT technician performing the scans were used in reporting the results to the patients. The average of vertebral

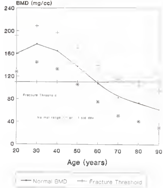

Dashed lines indicate normal range
of + or - 1 standard deviation

Figure 3-1. Age matched bone mineral density values for females.

densities for both exams was used as the reported value. The results of the study were communicated to the patient by letter and included a graph of their measured bone mineral densities as compared to age matched normals. An example of one such graph is shown as Figure 3-1.

Of primary interest to this research is the degree of reproducibility obtained between the two examinations performed on each patient. The results of the bone mineral analysis for all patients by each technician and the author is shown in Table 3-15. These results are a comparison of the overall patient bone mineral density for the first QCT examination regressed against those from the second QCT examination for the 18 patients imaged. The overall patient bone mineral density is the average value of all vertebrae measured for that patient.

All analyses showed a high degree of correlation from the first examination to the second with an R^2 of 0.99. The reproducibility is taken to be the value of the standard error divided by the average BMD. The reproducibilities obtained range from 1.3% to 2.9%.

Table 3-15 Regression output by QCT analyst.

Regression Data	Analysis by CT Tech 1	by Author	Analysis by CT tech 2
Constant	0.00	0.00	0.00
Std. Error	1.53	2.68	3.53
R squared	0.997	0.991	0.986
# of Patients	18	18	18
Degrees of Freedom	17	17	17
X coefficient	0.998	1.005	1.006
Std Error of Coefficient	0.003	0.005	0.006
Average BMD (mg/cc)	120.5	121.0	122.3
Reproducibility (%)	1.3	2.2	2.9

Dose Assessment

This section tabularizes the results of the dosimetry research. It specifies the dose to radiosensitive tissues of the body irradiated directly or by scattered radiation during the QCT examination. The dose contribution is indicated as resulting from direct axial scanning, axial scattering, and lateral scout examinations where ever possible.

Dose to Skin and Bone

The skin dose is taken to be the dose measured by the TLDs located on the surface of the Rando phantom. The dose to other soft tissues are indicated by their respective depths in cm from the skin surface. The bone dose is categorized according to dose to mineralized bone, bone marrow, and endosteum.

Dose from direct axial scanning

The dose in millirads from a single axial scan to skin, bone, bone marrow, endosteum, and soft tissue is shown in Table 3-16. The dose to all radiosensitive tissues is strongly dependent on the tube potential selected for the examination. The increase in dose from selecting a technique of 120 kVp and 40 mA over 80 kVp and 40 mA is on the order of 300% for all radiosensitive tissues.

Table 3-16. Dose (mrad) from single axial scan to skin, mineralized bone, bone marrow, endosteum, and soft tissue.

DOSE FROM SINGLE AXIAL SCAN

Technique	Location						
(kVp/mA/s)	Skin	2 cm	5 cm	8 cm	Bone	Endosteum	Marrow
140/40/2	769	626	411	298	916	534	254
120/40/2	580	459	283	202	592	323	157
80/40/2	182	152	101	62	173	82	41
80/10/2	56	40	26	16	48	23	11

Dose from axial scattering

Table 3-17 below tabularizes the dose contribution from scattered radiation from adjacent axial scans. The doses reported assume that each axial slice receives scattered radiation from two adjacent axials and therefore represents a worst case estimate of axial scattering. The dose reported at a depth of 5 cm was interpolated from the doses measured at 2 and 8 cm.

Table 3-17 Dose contribution (mrad) from axial scattering.

Technique	Location						
(kVp/mA/s)	Skin	2 cm	5 cm	8 cm	Bone	Osteoblasts	Marrow
140/40/2	54	91	95	100	242	141	67
120/40/2	40	63	67	71	165	90	43
80/40/2	17	30	33	36	97	46	23
80/10/2	4	7	8	9	24	11	6

Dose from Lateral Scouts

The dose contribution from the two lateral scout scans are tabularized in Table 3-18. The dose contribution is based on the sum of two lateral scout exams in keeping with the normal QCT procedure. The doses shown are measured along the vertical midplane of the phantom. Additionally the dose to skin as measured from the side of the phantom proximal to the x-ray tube head is shown.

Table 3-18. Dose contribution from two lateral scouts at 120 kVp and 40 mA.

Technique	Phantom Location or depth (cm)						
Along Midplane							Lateral
Skin	2 cm	5 cm	8 cm	Bone	Osteoblast	Marrow	Proximal Skin
11	4	9	10	61	33	16	72

Total Dose

The total dose from direct axial scanning, axial scattering, and lateral scout scans as a function of technique factor used is summarized in Table 3-19 below. The dose sparing with decreasing technique is less than that shown previously for direct axial scanning and reflects the constancy of the two lateral scout exams. The technique used for the two lateral scout exams was not changed even though the technique factors for the axial scans were modified. This fact moderates the dose sparing that would otherwise have occurred at decreased techniques.

Table 3-19. Total dose (mrad) from one QCT examination.

Technique	Phantom Location or depth (cm)						
(kVp/mA/s)	Skin	2 cm	5 cm	8 cm	Bone	Osteoblast	Marrow
140/40/2	895	721	515	408	1219	708	338
120/40/2	692	526	359	263	818	447	216
80/40/2	271	186	143	108	331	160	81
80/10/2	133	51	43	35	133	67	33

The percent contributions to the total dose from axial scans, axial scattering, and lateral scout scans are tabulated in Table 3-20. Due to rounding errors, dose contributions may not sum to 100%. As indicated, the majority of the dose is attributable to direct axial scanning and axial scattering. The percent contribution from the lateral scout exams is more pronounced at lower technique factors.

Table 3-20 Percent of total dose from direct axial scans, axial scattering, and lateral scout exams at various locations

	Percent of Total Dose Location or depth (cm)						
Procedure	Skin	2 cm	5 cm	8 cm	Bone	Endosteum	Marrow
140 kVp/40 mA							
Axial Scan	86	87	80	73	75	75	75
Axial Scatter	6	13	19	25	20	20	20
Lateral Scouts	8	1	2	3	5	5	5
120 kVp/40 mA							
Axial Scan	84	87	79	71	72	72	72
Axial Scatter	6	12	19	25	20	20	20
Lateral Scouts	10	1	3	4	7	7	7
80 kVp/40 mA							
Axial Scan	67	82	71	57	52	51	51
Axial Scatter	6	16	23	33	29	29	29
Lateral Scouts	27	2	6	9	18	20	20
80 kVp/10 mA							
Axial Scan	43	78	60	46	36	35	34
Axial Scatter	3	14	19	26	18	17	17
Lateral Scouts	54	8	21	29	46	49	49

Gonadal Dose

During the QCT procedure, the gonads are not normally directly irradiated by either axial or lateral scans. The axial scans are taken at too great a distance to contribute significantly to the gonadal dose. The two lateral scouts, since they include the top of the sacrum and iliac crest, do contribute scattered radiation to the gonads. The gonadal dose contribution from two lateral scout exams are shown in Table 3-21.

Table 3-21. Gonadal dose contribution from two lateral scouts exams.

	GONADAL DOSE CONTRIBUTION FROM 2 LATERAL SCOUTS (mrad)	
	Location	
Technique (kVp/mA)	Proximal ovary	Distal ovary
120/40	11.5	10.1

Dose Reduction Effects on Accuracy

The average BMD results, tabularized by patient and imaging technique used, are listed in Table 3-22. The results show excellent consistency at all tube currents for 140 and 120 kVp. At 80 kVp, measured BMD values show a small (1 mg/cc) increase when the tube current is decreased from 20 mA to 10 mA.

Table 3-22 Average patient BMD (mg/cc) at various imaging technique factors.

TECHNIQUE		AVERAGE BMD FOR THE PATIENT NUMBER SPECIFIED						
KVP	MA	5468	5472	5494	5513	5513	5563	5571
140	20	79.17	75.33	54.73	77.94	71.18	102.61	50.74
140	40	78.77	75.11	54.14	78.46	72.12	102.68	50.59
140	70	79.41	74.66	55.05	79.04	72.11	102.28	51.50
140	100	79.27	75.41	55.09	78.16	72.54	102.64	51.50
140	120	79.51	75.18	54.23	78.16	71.71	101.41	51.18
120	20	79.09	75.76	56.34	78.50	71.47	101.31	52.20
120	40	79.61	75.47	54.66	78.74	71.49	102.50	51.59
120	70	79.13	75.41	54.59	78.85	70.92	102.24	52.48
120	100	79.15	75.31	54.55	78.73	71.06	101.76	52.42
120	120	78.95	75.19	55.03	78.26	70.83	102.08	51.92
80	10	85.13	78.42	60.50	81.55	73.73	108.56	57.68
80	20	83.50	77.86	57.80	82.08	74.08	106.34	55.30
80	40	82.72	77.10	59.34	82.37	74.24	103.59	54.88
80	70	82.21	76.91	58.48	82.22	72.77	103.33	55.88
80	100	81.81	76.63	58.25	81.10	73.30	103.80	54.84
80	120	81.94	76.36	58.79	82.17	73.56	103.22	54.30

Accuracy and Precision of Single Slice Scanning

The ability of a reduced number of vertebrae to predict the overall average BMD was determined by regressing the vertebrae against the overall average patient BMD. The degree to which the vertebrae match the overall average patient BMD is reflected in the dispersion about the regression curve. The standard errors for different combinations of vertebrae when regressed against the average patient BMD is tabulated below.

Table 3-23. Standard errors of vertebral BMD values regressed against overall patient BMD.

Vertebrae/Vertebral Combination	Standard Error
T-12	6.25
L-1	6.32
L-2	5.32
L-3	3.56
L-4	9.51
L-1 + L-2	4.86
L-2 + L-3	3.72
Most Extreme Vertebrae	3.71

The reproducibility of a reduced number of vertebrae was determined by regressing the vertebrae in examination number one against the same vertebrae for examination number two. The standard error divided by the average BMD for those vertebrae is one measure of reproducibility. The reproducibility for different combinations of vertebrae when regressed for exam one against exam two is tabulated below:

Table 3-24. Reproducibility of vertebrae for exam one regressed against exam two

Vertebrae/Vertebral Combination	Reproducibility (%)
T-12	2.22
L-1	1.78
L-2	1.85
L-3	1.76
L-4	3.32
L-2 + L-3	1.30
Most Extreme Vertebrae	1.40

CHAPTER IV
DISCUSSION

This chapter discusses the results for each research objective presented in Chapter I. Graphic presentations of tabularized numerical data presented in Chapter III are also provided. Conclusions and recommendations based on these findings will be presented in Chapter V.

Field Nonuniformity Effects

The effects on measured BMD values due to field nonuniformities are discussed in terms of vertical decentering and lateral decentering. The clinical impact of such nonuniformities is also assessed.

Vertical Decentering

The effects of vertical decentering were assessed both at constant table position with varying distances between the CIRS and Cann-Genant phantoms and at a constant CIRS-Cann-Genant phantom distance with varying table positions. Figure 4-1 shows the field nonuniformity effects resulting from variations in vertical positioning of the gantry table within the scan field. Table position values indicate the distance of the gantry table from the isocenter of the scan field. Since the table is restricted to positions below

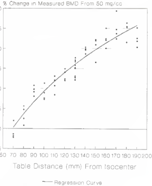

Figure 4-1. Change in measured BMD as a function of vertical table position within the scan field.

scan field isocenter, all values are positive. Larger position values indicate that the gantry table is being lowered while smaller numbers indicate that the table is being raised closer to the scan field isocenter.

As indicated, measured BMD increases approximately 25% (13 mg/cc) as the scan field isocenter to table top distance increases from 70 mm to 190 mm. Although this percent change is very large, its clinical significance for those institutions using a specified table height for QCT is minimal. The large percent change in measured BMD values does, however, underscore the importance of calibrating and maintaining a constant table position when performing QCT.

Of more import clinically, is the effect of patient vertical decentering at one table height. This vertical decentering is determined by the patient's spinal curvature, dorsal thickness, and the thickness of the water bolus. The technician may exert limited control over the magnitude of vertical decentering by using a knee elevating pad to reduce the patient's spinal curvature.

Figure 4-2 shows the percent change in measured BMD as a function of vertically decentering the phantom above isocenter while maintaining a constant table height. The results show a relative plateau in measured BMD values from the isocenter vertically to a height of approximately 4 cm. In this range, measured BMDs vary by less than 1% from

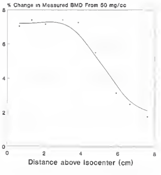

Figure 4-2. Percent change in measured BMD at a constant table height as a function of vertical decentering above isocenter.

those measured at isocenter and are about 7% higher than true BMD. Above 4 cm, the percent change from true BMD decreases rapidly, approaching 2% at 8 cm above isocenter. In the range of 4 cm to 8 cm above isocenter, measured BMD values vary by about 5%.

Where high precision is important, such as in longitudinal studies, maintaining the patient spine within the 0 to 4 cm plateau range will introduce less than 1% variability. To prevent increased measurement variability and degraded precision, the technologist should make every effort to prevent patient spinal position from exceeding this range.

Lateral Decentering

Figure 4-3 shows the percent change in measured BMD as a result of lateral decentering at a constant gantry table height. As indicated, the percent change in measured BMD relative to the BMD measured isocentrically, decreases as the phantom is moved laterally in either direction. The rate of decrease is relatively minor (less than 2%) out to a distance of approximately 4 cm. At distances greater than 4 cm, the rate of decrease in measured BMD values increases, reaching approximately 7% at a decentered position of about 5 cm.

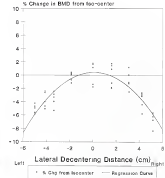

Figure 4-3 Percent change in measured BMD as a function of lateral decentering at a constant table height.

Although changes in measured BMD resulting from lateral decentering are as great as those from vertical decentering, the clinical significance of lateral decentering is much less. This is because lateral decentering, unlike vertical decentering, can be completely controlled by the technician. Further, laser alignment lights assist the technician in precise lateral repositioning of the patient. Using the data from the reproducibility study, the average scan was laterally decentered only 0.6 cm. The maximum decentering that occurred was 1.68 cm. Accordingly, all scans obtained would be expected to vary by less than 1% of the isocentric value as a result of lateral decentering alone. These data confirm the reduced clinical importance of lateral decentering.

Patient Geometry

To compare the significance of the differences between the means of bone mineral density measurements taken at different phantom geometries, an analysis of variance was performed. As can be seen from Table 4-1, a significant difference exists among the mean bone mineral density values obtained from the three varying geometries. The F-value derived is 26.29, which is highly significant with a probability of less than 10^{-6}.

Table 4-1. Analysis of variance for patient geometric effects.

	ANALYSIS OF VARIANCE				
EFFECT	SS	DOF	MS	F	PROBABILITY
BETWEEN	54.21	2	27.11	26.29	$<10^{-6}$
WITHIN	74.22	72	1.03		

Pair-wise comparisons of the means of each phantom geometry was accomplished by using paired t-tests and applying the Bonferroni correction for multiple comparisons. The t-statistics for this intracomparison are shown in Table 4-2.

Table 4-2. Pair-wise comparisons of the means for the geometric phantom configurations.

	Compared to		
Geometric Ratio	Geometric Ratio	t-value	Probability
1:1	1.3:1	2.67	0.01346
1:1	1.6:1	7.41	0.000001
1.3:1	1.6:1	4.84	0.000062

As can be seen from the table, the t-value of the 1:1 elliptical geometry when compared with the 1.3:1 geometry is 2.67. This value equates to a probability of 0.013 which exceeds the 0.05 rejection region even after applying the Bonferroni correction of $a = 0.02$. It therefore indicates a significant difference between the means of these two geometries.

The t-statistic determined from the 1:1 elliptical geometry compared against the 1.6:1 elliptical geometry yields a value of 7.41 which is significant at the 99% confidence level. Similarly, the t-statistic between the 1.3:1 and 1.6:1 geometries yield a value of 4.84 which is also significant at the 99% confidence level.

While the differences among the patient geometries is statistically significant, the clinical significance of an approximate 2 mg/cc (3%) change is not great from the standpoint of accuracy. Since normal patient variability is on the order of ± 30 mg/cc, the significance of a change in accuracy of 2 mg/cc is slight. This is not true, however, from the standpoint of reproducibility. Geometric changes may occur over time as the result of diet, disease, or kyphosis resulting from osteoporosis. Such changes could significantly degrade precision.

It is interesting to note that the most accurate BMD measurement was obtained at the 1.6:1 geometric ratio. The reason for this is unclear, but may have to do with the fact that the flattened elliptical geometry more closely approximates the shape of the Cenn-Genant phantom, allowing the patient closer proximity to the Cenn-Genant phantom bone mineral equivalent tubes. This may reduce the effects of field nonuniformities in the vertical direction and allow the mineralization tubes exposure similar to that of the patient in the lateral direction. Additionally, the flattened geometry shows less air gap at the lateral margins of the phantom when compared to the circular geometry, presenting fewer nonuniformities.

Patient Size Effects

To compare the significance of the differences between the means of bone mineral density measurements taken at different phantom sizes, an analysis of variance was performed. As can be seen from the ANOVA (Table 4-3) very little of the variability between the means can be accounted for by the effects of phantom size. The F-value derived is only 1.123 which is non-significant at the 95% confidence level.

Table 4-3. Analysis of variance for patient size effects data.

	ANALYSIS OF VARIANCE				
EFFECT	SS	DOF	MS	F	PROBABILITY
BETWEEN	3.698	2	1.849	1.123	NS
WITHIN	113.614	46	1.646		

A comparison of the variance between the three sizes of phantom was accomplished by using the F-statistic. This statistic is formed by the ratio of the two sample variances. The numerator and denominator degrees of freedom are both equal to one less than the number of images within each sample. The F-statistics for comparison of the variances in BMD measurements made with the various size phantoms are shown in Table 4-4.

Table 4-4. Comparison of variances of BMD measurements for different phantom sizes (circumference).

	Compared to		
Circumference	Circumference	F-value	Significant at α=0.05
80	96	1.07	Not Significant
80	106	2.92	Significant
96	106	2.73	Significant

As can be seen from the table, the ratio of the variances between the 80 cm circumference phantom and the 96 cm circumference phantom is very small and almost equal to unity. It's value of 1.068 falls short of the rejection region value of 2.02 and therefore does not indicate that a significant difference exists between the variances of these two samples.

The ratio of variances between the 80 cm and 106 cm circumference phantoms yield a value of 2.918 which is significant at the 95% confidence level. Similarly, the ratio of the variances between the 96 cm and 106 cm circumference phantoms yield a value of 2.73 which is also significant at the 95% confidence level.

Air Gap Effects

As shown in Figure 4-4, all techniques show essentially the same pattern of increasing percent change in measured BMD with increasing air gap size. When grouped by tube potential, scans made at lower mAs settings tend to show larger percent changes than scans made at higher mAs values. Whether this may be entirely accounted for by quantum effects is unclear. In all groups, after an initial rise of approximately 5% for a 1 cm air gap, the percent change plateaus at approximately 5% for air gap sizes between 1 and 2.5 cm, then rises steadily at air gaps

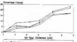

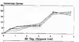

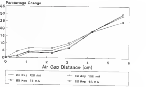

Figure 4-4. Percent change in measured BMD as a function of air gap size with a 2 s scan time at various kVps and mA values.

distances greater than 2.5 cm. In some cases, a 4% to 5% change in measured BMD was obtained at air gap distances as small as 0.5 cm.

This finding has marked clinical significance, especially in light of the high variability in air gap distances occurring during QCT. In the reproducibility study, for example, no patient showed a zero air gap distance on any axial scan. The average air gap distance, measured directly below the spine, was 1.45 cm with a maximum air gap of 3.28 cm. Similarly, no patient showed a zero air gap distance when measured from the lateral dorsal surface, the minimum air gap distance measured was 0.46 cm. When air gap measurements were measured from the lateral dorsal surface, the average air gap distance was 1.03 cm with a maximum air gap of 2.53 cm.

Perhaps more importantly, the average difference in air gap distance measured during the first and second examinations, was 0.35 cm measured directly below the spine and 0.31 cm when measured from the lateral dorsal surface. This degree of variability in air gap distance, which can be expected to occur during the course of a longitudinal study, has the potential for degrading reproducibility by introducing substantial variability into measured BMD values. These results emphasize the need to eliminate air gaps and point out the inadequacy of the conventional saline bag used as a water bolus to do so.

Longitudinal Slice Off-Set

Measured BMD was expected to change slowly with increasing distance from the vertebral midplane. Such a finding would indicate that small changes in longitudinal slice off-set would not significantly reduce QCT reproducibility. This was found to be true in about 80% of the vertebrae scanned.

Figure 4-5 shows one such typical case in the L-2 through L-4 vertebrae on one cadaver. The data, plotted as percent change in measured BMD relative to the midplane BMD against longitudinal off-set distance, show that within ±4 mm of the vertebral midplane measured BMD did not vary appreciably. At distances greater than ±6 mm, measured BMD began to depart more rapidly from midplane values.

Given the initial expectation, it was surprising to find that in 4 of the 35 vertebrae imaged within ±2 mm of the midplane, measured BMD varied by nearly 10% of the midplane value. Figure 4-6 shows vertebrae L-2 and L-3 from one such cadaver. Variability on the order of a 15% change in BMD relative to the midplane was noted within 4 mm of the vertebral midplane in some cases. This high degree of variability in approximately 20% of the vertebrae imaged indicates that small changes in longitudinal slice off-set can have an important influence on QCT reproducibility.

Gantry Angular Positioning

It is clear that changes in gantry angulation on the order of ± 4° do not adversely affect measured BMD relative to the midplane value in most cases. Within this range of angulation, over 80% of the scans varied by less than 4% of the midplane value. This fact should allow for more flexibility in clinical judgment when considering the need to repeat the QCT procedure based on small changes in gantry angulation. The quantification of the magnitude of impact of changes in gantry angulation on clinical reproducibility should aid the clinician in determining how tightly these factors must be controlled and when changes in these factors warrant repetition of the QCT procedure.

Aortic Calcifications

A statistical analysis of the data indicates a mean bone mineral density of 58.2 mg/cc and a standard deviation of 1.19 mg/cc for the phantom configured without aortic calcifications. With the two aortic calcification rings inserted, the mean bone mineral density was 58.3 mg/cc with a standard deviation of 0.93 mg/cc. The average bone

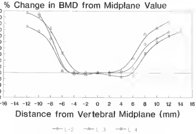

Figure 4-5. Percent change in BMD relative to the midplane as a function of longitudinal slice position for cadaver one.

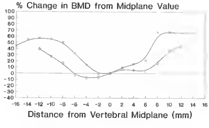

Figure 4-6. Percent change in BMD relative to the midplane as a function of longitudinal slice position for cadaver two

mineral densities measured with and without calcifications varied by less than 0.2%. A paired t-test of the data with 23 degrees of freedom yielded a t-value of 0.3 with a two tailed probability of 0.77. This indicates that the means of the distribution of measurements with and without aortic calcification rings are not significantly different.

Aortic calcifications as thick as 2 mm and as dense as 100 mg/cc of bone mineral equivalent material do not adversely affect the accuracy of vertebral BMD measurement. This is an important outcome since it verifies the insensitivity of QCT to extra-osseous arterial calcifications which are known to adversely effect other methods of bone densitometry

Simulated Bowel Gas

As indicated in the results of BMD measurements taken from a constant volume of simulated bowel gas at varying distances from the vertebral mineral insert, the average measured bone mineral density changed by less than 1 mg/cc regardless of defect (hole) to vertebral insert distance. Interestingly, the difference in measured BMD between the phantom with no defect compared to the phantom with the innermost insert removed (which would be expected to show the greatest impact on measured BMD) showed only a 0.2 mg/cc change. The analysis of variance shows no significant difference among the four constant volume simulated bowel gas phantom configurations at the 95% confidence level.

The results of varying volumes of simulated bowel gas at approximately the same distance from the mineral insert again show less than 1 mg/cc change in measured BMD. This is reflected in the analysis of variance which with a F-value of 1.216 indicating no significant difference in measured BMD among the various simulated bowel gas volume configurations.

The mean measured BMD changed minimally when the large transverse colon insert was compared to the unmodified phantom configuration. The net change was less than 0.5 mg/cc. A paired t-test showed no significant difference in measured BMD between these two phantom configurations.

Reproducibility Study

If perfect reproducibility existed from one examination to the next for a set of patients, a plot of overall BMD for the first examination versus overall BMD for the second examination would show a regression without error. In the regression of average patient BMD for exam one plotted against the average BMD for exam two by each QCT analyst, the dispersion of data points about the regression line is indicative of the lack of reproducibility of the technique. Figures 4-7, 4-8, and

4-9 graphically show the level of reproducibility obtained by each QCT analyst.

The variances in reproducibility result from variability introduced only during the process of bone mineral analysis. The variability is not due to errors in patient positioning or scanning technique since each analyst utilized the same images for data analysis. The variability is a result of imprecision introduced during analysis such as size and placement of the ROI and, to a lesser extent, positioning of computer cursor cross-hairs with the alignment pins on the Cann-Genant phantom.

As can be seen from figures 4-7, 4-8, and 4-9, the overall reproducibility varied considerably by analyst. The best reproducibility was obtained by CT technician number one with a reproducibility of 1.27% and the worst by CT technician number two with a reproducibility of 2.88%. The reproducibility based on the author's scan analysis was intermediate at 2.21%.

These results are important since reproducibility is generally more important than accuracy for longitudinal studies of bone mineralization. The best reproducibility obtained, 1.27%, compares favorably to published values by Cann (1987) of 1 to 3%. This level of reproducibility enables the clinical determination of bone mineral changes as small as 3.6% for any two consecutive examinations

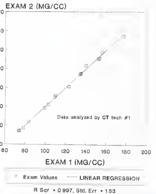

Figure 4-7 Regression of average patient BMD for exam one regressed against the average patient BMD for exam two (data analyzed by CT tech one).

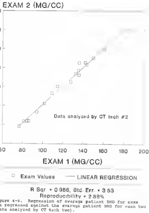

Figure 4-8. Regression of average patient BMD for exam one regressed against the average patient BMD for exam two (data analyzed by CT tech two).

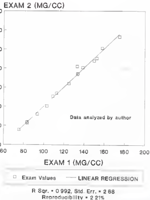

Figure 4-9. Regression of average patient BMD for exam one regressed against the average patient BMD for exam two (data analyzed by author).

In an effort to determine the reason for the wide difference in reproducibility, the analysis technique of each technician was observed. No differences were noted in positioning of the ROI. All individuals placed the ROI approximately one pixel from the anterior cortical margin of the vertebral body.

Although the QCT software will correctly position the cursors automatically over the Cann-Genant index marks in some cases, it is sporadic in nature and very frequently the technologist is required to manually reposition the cursors. All individuals, however, appeared equally accurate in the placement of the cursors over the reference alignment pins of the Cann-Genant phantom.

One difference was, however, apparent. All three individuals chose very different ROI sizes. CT technician number one used the largest possible ROI which could just be inscribed within the trabecular volume of the vertebra without overlapping the cortical margins. This ROI area varied from vertebra to vertebra but was usually larger than the ROI used by the author. The author used the 2.6 cm^2 computer default ROI. The third CT technician used a ROI that also varied but was noticeably smaller in almost every case than that used by either CT technician one or the author. Her ROI was normally selected to fill only the anterior half of the trabecular region of each vertebra

On a statistical basis alone, a larger ROI containing more pixels, would be expected to yield a more consistent average BMD. From observation, the average ROI used by CT technician one was approximately 6.6 cm^2 and contained approximately 750 pixels. The average ROI used by CT technician two was approximately 3.1 cm^2 and contained approximately 350 pixels. If it is assumed the pixel values are normally distributed and centered around the same mean value, the standard deviation of values around the mean may be calculated by

$$\pm \ (1.96 \times \sigma)/(\sqrt{N})$$

where N is equal to the number of pixels. The deviation about the population mean then is inversely proportional to the square root of the number of pixels sampled. Comparing the number of pixels sampled, the deviation about the population mean for the two technicians is proportional to

$$\pm \sqrt{N_1}/\sqrt{N_2} = \sqrt{750}/\sqrt{210} = 1.89$$

It would be expected, on a statistical basis alone, for CT technician two to have a deviation about a mean value 1.89 times that of CT technician one. Based on the reproducibility of 1.27% obtained by CT tech #1, it could be predicted that CT tech #2 would have a reproducibility of 1.89 x 1.27% or 2.40%. The actual reproducibility obtained by CT tech #2 was 2.88%, slightly higher than the

2.40% predicted. This finding does indicate, however, that 70% of the increase in variability is accounted for on the basis of number of pixels imaged alone. The remaining variability is most likely due to differences in the actual area inscribed when positioning the ROI within the vertebral body.

The results of this study emphasize the importance of properly trained and experienced technicians in achieving high reproducibility. Since clinical reproducibility is heavily dependant upon the technician, published reproducibility values may be valid only for the specific site, scanner, and technician employed. This underscores the need for research centers and centers which are closely monitoring the effects of therapy to independently determine QCT reproducibility.

Dose Assessment

The assessment of patient dose is discussed in terms of the dose to radiosensitive tissues of the body which are irradiated directly or through photon scattering during the QCT examination. Dose contributions from direct axial scanning, axial scattering, and lateral scout scans are specified. A discussion of the health implications of a QCT examination is provided as a risk versus benefit analysis.

Dose to Skin and Bone

The dosimetric analysis specifies the dose to skin, soft tissue, bone mineral, red bone marrow, and osteogenic cells. Doses to soft tissues are provided at various depths from the phantom surface.

Dose from direct axial scanning

The dose from a single axial scan to both skin and bone marrow as a function of technique factor utilized for the study is shown in Figure 4-10.

The dose to both the skin and to the bone marrow decreases with decreasing radiographic technique. The skin dose, 182 mrad, measured at 80 kVp, 40 mA, with a 2 s scan time, reflects the dose from the standard QCT protocol. Of particular interest is the magnitude of decrease in dose from direct axial scanning as a function of technique factors from 120 kVp and 40 mA to 80 kVp and 10 mA. The skin dose at 120 kVp and 40 mA (580 mrad) is over ten times greater than that at 80 kVp and 10 mA (57 mrad) and over three times greater than at 80 kVp and 40 mA (182 mrad). This dramatic reduction in dose with decreasing radiographic technique mandates the need to perform QCT exams at the recommended technique of 80 kVp and 40 mA whenever practicable.

Additionally, it should be noted that the axial dose measured with a technique of 80 kVp and 10 mA is approximately one fourth that of normal QCT technique. This represents a substantial dose sparing. The accuracy and precision of bone mineral determination utilizing such low dose technique is investigated as a separate research objective.

Dose from axial scattering

The higher dose to bone compared to that of soft tissue reflects the higher f-factor for bone (4.12) at this energy than for soft tissue (0.89). This is due to bone's higher x-ray absorption coefficient resulting from the Z-dependent increase in photoelectric interactions at this energy range. The dose to red marrow and endosteal tissues includes a dose enhancement factor to account for the dose contribution of secondary electrons from the surrounding bone.

Dose from lateral scouts

The dose distribution from the proximal to the distal side of the lateral scout axes was not mapped in detail. The dose at the lateral skin surface on the proximal side of the scout was 36 mrad/scan. Five centimeters medial to the skin surface the dose decreased to 22 mrad/scan and at

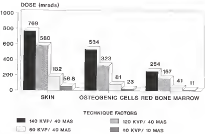

Figure 4-10. Dose from direct axial scanning to radiosensitive tissues.

the midline of the phantom the dose had decreased to approximately 5 mrad/scan. The dose to the lateral surface of the phantom most distal to the tube head was 1 mrad.

Taken on a percentage basis relative to the total dose from the QCT procedure, the dose contribution from the two lateral scans is approximately 27% of the total skin dose and approximately 20% of the dose to the red marrow and endosteum at a tube potential of 80 kVp and a tube current of 40 mA.

Total dose

As shown in Figure 4-11, the total dose from the standard QCT procedure decreases with increasing tissue depth. Due to the 360° irradiation from the CT beam, the rate of decrease in dose as a function of depth in tissue is much less in CT than that in typical diagnostic units. While a diagnostic unit may have an exit dose only 1% of its entrance dose, the minimal CT dose normally occurs at the isocenter, increasing isotopically toward the body surface. This results in a more uniform dose distribution and a higher average dose over the region irradiated than with conventional xray The dose for the standard QCT technique measured at the isocenter of the phantom was approximately one third of the dose measured at the surface of the phantom.

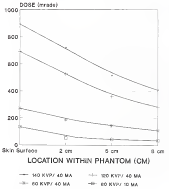

Figure 4-11. Soft tissue dose distribution as a function of depth (cm) from phantom surface.

The dose equivalent to the most radiosensitive organs, the skin, osteoblasts, and red bone marrow, are 271 mrem, 160 mrem, and 81 mrem respectively at a technique of 80 kVp, 40 mA, and 2 s. These doses are consistent with most citations in the literature. Genant et al. (1987) cite the single energy CT dose equivalent to be in the range of 100 to 300 mrem.

The dose contribution from the axial scans to the total dose is shown in Figure 4-12. At standard QCT technique, the dose contribution from axial scans, to include axial scattering, accounts for at least 75% of the total patient dose. This percentage is higher for larger kVps and only slightly lower when measured at a technique of 80 kVp and 10 mA. The large axial dose contribution to the total dose lends increased impetus to the need to investigate the potential for performing QCT examinations with a reduced number of axial scans. The impact of using a reduced number of vertebrae for QCT examinations is examined in detail in a later section.

Gonadal dose

The gonadal dose equivalent from the QCT procedure is seen to be extremely minimal, on the order of 10 mrem for each gonad. The dose (10.45 mrad) to the ovary proximal to the tube head during the lateral scout exams is only slightly increased over that of the distal ovary (10.1

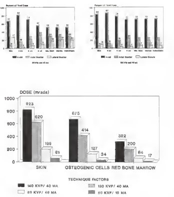

Dose from direct axial scanning
and axial scattering

Figure 4-12. Dose and percent dose contribution from axial scanning to total patient dose.

mrad). The minimal gonadal dose is reflective of the fact that the ovaries are irradiated only by scattered radiation from the procedure and are afforded some protection from scattered radiation by their location within the pelvis.

Health Implications

The QCT procedure results in a dose to four radiation sensitive areas of the body. These areas and the total dose equivalent as measured from the standard QCT procedure are tabularized below.

Table 4-5. Dose equivalent to radiosensitive tissues.

Organ/tissue	Dose Equivalent (mrem)
Skin	271
Red bone Marrow	81
Osteogenic Cells	160
Ovaries	11

Risks

The adverse health risk associated with each radiosensitive organ or tissue can be calculated from the measured doses and published risk estimates. Note, however, that risk estimates represent extrapolations of adverse health consequences from much higher doses. No adverse health effects have been directly measured from diagnostic doses of this magnitude.

The published risk estimates assume that the adverse health effects occurring at high radiation doses may be extrapolated down to very low doses without threshold. While this is a conservative approach to risk estimation, its accuracy is subject to argument on several fronts. Although there is no direct evidence that small doses of radiation comparable to those used in diagnostic radiology cause harmful effects (Hall, 1988), conservative risk estimates will be utilized in this risk assessment consistent with the "worst case" approach employed to this point.

The adverse health consequences from QCT are related to the portion of the body irradiated, either directly or through scattered radiation, during the procedure. This area includes the region of the body bounded by vertebra T-12 through the superior iliac crest. The ovaries receive only a small quantity of radiation due to scatter. Radiosensitive tissues within this region include the red bone marrow, osteogenic cells, dermal skin cells, and the gonads. Irradiation to these tissues may result in leukemia, bone cancer, skin cancer, and genetic effects respectively.

In order to make reasonable estimates of adverse health effects, a number of assumptions were made in the dose calculations. These assumptions are as follows:

1. Risk estimates based on a uniform whole body exposure may be scaled to the fraction of the body tissue irradiated during the QCT procedure.

2. Although the entire active marrow of a lumbar vertebra is approximately 30 mm thick, it is assumed that the 10 mm wide axial slice fully irradiates the entire width of the vertebra. This assumption was made to fully account for scattered radiation and to present a very conservative risk estimate. Additionally, this obviates the need to measure the change in dose distribution over the 30 mm width of the vertebral marrow.

3. During the axial scans of the vertebrae, the fraction of the total body skin that is irradiated is assumed to be identical to the fraction of the skin irradiated during the lateral scans. This assumption again simplifies calculations and presents a very conservative health risk estimate.

4. The dose measured at the skin surface closely approximates the dose at a depth of approximately 70 microns to the germinal layers of the skin. Additionally, the skin dose contribution from the lateral scouts was taken to be one half of dose measured at the phantom's lateral surface, proximal to the x-ray tube head.

5. All risk estimates used, unless otherwise specified, represent the risk of developing a fatal cancer.

Leukemia. Leukemia is a cancer of the blood forming organs characterized by the replacement of bone marrow with immature white blood cells (leukocytes) and an abnormal amount of leukocytes in the circulating blood stream. The red bone marrow is considered to be the main tissue involved in the causation of radiation induced leukemia. Since the hematopoetic cells are considered to be randomly distributed within the marrow of the trabecular bone (ICRP 11, 1968), the dose equivalent to these cells is averaged over the entire marrow volume of the trabecular bone. From data listed for Reference Man (ICRP 23, 1975), by age 44, vertebrae L-1 through L-4 contain 90.5 grams of red bone marrow. The total red bone marrow in the body is also specified as 1045.7 grams. Vertebrae L-1 through L-4 represent approximately 8.6% of the total red bone marrow of the body. The whole body risk estimate for induction of leukemia is 2 x 10-6 per mrad (ICRP 26, 1977).

The doses used in the risk assessment for leukemia are the doses to red bone marrow at each technique as previously determined. The calculations are tabularized below:

Table 4-6 Risk of a fatal leukemia per QCT procedure.

TECHNIQUE (kVp,mA,s)	PROCEDURE	RISK FACTOR PER mrem	% OF BODY SCANNED	DOSE (mrem)	RISK
80/10/2	AXIAL	2×10^{-8}	8.6	17	2.9×10^{-8}
80/10/2	LATERALS	2×10^{-8}	9.8	16	3.1×10^{-8}
80/40/2	AXIAL	2×10^{-8}	8.6	65	11.0×10^{-8}
80/40/2	LATERALS	2×10^{-8}	9.8	16	3.1×10^{-8}
120/40/2	AXIAL	2×10^{-8}	8.6	200	34.0×10^{-8}
120/40/2	LATERALS	2×10^{-8}	9.8	16	3.1×10^{-8}
140/40/2	AXIAL	2×10^{-8}	8.6	322	55.0×10^{-8}
140/40/2	LATERALS	2×10^{-8}	9.8	16	3.1×10^{-8}

The total risk of developing leukemia per procedure as a function of technique factor selected is 6.0×10^{-8} at 80 kVp,10 mA, and 2 s, 14.1×10^{-8} at 80 kVp,40 mA, and 2 s, 37.1×10^{-8} at 120 kVp, 40 mA, and 2 s, and 58.1×10^{-8} at 140 kVp, 40 mA, and 2 s.

Graphically, the results are shown in Figure 4-13. As expected, the risk is proportional to the dose received and increases with increasing technique factors. This increase in risk is not a linear function. Holding other technique factors constant, the risk of induction of leukemia nearly triples when the tube potential is increased from 80 to 120 kVp while increasing 150% from 120 to 140 kVp.

The risk at tube potentials of 80 kVp and 10 mA with a 2 s scan time is not one fourth that of a tube potential of 80 kVp and 40 mA with a 2 s scan time as would be expected. This is due to the dose contribution from the lateral scout

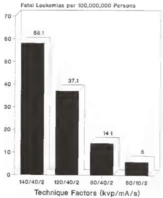

Figure 4-13. Risk of developing a fatal leukemia as a result of one QCT examination

scans whichis not reduced when the axial technique factor is changed. The risk at 80 kVp, 10 mA, and 2 s is approximately half that at 80 kVp, 40 mA, and 2 s.

Bone cancer. Primary bone cancer is sarcoma resulting from the malignant transformation of osteogenic cells. These osteogenic cells lie very near the surface of the trabecula. Because of their proximity to mineralized bone and its high atomic number, they are subjected to an enhanced electron fluence arising from the mineralized bone. Dose enhancements to the soft tissue dose measured at the trabecula are based on a dose averaged over a 10 micron distance from the trabecular surface. Consequently, the dose to these osteogenic cells is greater than the dose to the red bone marrow at a given technique. Fortunately, the radiosensitivity of the osteogenic cells is less than that of the hematopoetic cells resulting in a lower risk factor per unit dose equivalent for bone cancer than for leukemia.

Using the previously determined doses to osteogenic tissue, calculations for the incidence of fatal bone cancers per QCT procedure is summarized below.

Table 4-7. Risk of fatal bone cancers per QCT procedure.

TECHNIQUE (kVp/mA/s)	PROCEDURE	RISK FACTOR PER mrem	% OF BODY SCANNED	DOSE (mrem)	RISK
80/10/2	AXIAL	5×10^{-9}	8.6	34	1.5×10^{-8}
80/10/2	LATERALS	5×10^{-9}	9.8	33	1.6×10^{-8}
TOTAL RISK AT 80 kVp and 10 mA......3.1×10^{-8}					
80/40/2	AXIAL	5×10^{-9}	8.6	130	5.6×10^{-8}
80/40/2	LATERALS	5×10^{-9}	9.8	33	1.6×10^{-8}
TOTAL RISK at 80 kVp and 40 mA......7.2×10^{-8}					
120/40/2	AXIAL	5×10^{-9}	8.6	410	18.0×10^{-8}
120/40/2	LATERALS	5×10^{-9}	9.8	33	1.6×10^{-8}
TOTAL RISK at 120 kVp and 40 mA......19.6×10^{-8}					
140/40/2	AXIAL	5×10^{-9}	8.6	670	29.0×10^{-8}
140/40/2	LATERALS	5×10^{-9}	9.8	33	1.6×10^{-8}
TOTAL RISK at 140 kVp and 40 mA......30.6×10^{-8}					

As indicated, the total risk of developing bone cancer per procedure as a function of technique factor selected is 3.1×10^{-8} at 80 kVp, 10 mA, and 2 s, 7.2×10^{-8} at 80 kVp, 40 mA, and 2 s, 19.6×10^{-8} at 120 kVp, 40 mA, and 2 s, and 30.6×10^{-8} at 140 kVp, 40 mA, and 2 s. Graphically, the results are shown in Figure 4-14.

The risk of developing bone cancer increases with increasing technique. The risk of bone cancer induction is approximately half the risk for induction of leukemia at each technique factor. The rate of increase in risk of bone cancer with increasing technique is essentially the same as described for leukemic risk above

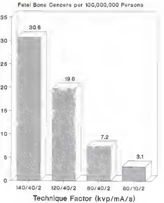

Figure 4-14. Risk of developing a fatal bone cancer as a result of one QCT examination.

Skin Cancer. Skin cancer results from malignancy within the germinal layers of the skin, the stratum spinosum and the stratum basale (Tortora and Anagnostakos, 1984). This layer is generally located at a depth of 50 to 100 microns (0.05 to 0.1 mm) from the skin surface. For the purposes of this study, the doses measured at the phantom surface were utilized as a measure of the basal skin dose. The skin dose contribution from the two lateral scout examinations was taken to be one half the dose measured at the lateral surface of the phantom, proximal to the tube head.

Table 4-8. Risk of fatal skin cancers per QCT procedure

TECHNIQUE (kVp/mA/s)	PROCEDURE	RISK FACTOR PER mrem	% OF BODY SCANNED	DOSE (mrem)	RISK
80/10/2	AXIAL	1×10^{-9}	8.6	61	5.2×10^{-9}
80/10/2	LATERALS	1×10^{-9}	9.8	36	3.5×10^{-9}
80/40/2	AXIAL	1×10^{-9}	8.6	200	17.0×10^{-9}
80/40/2	LATERALS	1×10^{-9}	9.8	36	3.5×10^{-9}
120/40/2	AXIAL	1×10^{-9}	8.6	620	53.0×10^{-9}
120/40/2	LATERALS	1×10^{-9}	9.8	36	3.5×10^{-9}
140/40/2	AXIAL	1×10^{-9}	8.6	820	71.0×10^{-9}
140/40/2	LATERALS	1×10^{-9}	9.8	36	3.5×10^{-9}

The risk per area of developing a fatal skin cancer is less than for any of the other radiation induced malignancies. This is not due to a lack of radiosensitivity of the skin but rather is a function of the ease with which most skin cancers may be excised or cryogenically removed with a non-fatal outcome. The rate of induction of non-fatal skin cancers is approximately 100 times that of fatal skin cancers (Hall, 1988).

The total risk of developing fatal skin cancer per procedure as a function of technique factor selected is 8.7 x 10^{-9} at 80 kVp, 10 mA, and 2 s, 20.5 x 10^{-9} at 80 kVp, 40 mA, and 2 s, 56.5 x 10^{-9} at 120 kVp, 40 mA, and 2 s, and 74.5 x 10^{-9} at 140 kVp, 40 mA, and 2 s.

Graphically, the results are shown in Figure 4-15. In all cases, the incidence of fatal skin cancers is low, on the order of 10^{-9} per procedure. As expected, risk increases with increasing technique with the largest percent increase occurring between 80 and 120 kVps.

All Cancers. Figure 4-16 compares the risk of developing a fatal cancer by type as a function of technique selected. When taken collectively as a function of technique factor, as shown in Figure 4-17, there is approximately a two fold increase in fatal cancers when the technique factor used is increased from 80 kVp and 10 mA to 80 kVp and 40 mA Nearly a three fold increase in fatal cancers is encountered when going from 80 kVp and 40 mA to

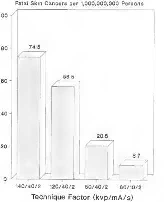

Figure 4-15. Risk of developing a fatal skin cancer as a result of one QCT examination.

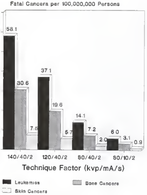

Figure 4-16. Risk of developing a fatal cancer by type at various QCT technique factors as a result of one QCT examination.

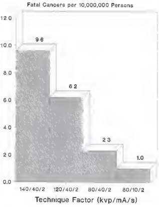

Figure 4-17. Total fatal cancer risk as a result of one QCT examination.

120 kVp and 40 mA. These large incremental increases incancer incidence with increasing radiographic technique underscore the need to perform QCT at the lowest technique possible and give further impetus to determining the feasibility of performing QCT at techniques lower than the standard 80 kVp and 40 mA. The impact of reducing the technique below the normal QCT technique is investigated in a later section.

Using the standard QCT protocol, the number of excess fetal cancers of any type on a per procedure basis, is 23×10^{-8} fetal cancers/procedure. To put this risk in better perspective, an individual receiving a standard QCT examination would have about three chances in ten million of developing a fetal cancer as a result of this procedure.

Using published comparative risk estimates from Hall (1988) of 1.37×10^{-7} deaths per cigarette smoked and 5.6×10^{-8} deaths per mile driven, the risks of fatality from QCT may be compared to other more common risks. Figure 4-19 shows a comparison of fatality incidence from QCT with that of cigarette smoking and driving an automobile. As indicated, the risk of fatality from one standard QCT procedure is equivalent to driving approximately four miles or smoking one and a half cigarettes. Therefore, it is likely that the patient, in driving to and from her appointment for the QCT examination, would incur a greater risk than from the QCT procedure itself.

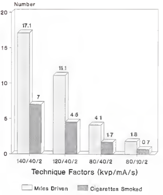

Figure 4-18. Comparison of QCT risk with other common risks.

Many areas of the world have high natural background rates of similarly low LET radiation. Areas of Brazil, India, and Niue Island in the Pacific Since have background dose rates of 500, 1300, and 1,000 mrem/year respectively (Hall, 1978). There is no epidemiological evidence that populations in these areas suffer increased incidences of fatality or other adverse health consequences as a result of their increased exposure. Since the dose equivalent to the radiosensitive areas of the body irradiated during a standard QCT examination is less than 300 mrem, one third the annual background radiation in the same parts of the world which show no increased incidence of adverse health consequences, it may be argued that any increase in mortality or morbidity from QCT would be statistically insignificant.

Benefits

As discussed in the introduction, osteoporosis is not a benign postural condition, but one that has a surprisingly high mortality rate. The most life threatening consequence of osteoporosis is hip fracture. According to Cummings (1987) the number of hip fractures occurring in the U.S. in 1986 was approximately 250,000 It is the female with advanced osteoporosis who is most likely to experience such hip fractures. The consequences of hip fracture are severe. According to Notelovitz and Ware (1982), less than half of the women who have a hip fracture regain normal function. Fifteen percent of such women die shortly after hip fracture and 30% die within a year of such injury. Deaths are usually caused from blood clots, fat embolism (from bone marrow fat trapped in the lung), and complications occurring from supportive care such as pneumonia. Additionally, if the blood supply to the head of the femur is disrupted for any substantial length of time, avascular necrosis may occur resulting in the need for hip replacement surgery. It has been estimated that a hip fracture reduces a woman's life span by 12%. Clearly, any procedure with low risk to the patient which is capable of accurately diagnosing osteopenia should be employed in an effort to reduce the severe consequences of osteoporosis.

It should not be inferred from the preceding that the low risk of adverse health consequences from the QCT procedure warrants routine screening of all women. In such cases, large numbers of perfectly healthy women would be needlessly exposed to radiation. It is the belief of the author, however, that the morbidity and mortality of this condition warrants screening for those most at risk. The relevant questions are who should be screened and by which method of bone density measurement?

At present, the only viable methods of assessing bone mineralization are through single photon absorptiometry, dual photon absorptiomety, or QCT. Typical doses from single photon absorptiometry are generally less than 5 mrad and have been reported by Kiesel (1984) to be as little as two mrad to the wrist. SPA's suitability for measurement of only the appendicular skeleton with its low metabolic turnover make SPA's predictive ability of bone loss suspect. Several studies have also shown low correlation between bone loss in the appendicular and axial skeleton. The National Osteoporosis Foundations (Peck et al., 1987) states

> the rates of (bone mineral) change in the appendicular skeleton may be low, however, and the measurement of bone density or changes in bone density at these sites do not accurately reflect bone density or changes in any other area, such as the axial skeleton, which is the area of greatest clinical interest

Dual photon absorptiometry allows direct measurement of the axial skeleton with doses on the order of 4 to 5 mrad. Unfortunately, DPA measures an integral amount of bone mineral in the path of the beam and, therefore, is adversely affected by extra-osseous calcifications. Such ossifications become more common with age, further limiting the usefulness of this technique for screening a mature population

QCT is unquestionably the most sensitive method of bone mineral determination. Its clinical reproducibility was on the order of 1% for the most qualified technologist. This reproducibility is equal to or better than that reported for the competing methods. It would seem, therefore, that the most sensitive and reproducible method for bone mineral assessment for osteoporosis is QCT. The comparatively high dose from QCT requires a careful selection of the population to be screened. The lack of availability of CT scanners at some locations and the relatively high cost of a QCT exam further underscore the need for a select patient population.

The American Osteoporosis Foundation acknowledges the need for radiologic assessment of patients with idiopathic osteoporosis, established osteoporosis, disease entities strongly associated with osteoporosis, and in the deciding whether or not estrogen therapy should be administered (Peck et al., 1987). There should be little argument regarding the appropriateness of bone mineral evaluation by QCT for these groups. The more thorny question regards the value of screening premenopausal and newly menopausal women.

Numerous studies have shown the efficacy of estrogen therapy in retarding bone mineral loss in postmenopausal women. For premenopausal women, however, estrogen therapy is inappropriate. For these individuals, treatment for prevention of bone loss consists of calcium supplementation, adequate vitamin D intake, exercise, and the reduction of secondary contributing factors such as smoking, red meats, salt intake, and alcohol consumption. Except in persons predisposed to kidney stones, where calcium supplementation may not be appropriate, all of the above treatments are considered good health practices. "Treating" all premenopausal women in this way would be prudent. The evaluation of bone loss through QCT would not change this treatment regimen and is therefore considered unnecessary.

There are a number of factors which are recognized as effecting an individual's risk of developing osteoporosis. Kotelevitz (1982) cites such factors as age at onset of menopause, genetic factors, race, body size, certain diseases, a history of bone fracture, fecundity, use of oral contraceptives, vegetarianism, smoking, alcohol consumption, and exercise. For those at risk, long term estrogen therapy has been shown to reduce the incidence of hip and vertebral fractures by about 50% (Cummings, 1987). The average rate of postmenopausal bone loss is 4% per year, although these rates may be much higher in some women. The greatest rates of bone loss occur during the first five years postmenopause. Since estrogen therapy can only slow the rate of bone loss, not replace bone that has already been lost, it is important that estrogen therapy be started as soon as possible after menopause.

The author would argue that given the high morbidity and mortality arising from fractures resulting from osteoporosis and the very low risk of fatal cancers from QCT, newly postmenopausal Caucasian women for whom estrogen therapy is not specifically contraindicated, should be afforded the opportunity for QCT. For women who show below normal bone mineralization, estrogen therapy should be considered.

Since estrogen therapy is a long term regimen, lasting from five to fifteen years, there is little value in frequent reassessment of bone mineralization prior to completing the treatment regimen. The assessment of rates of bone loss prior to such time to determine how the patient is responding to treatment is only warranted if, due to complications from estrogen therapy, termination of the treatment is being considered or to assess patient response to the therapy. In most other cases, information about the rate of bone loss would only be anecdotal. If a slowed rate of bone loss were noted, the therapy would be continued. If the rate of bone loss was unchanged or even accelerated, it is likely that therapy would be continued under the assumption that the rate of bone loss would be even greater without estrogen supplementation. Routine QCT

---

examinations throughout the course of estrogen therapy, therefore, are seldom justified and subject the patient to increased risk of radiation induced malignancy without minimal benefit.

The advantages of QCT leading to a decision to begin estrogen therapy can be seen from a risk versus benefit perspective. According to the World Almanac and Book of Facts (1987), there are currently 20.6 million women in the U.S. between the ages of 45 and 65 who are predominantly Caucasian. Assuming these women are evenly distributed by age, there are approximately 1.03 million women who are age 50, the average age for onset of menopause. If it is assumed each women will have two standard QCT examinations (one at menopause and one at five years postmenopause) a total of 2.06 million QCT examinations will be performed. Applying this value to each sub-population of women as they turn 50 for the next 30 years, at the end of the 30 years of QCT evaluations, a total of 61.8 million scans will have been performed. Using the previously determined risk factor for cancer fatalities of all types for a standard QCT examination, 2.3 x 10^{-7} fatal cancers/examination, a total of 14 fatal cancers would be caused by these examinations. According to the American Cancer Society, 20% of all deaths in the U.S. are caused by cancer. For this population, 20%, or 4.12 million deaths would be from cancer (Cancer Facts and Figures, 1987). Thus, the 30 years of QCT examinations would raise the natural incidence of cancer fatalities from 4,120,000 to 4,120,014. This represents an increase of less than 1/1000 of one percent. Even this miniscule increase in fatalities, however, would be unacceptable if not offset by comparable benefit.

Each year, 200,000 post- and peri-menopausal women fracture a bone. Of these, about 20% or 40,000 die from complications following fracture. If it is assumed a QCT examination leading to a decision to begin estrogen therapy prevents just one in ten women from having a fracture, the number of fractures occurring each year would be reduced by 20,000. Since about 20% of the fractures have fatal outcomes, approximately 4,000 lives would be saved annually. Comparing this benefit to the risk of cancer induction, QCT screening and estrogen therapy is 290 times more likely to save a life than cause a death.

Dose Reduction Effects on Accuracy

A high degree of consistency in average patient BMD values is noted at all techniques factors. The average patient BMD varies only about 1 mg/cc for all mA settings at tube potentials of 140 and 120. At a tube potential of 80 kVp, the consequences of increased photoelectric interactions with bone yield higher average BMD values at all tube current settings.

Since the accepted QCT scanning protocol calls for a technique factor of 80 kVp and 40 mA, and the objective of this study was to determine the effect on BMD measurements of reducing the patient dose, only the data obtained at 80 kVp for various mA's were statistically analyzed. The mean and standard deviations for the average patient BMD at a technique setting of 80 kVp for 40, 20, and 10 mA are shown in Table 4-9.

Table 4-9. Average BMD and standard deviation at various mA settings for 80 kVp

Technique Setting			
kVp	mA	Avg. BMD	Standard Deviation
80	10	77.94	17.00
80	20	76.71	17.21
80	40	76.32	16.20

These differences are rather small. The t-values obtained from pair-wise comparisons at various technique factors and their associated probabilities are listed in Table 4-10. Not surprisingly, pair-wise comparisons using t-tests on the data at 80 kVp associated by mA, fail to show a significant difference in patient BMD as a function of imaging technique used.

Table 4-10. Paired t-test comparisons at 80 kVp and various tube current settings.

compared to			
Technique (kVp/mA)	Technique (kVp/mA)	t-value	Probability
80/40	80/20	0.783	0.460
80/40	80/10	2.13	0.077
80/20	80/10	2.44	0.051

A more clinically relevant way to view this data is shown in Figure 4-19. As indicated in the graph, the patient BMD measured at a technique of 80 kVp with 40, 20, and 10 mA, are very similar.

Table 4-11 provides a more detailed account of the differences in technique grouped by patient. As indicated, the average difference in patient bone mineral at technique settings of 80 kVp and 20 mA compared to that at 80 kVp and 40 mA is less than 1 mg/cc. At 10 mA, the average difference is less than 2 mg/cc. On an individual patient basis, the maximum difference obtained when axial images were taken at a tube current of 20 mA compared to images taken at 40 mA was 2.75 mg/cc. This difference increases to almost 5 mg/cc for images made at a technique of 80 kVp and 10 mA.

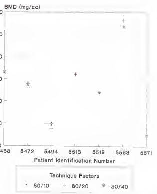

Figure 4-19. Average patient BMD as a function of radiographic technique used for QCT examination.

Table 4-11. BMD differences (mg/cc) from values measured at technique settings of 80 kVp and 40 mA.

	BMD difference from 80 kVp/40 mA	
Patient #	80 kVp/20 mA	80 kVp/10 mA
5468	0.78	2.41
5472	0.76	1.32
5494	1.54	1.16
5513	0.29	0.82
5519	0.16	0.50
5563	2.75	4.97
5571	0.42	2.75
Average Difference	0.96	1.99
Maximum Difference	2.75	4.97

This level of accuracy would probably be clinically acceptable for a non-longitudinal study, especially when the dose sparing effects are considered. A reduction in technique to 80 kVp and 20 mA would reduce the axial dose to the patient by 50%. A reduction to 80 kVp and 10 mA would reduce the axial dose to 25% of that at 80 kVp and 40 mA. Such reductions would also decrease the dose contributions due to axial scattering by the same percentages.

Figure 4-10 indicates that a reduction in technique from 80 kVp and 40 mA to 80 kVp and 10 mA would result in a dose sparing of approximately 60 mrad to osteogenic cells of the bone and 30 mrad to red bone marrow for a single axial scan. When the reduction in axial scattering is included, the total dose sparing over the dose at 80 kVp and 40 mA would be approximately 100 mrad to osteogenic cells and 50 mrad to red bone marrow. This represents a reduction in overall patient dose of approximately 60% to both osteogenic cells and red marrow.

Accuracy and Precision of Single Slice Scanning

As can be seen from figures 4-20 and 4-21, the standard error of the regression curves range from a low of 3.96 to a high of 9.51 for a single vertebra. Vertebra L-3 shows the best predictive value of a single vertebra to overall BMD with a standard error of 3.96. L-2 and L-3, when averaged together show slightly better predictive ability with a standard error of 3.72. This is essentially equal to the standard error of 3.71 found when the two most extreme vertebrae, usually L-1 and L-4, are averaged and regressed against the overall patient BMD. A more detailed accounting of the effects of using a reduced number of vertebrae to predict average patient BMD is shown in Table 4-12.

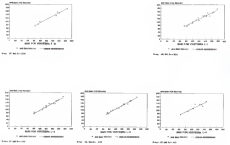

Figure 4-20. Individual vertebral BMDs plotted against average patient BMD.

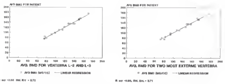

Figure 4-21. Vertebral pair BMDs plotted against average patient BMD.

Table 4-12. Accuracy data for individual vertebrae and vertebral combinations.

Vertebrae	Maximum Change (mg/cc)	Maximum Percent Change	Percent of Vertebrae with ≤2% Maximum Change	Percent of Vertebrae with ≤5% Maximum Change	Average Change (mg/cc)	Average Percent Change
T-12	14.5	10.8	29	29	7.7	6.7
L-1	18.3	13.6	31	37	6.1	5.2
L-2	13.9	10.4	35	53	4.7	4.3
L-3	10.4	12.4	11	53	6.0	5.1
L-4	23.2	17.3	10	40	8.9	8.3
Extreme	7.3	4.2	66	100	3.0	1.7
L-2+L-3	14.0	8.0	63	95	3.5	2.0

Table 4-12 indicates the magnitude of change that would occur if a reduced number of vertebrae were used to predict the average patient BMD. The columns labeled "Maximum Change" and "Maximum Percent Change" indicate the maximum difference in BMD, in mg/cc and percent, of that particular type of vertebrae compared to the patient's overall average BMD. The columns labeled ≤2% and ≤5% maximum change show the percentage of the vertebrae of each type that showed a maximum change from the overall patient BMD of less than or equal to 2 and 5% respectively. The last two columns indicate the average difference between each type of vertebrae and the average patient BMD.

The maximum difference of vertebra L-3, 10.4 mg/cc, from the average patient BMD is less than that shown by other individual vertebra. On a percent change basis, however, L-2 shows the greatest accuracy with a maximum percent change of 10.4% and an average percent change of 4.3%. For a vertebral combination, the average of the two most extreme vertebrae showed a maximal difference of 7.3 mg/cc from the overall patient BMD and an average percent change of 4.2%. The average of the two most extreme vertebrae also had the lowest average difference of 3.0 mg/cc and showed only an average 1.7% change in BMD from the average patient BMD.

Figures 4-22 and 4-23 show multiple graphs of vertebrae and vertebral combinations plotted against themselves for exam one and exam 2. It indicates that the reproducibility of various vertebrae and vertebral combinations ranges from 3.32% for L-4 to 1.30% for the average of L-2 and L-3. For a single vertebra, L-3 showed the best reproducibility at 1.76%, while L-4 showed the worst at 3.32%.

The reproducibility of the averaged L-2 and L-3 vertebrae, 1.3%, compares favorably with the overall reproducibility of 1.27% found by regressing the average of all vertebrae imaged. The actual trade-offs in reproducibility that would occur as a result of repeat imaging of a reduced number of vertebrae may be seen from Table 4-13.

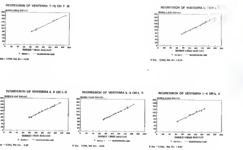

Figure 4-22. Measured BMD of individual vertebra for exam one plotted against the measured BMD of individual vertebra for exam two.

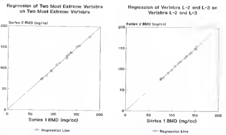

R Sqr = .998, Std Err = 1.71
Reproducibility = 1.4 %

R Sqr = .998, Std. Err = 1.53
Reproducibility = 1.3 %

Figure 4-23. Measured BMD of vertebral pairs for exam one plotted against measured BMD of vertebral pairs for exam two.

Table 4-13. Reproducibility data for individual vertebra and vertebral combinations.

			Percent of Vertebrae with			
Vertebrae	Maximum Change (mg/cc)	Percent Maximum Change	<2% Maximum Change	≤5% Maximum Change	Average Change (mg/cc)	Percent Average Change
T-12	7.0	5.8	71	88	2.6	1.9
L-1	5.6	3.1	75	100	1.6	1.3
L-2	6.0	7.0	71	94	1.9	1.7
L-3	5.0	3.5	82	100	1.7	1.5
L-4	6.5	4.8	40	100	2.5	2.4
Extreme	4.1	3.2	76	100	1.4	1.2
L-2+L-3	3.0	2.2	88	100	1.2	1.0

The maximum change in BMD for any single vertebra imaged range from a high of 7 mg/cc for a T-12 vertebra to a low of 3 mg/cc for an averaged L-2 and L-3 vertebrae. The average change in BMD was significantly better with a maximal average change in BMD of 2.4 mg/cc for all L-4 vertebrae to a low of 1.0 mg/cc for the average of all averaged L-2 and L-3 vertebrae. On a percentage change basis, the maximum percentage change occurred with a L-2 vertebra which showed a 7% change in BMD. The lowest percent change occurred with an averaged L-2 and L-3 vertebrae which showed only a 2.2% change.

With the exception of L-4, 70% or more of all vertebrae showed a change of less than or equal to 2% Eighty-two percent of L-3 vertebrae and 88% of the averaged L-2 and L-3 vertebrae showed a change of less than or equal to 2% on repeat scans. More than 85% of all vertebrae imaged showed a change of less than or equal to 5%. No change in BMD greater than 5% was obtained upon repeat imaging of vertebrae L-1, L-3, and L-4. Similarly, the average of the two most extreme vertebrae and the average of L-2 and L-3 showed no case in which the maximal change in BMD on repeat scans differed by more than 5% of value for the first scan.

Again, with the exception of L-4, the average percent change in BMD for all other vertebrae was less than 2%. The lowest average percent change for a single vertebra was 1.3% for L-1 and 1.0% for the averaged L-2 and L-3 vertebrae.

CHAPTER V
CONCLUSIONS

This chapter recaps significant findings from the preceding chapters and draws conclusions from the analysis of those findings. It contains conclusions based on each research objective as well as recommendations for modifications of the standard QCT protocol and areas requiring further research.

Field Nonuniformity Effects

The clinical significance of the effect of scan field nonuniformities are judged. The ease of controlling and magnitude of their effect is also assessed.

Vertical Decentering

The vertical decentering results indicate a plateau in values for spinal positions within 0 to 4 cm above isocenter. In this range, the change in measured BMD values relative to the isocentric value is less than 1%. For spinal positions 4 to 6 cm above isocenter, the change in measured BMD values relative to the isocentric value varies by as much as 4%.

Some idea of the clinical relevance of this change may be obtained by using the data obtained in the reproducibility study. That data indicate 66% of the axial images obtained were made within 4 cm of isocenter. Twenty-nine percent of the images were made at locations between 4 and 6 cm above isocenter. Only 3% of the images were made at distances exceeding 6 cm above isocenter. Vertical decentering to distances 4 to 6 cm above isocenter, which was seen in almost a third of the study patients, would seem to be a common clinical occurrence.

Since BMD measurements obtained 4 to 6 cm above isocenter varied as much as 4%, measurement precision in this range may be significantly degraded. This underscores the importance of insuring patient spinal position within 0 to 4 cm above isocenter for longitudinal studies where high precision is required.

Lateral Decentering

Although changes in measured BMD resulting from lateral decentering are as great as those from vertical decentering, the clinical significance of lateral decentering is much less. Data from the reproducibility study showed the average scan to be laterally decentered only 0.6 cm. The maximum decentering that occurred was 1.68 cm. On the basis of lateral decentering alone, all scans obtained would be expected to vary by less than 1% of the isocentric value. It may be concluded from the foregoing that small changes in lateral decentering of the magnitude normally encountered clinically would not be expected to significantly impact on measured BMD values.

Patient Geometry

The analysis of variance indicates that a statistically significant difference occurs among the three phantom geometries utilized in this study. While the differences among the patient geometries is statistically significant, the clinical significance of an approximate 2 mg/cc (3%) change is not great from the standpoint of accuracy. From the standpoint of reproducibility, where clinical precision is 1 to 3%, a 3% change in measured BMD is highly significant. It may be concluded that, while changes in patient geometry would have little effect on QCT accuracy, changes in patient geometry during the course of a longitudinal study would adversely impact on QCT reproducibility.

Whether geometric effects could be corrected by scaling the measured decrease in average BMD to changes in patient geometry is uncertain. It would seem prudent, however, to record the anterio-posterior and lateral dimensions of each patient during the course of the QCT examination. This would allow such information to be available for use in the interpretation of future QCT evaluations.

Patient Size Effects

The analysis of variance shows that no significant difference can be proven among the samples observed from the three sizes of phantom utilized in this study. The extremely small F-value observed when testing for difference effects leads one to the conclusion that changes in patient size in longitudinal studies would not have a significant effect on the mean bone mineral density measurements.

The changes in variances between the phantom sizes do show an effect. The variance between the 80 cm and 96 cm as well as the 80 cm and 106 cm circumference phantom configurations are significant at the 95% confidence level. The variance increases with increasing phantom size. This is to be expected since the number of photons reaching the detectors will be progressively reduced with increasing phantom size. This increase in measurement variability would be expected as a result of quantum effects

Air Gap Effects

It is apparent from the research that even very small air gaps can impact on QCT accuracy. The rather sharp initial rise of 5% in measured BMD induced by an air gap of only 1 cm indicates a need to tightly control this clinical variable. Ideally, air gaps would be eliminated during scanning. The plateau in the rate of change in measured BMD occurring from about 1 to 2.5 cm air gap distance would suggest that if a zero air gap size is not consistently obtainable in a clinical setting, a method to insure a consistent 1 to 2.5 cm air gap size would be useful in reducing variability. Alternatively, on future scans it may be possible to record air gap sizes and apply correction factors in order to compensate for variability introduced by differences in air gap sizes.

Longitudinal Slice Off-Set

These results show that small differences in longitudinal slice off-set have a significant effect on QCT reproducibility. Based on these findings, if longitudinal patient movement is noted during a scan, a decision not to repeat the QCT procedure should be made with care guided by the clinical need for high precision for a particular study balanced against the increased patient dose incurred. This decision by the clinician can be assisted by determining the maximum acceptable percent BMD change for the study, the movement from the midplane that occurred, and the percentage of scans showing less than or equal to the maximum acceptable change at that distance based on this study data.

Gantry Angular Positioning

It may be concluded from the results of this study that small changes in gantry angulation have minimal adverse impact on measured BMD values relative to the midplane value. This fact should allow the clinician to have greater confidence in BMD measurements for those cases where only changes in gantry angulation have occurred. When considering the need to repeat the QCT procedure the clinician will be able to use the data quantified on the magnitude of impact of gantry angulation in determining when repetition of the QCT procedure is warranted.

Aortic Calcification Effects

It may be concluded that QCT is insensitive to aortic calcifications as thick as 2 mm and as dense as 100 mg/cc of bone mineral equivalent material. Such extra-osseous aortic calcifications do not adversely affect the accuracy of vertebral bone mineral density measurements using QCT

Additionally, these results would imply that similar areas of calcification within the body such as kidney and pancreatic calcifications may have little effect on spinal bone density measurements using QCT. Such effects were not specifically evaluated, however, since their frequency of occurrence is much less than that of aortic calcifications

Simulated Bowel Gas

This study does not address the issue of large volumes of gas within the body such as the lungs or volumes of gas larger that 3.1 cm^3 immediately adjacent to the vertebral body. It is clear from the research, however, that small amounts of simulated internal bowel gas do not significantly degrade the accuracy or precision of measured bone mineral density. This appears to hold for the normal amounts of internal bowel gas seen clinically. Based on these results, it may be concluded that a high degree of confidence can be placed in measured BMD values imaged when small amounts of extra-vertebral air are present The repetition of such scans on the basis of the presence of air within the scan field is not justified.

Reproducibility Study

Reproducibility is generally considered to be more important than accuracy in longitudinal studies of bone mineralization. The best reproducibility of the QCT technique obtained under clinical conditions was 1.27%. This compares very favorably to published values of 1 to 3% (Cann, 1987). This level of reproducibility will allow the clinical determination of bone mineral changes as small as 3.6% for any two consecutive examinations. It may be concluded that clinical QCT is a sensitive indicator of small changes in bone mineralization. This makes QCT a very useful tool in monitoring both therapies to restore bone mineral and in disease processes, to include osteoporosis, which reduce bone mineralization.

The results of this study emphasize the importance of properly trained and experienced technicians in achieving high reproducibility. Proper training should underscore the critical nature of selecting the largest possible ROI to measure trabecular bone mineral. The significant impact of this parameter demands added emphasis in protocol and procedural manuals. Further, since clinical reproducibility is heavily dependent upon the technician, research centers and centers conducting longitudinal QCT studies should independently assess the reproducibility obtained at their specific institution. Published reproducibility values for QCT should be viewed as valid only for the specific location, equipment, and personnel employed.

Dose Assessment

The dose assessment presents conclusions based on experimental results. The conclusions are made relative to type of radiosensitive tissue irradiated and mode of irradiation, either by direct or scattered radiation. Conclusions are drawn as to health consequences and dose sparing measures are specified.

Dose to Skin and Bone

The dose to soft tissue and to radiosensitive tissues such as the skin and bone are discussed. The dose is specified according to technique, axial, and lateral scans and conclusions drawn regarding the total dose for a QCT examination.

Dose from direct axial scanning

The dramatic reduction in dose with decreasing radiographic technique underscores the need to perform QCT exams at the recommended technique of 80 kVp and 40 mA whenever practicable. The potential for even greater dose sparing warrants a more complete investigation into the feasibility of imaging at still lower technique factors.

Dose from axial scattering

The dose contribution from axial scattering contributes approximately 55% of the total dose to bone marrow and osteogenic cells at standard technique. The dose contribution to soft tissue components is less with a maximum of 33% to isocentrically located tissues. This fact again indicates the high degree of dose sparing that could be achieved by reducing the number of axial scans required per QCT examination.

Dose from lateral scouts

Using the dose to skin located proximal to the tube head for all skin dose calculations, the dose contribution from the lateral scout scans was 27% of the total QCT dose at technique settings of 80 kVp and 40 mA. This dose contribution could be substantially reduced by performing the two lateral scout examinations at reduced technique. Since the laterals are used only to visualize the vertebral bodies, there appears to be little clinical advantage to scanning at the standard lateral technique of 120 kVp and 40 mA.

Total dose

From the dosimetry measurements obtained, it appears that the total dose equivalent from the QCT procedure when performed using the standard QCT protocol is approximately 271 mrem to skin, 160 mrem to osteogenic cells, and 81 mrem to bone marrow. These dose equivalents are well within those generally cited in the literature for the standard QCT technique. As indicated previously, these doses may be reduced substantially if lower radiographic technique for axial and lateral scans are used or if fewer vertebrae are selected for imaging.

Gonadal Dose

The gonadal dose equivalent from the QCT examination is extremely minimal, on the order of 10 mrem. The risk of cancer induction from such a dose is vanishingly small. The genetic consequences of such doses to a postmenopausal population are nonexistent.

Health Implications

It may be seen that QCT is not without risk of cancer induction, although the risk is extremely small. When compared to the natural cancer incidence, the excess cancer fatalities that would be introduced from widespread use of QCT for evaluation of osteoporosis in postmenopausal females is less than 1/1000 of 1% over the natural cancer incidence. Using the standard QCT protocol, the health benefits of QCT examination far outweigh any risks to the individual from the procedure. By targeting only newly postmenopausal women for whom estrogen therapy is not otherwise contraindicated for QCT examination, the population risk is further limited while the potential for benefit is maximized.

Dose Reduction Effects on Accuracy

For the purposes of determining a patient's bone mineralization, an accuracy within 1 or 2 mg/cc is seldom required. It is only during longitudinal studies which monitor response to therapy or disease that small changes in bone mineralization become important.

A reduction in technique factor from the normal scanning protocol of 80 kVp and 40 mA appears to be a viable option for non-longitudinal studies of bone mineralization. Compared to the BMD obtained at 80 kVp and 40 mA, the average change in BMD is less than 1 and 2 mg/cc at 20 mA and 10 mA respectively. While the difference in accuracy would be minimal, the dose sparing effects of lowering the technique selected to 80 kVp and 10 mA would result in a dose reduction of 100 mrad to osteogenic cells and 50 mrad to red bone marrow. This represents a dose reduction of approximately 60% to both osteogenic cells and red bone marrow. Additionally, the author sees no reason why the two lateral scout scans could not be reduced to lower technique as a method to further decrease patient dose.

Accuracy and Precision of Single Slice Scanning

Decisions regarding acceptable limits on accuracy and reproducibility are clinical ones which must be governed by the nature of the examination and the judgment of the clinician. The results of this research presents the clinician with previously unavailable empirical data upon which to make such judgments.

For the purposes of estimating the overall patient BMD, the average of the two most extreme vertebrae had a maximal difference of 7.3 mg/cc from the overall patient BMD and an maximum percent change of 4.2%. The average of all of the two most extreme vertebrae differed by only 3.0 mg/cc, a 1.7% change, in BMD as measured against the average patient BMD. Given a natural biological variability in BMD of approximately 30 mg/cc, differences in the range of 3 to 7 mg/cc may, in many cases, be clinically acceptable.

When reproducibility is of prime interest, the average of vertebrae L-2 and L-3 showed a difference of only a 3 mg/cc or a 2.2% maximal change. The average change in BMD as measured by the L-2 + L-3 combination, was only 1.2 mg/cc or a 1.0% average difference This small degree of difference may also be clinically appropriate.

While this research points to the need for more in depth study with a larger patient population, it is clear that a reasonable potential exists for modifying the standard QCT procedure. By imaging fewer vertebrae, only small sacrifices in accuracy and reproducibility would result while the dose savings to the patient would be substantial.

Optimization of Parameters and Recommendations

Of the research objectives specified in Table 1-2, changes in patient size, gantry angulation, and the presence of aortic calcifications and bowel gas, have little or no impact on measured BMD values. Based on the findings of this study, the clinician may have high confidence in BMD measurements made in the presence of small changes in these parameters. Additionally, the effects of lateral decentering, while experimentally important, are easily controlled by competent CT technicians and, therefore, have minimal clinical impact.

The effects of vertical decentering were not easily controlled, however, and have the potential for significantly degrading the accuracy of BMD measurements. Changes in patient geometry, spine - water bolus air gap distance, and longitudinal slice position also significantly degrade the accuracy of BMD measurements.

The reproducibility study indicated that clinical reproducibility is strongly dependent upon the size of the ROI chosen for trabecular BMD analysis. The dosimetry study indicated that although the health risks from QCT examination are not great, the potential exists for substantially reducing the patient dose from QCT. Areas of dose sparing potential include imaging at lower technique factors for both axial and lateral scans as well as imaging fewer than normal vertebrae per examination.

Based on the above, it is recommended that the standard QCT protocol include recording

1. the vertical position of the patient relative to the scan field isocenter,

2. the patient geometric ratio (A-P/lateral distances), and

3. changes in longitudinal slice position relative to the vertebral midplane.

Such information will be of value to the clinician in interpreting the results of QCT examination and in determining the source of variability in the BMD measurements. It is further recommended that increased emphasis be provided the CT technicians in selection of the largest possible ROI to inscribe the spinal trabecula and in using the lowest technique factors possible, consistent with the accuracy and precision required by the type of examination. Specifically, the author believes that a technique of 80 kVp and 20 mA for axial scanning along with a reduced technique for lateral scanning is appropriate for screening of petite patients.

Further research with a larger patient population is recommended to determine the efficacy of replacing the standard QCT technique with one using a reduced number of vertebrae. Further, if QCT is to be dosimetrically evaluated relative to other methods of bone densitometry, a more complete dosimetric study is necessary. The dosimetry work performed in this study was approached from the standpoint of assessing health risk. It employed a series of worst-case assumptions in order to safe-side adverse health consequences. In order to more equally evaluate the patient dose from QCT relative to competing modalities of bone densitometry, more extensive measurements should be made.

APPENDIX A
DOSIMETRIC SYSTEMS

This appendix addresses the steps taken to insure that all systems associated with dosimetric analysis performed in this study were functioning properly. Additionally, the procedures utilized for TLD chip matching and the configuration of the diagnostic x-ray unit enabling it to approximate the spectrum of the CT scanner is discussed.

TL Dosimetry System

Thermoluminescent dosimetry was selected as the dosimetric method of choice for this study's dosimetric research. Unless the Rando phantom were to be physically modified, the small diameter of the holes bored within the phantom require a dosimeter with a diameter of less than 5 mm. Although TL dosimetry has a number of other advantages, the ability of a TLD chip to fit within the Rando phantom without modification was a primary consideration.

TLD 100's

Thermoluminescence is the property by which certain materials exposed to radiation will emit light when heated. According to conduction band theory, when a thermoluminescent material absorbs radiation energy, a valence electron is released to the conduction band leaving behind a hole in the valence band. The electron and hole are free to move through the material until they recombine or become trapped in meta-stable states. When trapped in a meta-stable state, the electron or hole may be freed if sufficient thermal energy is supplied. Upon the application of sufficient heat, the trapped electrons and holes are again free to wander throughout the material, eventually to recombine in the valence band. The energy lost in this process is given off in the form of light. The amount of light emitted is proportional to the amount of energy absorbed from the radiation received and thus may be used as a radiation dosimeter.

A graph of the light output of a TLD chip as it is heated is called a glow curve. It reflects light output as a function of temperature or heating time. The shape of the glow curve varies from one material to the next, showing peaks and valleys. The peaks represent traps at different energy levels. The integral of the glow curve is a measure of the total light emitted and is used to estimate the radiation energy absorbed by the crystal.

By exposing several TLD chips to known but varying amounts of radiation and then reading their light output, a curve of light emitted versus radiation received can be obtained. Such a curve is called a dosage calibration curve and can be used to determine the dose received from a similar TLD chip based on its measured light output. A typical glow curve is shown in Figure A-1. This curve shows several small peaks and one large peak in light output as a function of temperature.

Since the lower energy peaks may empty in response to daily temperature fluctuations and normal thermal absorptions, they could introduce undesirable variability in measured light output. To prevent this, most TLD chips are preannealed (heated at low temperatures) to remove the low energy peaks prior to reading. This provides a more consistent reading of radiation energy absorbed.

Of all the materials exhibiting thermoluminescence, one of the most commonly used for radiation dosimetry is lithium fluoride (LiF). This material is available commercially in a variety of forms, the most ubiquitous being pressed chips. Those used for this study were Harshaw TLD-100 chips. These were 0.32 x 0.32 x 0.09 cm in size and composed of LiF with minor impurities, primarily magnesium and titanium which are added to increase the number of trapping sites within the crystal. The lithium is present in its normal isotopic abundance of 7.5% ^{6}Li and 92.5% ^{7}Li.

Table A-1 taken from Armstrong (1987) shows a summary of properties of several commercially available TLD materials. As indicated, TLD-100 shows several properties which make it appropriate for dosimetry. Its effective

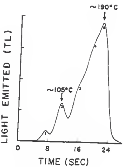

Figure A-1. Typical glow curve for Lithium Flouride TLD-100.

Table A-1. Properties of some commercially available [illegible]

TLD MATERIALS SUMMARY

Property/Type	LiF	$Li_2B_4O_7$: Mn	CaF_2: Mn	CaF_2 (TLD 200)	$CaSO_4$: Mn	$CaSO_4$: [illegible]
Density (gm/cc)	2.64 (Powder ~1.2)	~2.4 (Ribbon) ~1.2 (Powder)	3.18	3.18	2.61	2.61
Effective Atomic No (Z) for photoelectric absorption	8.2	7.4	16.3	16.3	15.3	15.5
TL Emission Spectra	3500-6000Å (4000 max)	5300-6300Å (6050 max)	4400-6000Å (5000 max)	Peaks at 4835Å at 5765Å	4500-6000Å (5000 max)	4800Å 5700Å
Temperature of main TL glow peak	195°C	200°C	260°C	180°C	110°C	220°C
Efficiency at ^{60}Co relative to LiF	1.0	0.15	10	30	70	30
Energy Response 30 Kev/^{60}Co	1.25	0.9	~13	~12.5	~10	~12.5
Useful Range	mR-3x10^5 R	50mR 10^6 R	mR-3x10^5 R	10μR 10^4 R	μR 10^4 R	μR ~10^6 R
Fading	Negligible 5%/yr at 20°C	<5% in 3 months	10% in first 24 hours 15% total in 2 months	10% in first 24 hours 16% total in 2 weeks	50% in first 24 hours	2% in 1 month 8% in 6 months
Physical Forms	Powder extruded teflon, glass encapsulated bulbs, chipped crystals	Powder Solid Glass, Teflon	Powder teflon pressed, glass encapsulated bulbs	Powder Crystals Glass bulbs	Powder Teflon	Powder Powder Ribbons
Available From	Harshaw supplies everyone	Harshaw	EG & G Harshaw (1)	Harshaw only	Harshaw (2)	Harshaw (2)

atomic number of 8.2 is close to that of both soft tissue (7.4) and air (7.6). This makes it especially suitable for soft tissue dosimetry. It has a stable main glow peak of 195°C which contributes to a fade rate of less than 5% per year. It has a useful dosimetric range of a few mR to approximately 300,000 R. Additionally, TLD-100 shows no dose rate dependence and little energy dependence over the range of interest for this study.

The only other TLD material which compares favorably to LiF in terms of suitability for this study is manganese doped lithium borate ($Li_2B_4O_7$:Mn). $Li_2B_4O_7$:Mn has an effective Z of 7.4 which is closer to the effective Z of both tissue and air than is LiF. Unfortunately $Li_2B_4O_7$:Mn's useful range begins at approximately 50 mR making it less suitable than LiF for very low dose measurements. In light of the above, and its ready availability, TLD-100 was selected as the dosimeter of choice for these dosimetric measurements.

TLD Reader

In order to determine the amount of radiation absorbed by a TLD, the dosimeter is heated at a uniform rate to a specific temperature. This temperature usually corresponds to the largest glow peak of interest The light output is then precisely measured using a photomultiplier tube. The entire area of sample, heating planchette, and photomultiplier are light insulated and flushed with nitrogen gas to eliminate spurious luminescence.

To insure consistency of readings, the Harshaw 2000 series TLD reader used in this study employs several refinements over the basic process just described. In order to minimize spurious readings caused by thermal effects to the electronics, the photomultiplier tube is thermo-electrically cooled. It is also located away from the heating planchette and employs lenses to bend and redirect the light away from the TLD-planchette location. A light filter is also used to filter out infrared radiation from the light emitted by the TLD. These enhancements, as well as others, insure a high signal to noise ratio which is very important, especially in the measurement of low dose radiation fields.

Initial annealing of TLD chips

Although the TLD chips which were used in this study were reported to be "good" chips, their exposure history was uncertain. In light of this fact, it was considered prudent to restructure all of the TLD chips. The restructuring of TLD chips is a preannealing procedure which can both increase the overall sensitivity of the TLD chip and reduce the size of the low dose glow curve peaks relative to that of the larger peaks. Additionally, this procedure will tend to "rezero" the response of the chips, helping to eliminate any cumulative effects from previous exposures. This type of annealing is routinely done by Harshaw prior to initial sale of their TLD-100 chips.

In order to restructure the TLD chips used in this study, all chips were annealed prior to use. This annealing consisted of heating each chip in a temperature controlled oven at 400°C for one hour followed by a two hour cool down period at 100°C. All TLD chips were placed in an aluminum crucible which had been milled out to hold TLD chips. The crucible was cleaned prior to use with anhydrous methyl alcohol to remove any foreign material. After the heating cycle was complete, the restructured chips were then returned to a lucite holder which was sealed inside a light tight pouch. The chips were now ready to be sensitivity matched

Sensitivity matching of TLD chips

Prior to using the TLDs for dosimetry measurements, it was necessary to match the chips for sensitivity and to calibrate them to a known radiation source

Ideally, the TLD chips would be matched and calibrated with the same unit used for dose measurements. This would insure that the TLD response would occur over the same range of exposure, exposure rate, and, beam energy as would be encountered during actual scanning. Unfortunately, the small diameter of the CT beam and the variability of beam energy across the breadth of the beam make the use of the CT scanner for TLD chip matching and calibration impractical.

Alternatively, a diagnostic x-ray unit was utilized. The diagnostic unit was adjusted to insure the TLD chips would be exposed to approximately the same energy beam on the diagnostic unit that they would experience on the CT scanner. This was accomplished by adjusting the tube potential and filtration of the diagnostic unit until the beam half value layer (HVL) measurements obtained matched those of the CT scanner.

CT HVL Determination

Bow-tie filter

The measurement of HVLs on the GE 9800 CT scanner is not a straightforward task due to the presence of a bow-tie filter. This filter is automatically selected when the scanner is used to scan areas of the torso such as during QCT examinations. The bow-tie filter serves to compensate for variations in photon intensity at the detector location that would otherwise be introduced by the cylindrical geometry of the patient. In such a geometry, the photon beam passing through the center of the torso would be attenuated more than the same beam passing through the periphery of the torso. This is due to the greater mass of material through which the photon beam must pass in the center of the torso relative to the periphery. To compensate for this effect, a filter which is thinner in the middle and thicker near the edges (hence the term, bow-tie filter) is used. Unfortunately, the bow-tie filter not only affects the intensity of the beam but also its energy. As a consequence, the beam energy is not uniform along its breadth, but increases in each direction from its isocentric value.

For this reason, HVL measurements of the CT beam were obtained at both an isocentric location and a location laterally decentered from isocenter. A Capintec electrometer (model 192, serial number 94C741) with ion chamber (model PR06G, serial number CIIG.64266) was used for these HVL determinations. The Capintec was calibrated by intercomparison with instruments calibrated by or directly traceable to the National Bureau of Standards in 1986 by K & S Associates of Nashville, Tennessee.

The active volume of the ion chamber was placed on the upper surface of a cardboard stand. The stand was placed within the CT scanner gantry so that the probe was centrally located (37 cm below the top of the gantry and 34 cm above the base of the gantry). The base of the stand was open and a 20 x 20 cm opening was cut from the top of the stand. This was done to minimize the effects of any scattered radiation from the stand and gantry. The active volume of ion chamber was localized laterally within the scan field using the laser alignment beams and taped into piece parallel to and within the axis of the beam. To confirm the ion chambers location within the 1 cm wide CT fan beam, a sheet of x-ray film was carefully placed under the ion chamber probe. An exposure was made using the CT scanner with the x-ray tube locked into position vertically over the chamber. The chamber position was confirmed to be fully within the beam by visual inspection of the film.

Effects of scattering on ion chamber

Efforts were made to minimize any influence from scattered radiation on the ion chamber. These efforts included positioning the chamber as far from gantry elements as practical, using a low atomic number material (cardboard) for support of the chamber, and removing a 20 x 20 cm portion of the cardboard stand immediately surrounding the active volume of the chamber.

Never-the-less, it was felt prudent to estimate the effect on the ion chamber from whatever scattered radiation might occur. To accomplish this, three measurements were taken with the active volume of the chamber suspended over the 20 x 20 cm opening on the top surface of the stand. The exposures were made with a technique of 80 kVp, 100 mA, with a 2 s scan time. A 20 x 20 cm square of cardboard was then placed over the opening and a second series of three measures were made as before. These two series of measures serve to illustrate the detector response with and without backscatter from the experimental apparatus.

The average reading of the detector with backscatter from the cardboard was found to be 256.5 milliroentgens (mR) and 255.0 mR without backscatter. These measures indicate less than a 1% (0.65 %) difference in detector response to backscatter from the cardboard support. From this, it may be concluded that backscattered radiation from the experimental apparatus will not greatly affect measurements used in HVL determinations

Ion chamber stem effects

In order to fully irradiate the ion chamber, it was necessary to align the chamber so that its entire length was completely within the CT beam This arrangement has the potential for introducing undesired ionizations within the stem of the chamber and its connecting cable. Such spurious and unwanted ionizations create a "stem effect" leading to measurement inaccuracies.

To test for the magnitude of the stem effect for this experimental arrangement, a Philips diagnostic x-ray unit (Sigma 45206,45207,45208 with 1.5 mm Al equivalent inherent filtration) with technique factors of 100 kVp and 110 mAs was used to irradiate the ion chamber in two different orientations.

In both orientations, a field size of 20 x 5 cm was used. In the first orientation, the ion chamber probe was aligned parallel to the long axis of the beam with its entire length contained within the beam. The chamber was then irradiated and the exposure reading recorded. In the second orientation, the chamber was reoriented perpendicular to the long axis of the scan field so that only the 3.5 cm active volume of the chamber was irradiated. A second exposure was made in this configuration. In order to determine the magnitude of the stem effects as a function of beam energy, this same procedure was repeated at 60 kVp and 250 mAs.

At both tube potentials, the readings recorded with the entire length of the probe irradiated were within 2% of those in which only the active volume of the probe was irradiated. The stem effect, then, appears to be minimal. Its small change at two different tube potentials indicates that it is relatively insensitive to changes in beam energy. It was, therefore, considered to be suitable for measurements using the more highly filtered CT beam and adequate for the purposes of this assessment.

CT HVL Measurements

Satisfied that the stem effect and scattering from the experimental apparatus would have minimal impact on the HVL measurements, the HVL of the CT scanner was determined. With the Capintec properly positioned within the 1 cm fan beam of the CT scanner, a series of HVL measurements were made. To bracket the range of energies used in this study, measurements were made with a technique of 80 kVp, 100 mA, and 2 s as well as with a technique of 120 kVp, 100 mA, and 2 s. To assess the variability in beam energy introduced by the bow-tie filter, HVL measurements were also made with the Capintec chamber laterally decentered 14 cm from isocenter.

A series of three measurements was made at 80 kVp, 100 mA, with a 2 s scan time at the isocentric position in the absence of any added aluminum absorbers. These measurements were averaged to obtain a more accurate value for the beam filtered only by the bow-tie filter.

Pure aluminum plates calibrated at the National Bureau of Standards were used as absorbers for HVL determinations. A 0.970 mm layer of aluminum absorber was taped to the top of the gantry housing directly below the tube location and an exposure was obtained. Additional layers of aluminum were added to the top of the gantry housing prior to each subsequent exposure. The measured exposure at each thickness of aluminum was recorded.

To assess the change in HVL over the breadth of the CT beam, this process was repeated at a location laterally decentered a distance of 14 cm from isocenter. Upon completion of these measurements, the entire process was repeated at 120 kVp.

The results of these measurements are tabulated below

Table A-2. CT HVL Measurements.

kVp	MA	S	Location	Aluminum (mm)	Total Aluminum (mm)	Exposure (Roentgen)	Normalized Exposure
80	100	2	isocenter	0.000	0.000	2.688	1.000
80	100	2	isocenter	0.970	0.970	2.172	0.808
80	100	2	isocenter	0.970	1.940	1.795	0.668
80	100	2	isocenter	0.991	2.931	1.514	0.563
80	100	2	isocenter	1.956	4.887	1.120	0.417
80	100	2	isocenter	2.040	6.927	0.836	0.311
80	100	2	isocenter	2.040	8.967	0.652	0.243
80	100	2	isocenter	3.284	12.251	0.452	0.168
120	100	2	isocenter	0.000	0.000	6.000	1.000
120	100	2	isocenter	0.970	0.970	4.826	0.804
120	100	2	isocenter	0.970	1.940	4.220	0.703
120	100	2	isocenter	0.991	2.931	3.735	0.623
120	100	2	isocenter	1.956	4.887	3.003	0.501
120	100	2	isocenter	2.040	6.927	2.418	0.403
120	100	2	isocenter	2.040	8.967	2.007	0.335
120	100	2	isocenter	3.284	12.251	1.519	0.253
80	100	2	decentered	0.000	0.000	0.196	1.000
80	100	2	decentered	0.970	0.970	0.171	0.875
80	100	2	decentered	0.970	1.940	0.152	0.777
80	100	2	decentered	0.991	2.931	0.137	0.701
80	100	2	decentered	1.956	4.887	0.110	0.563
80	100	2	decentered	2.040	6.927	0.090	0.460
80	100	2	decentered	2.040	8.967	0.069	0.353

Table A-2. CT HVL Measurements (continued).

kVp	MA	S	Location	Aluminum (mm)	Total Aluminum (mm)	Exposure (Roentgen)	Normalized Exposure
80	100	2	decentered	3.284	12.251	0.049	0.251
120	100	2	decentered	0.000	0.000	0.597	1.000
120	100	2	decentered	0.970	0.970	0.548	0.918
120	100	2	decentered	0.970	1.940	0.500	0.838
120	100	2	decentered	0.991	2.931	0.456	0.764
120	100	2	decentered	1.956	4.887	0.388	0.650
120	100	2	decentered	2.040	6.927	0.328	0.549
120	100	2	decentered	2.040	8.967	0.275	0.461
120	100	2	decentered	3.284	12.251	0.213	0.357

Graphically, the normalized CT half-value determination at the isocentric location is shown in Figure A-2. It depicts the exposure in Roentgens as a function of millimeters of aluminum absorber. As shown, at a tube potential of 80 kVp, a thickness of approximately 3.7 mm of aluminum is sufficient to reduce the exposure at the CT scanner's isocentric position by one half. Approximately 4.8 mm of aluminum is required for the same amount of reduction at 120 kVp.

Figure A-3 shows a similar plot of normalized exposure as a function of millimeters of aluminum absorber for the laterally decentered chamber position. Here the HVLs are approximately 6 and 8 mm of aluminum for tube potentials of 80 and 120 kVp respectively. As would be expected, the slope of the curves approach linearity at the decentered

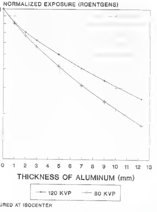

Figure A-2 Normalized CT HVL determination at technique settings of 120 and 80 kVp measured at isocenter.

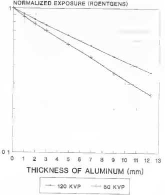

MEASURED AT DECENTERED
LOCATION, 14 CM FROM ISOCENTER

Figure A-3 Normalized CT HVL determination at technique settings of 120 and 80 kVp 14 cm laterally decentered from isocenter.

location due to the beam hardening effects of the bow-tie filter toward the periphery of the scan field.

The HVL of the CT scanner at a technique setting of 80 kVp was determined to be 3.7 mm of aluminum at isocenter and 6 mm of aluminum when decentered 14 cm laterally. The average HVL at 80 kVp was taken to be the average of these two values or 4.9 mm of aluminum. The HVL of the CT scanner at 120 kVp was determined to be 4.8 mm of aluminum at isocenter and 8 mm of aluminum when decentered 14 cm laterally. The average HVL at 120 kVp was taken to be the average of these two values or 6.4 mm of aluminum.

Match HVL of diagnostic unit to CT scanner

Having determined the HVLs of the CT scanner for the range of energies to be used during the dosimetry study, it becomes possible to match the HVL of the Phillips diagnostic unit to that of the CT scanner. This assures the TLD chips used for sensitivity matching and calibration will be exposed to the same beam energy as found during QCT scanning.

In order to determine the kVp and filtration required by the diagnostic unit to match the HVL of the CT scanner, a cardboard stand having a 20 x 20 cm opening in the top was placed on the table of the diagnostic x-ray unit (see

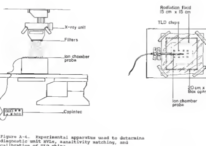

Figure A-4. Experimental apparatus used to determine diagnostic unit HVLs, sensitivity matching, and calibration of TLD chips.

Figure A-4). The Capintec chamber was placed over the opening of the box and taped in place so that the active volume was centrally located within the opening and suspended 30 cm above the table top. The x-ray tube was positioned directly over the active volume of the chamber and a 15 x 15 cm radiation field was selected. This allowed for a 5 cm "free space" around the x-ray field to minimize scattering effects. The x-ray tube head was raised as high as practicable (20 cm) above the probe. It was felt that this configuration would result in minimal scattered radiation at the location of the probe.

Iterative adjustments were made to the kVp and added filtration of the diagnostic unit until HVLs equivalent to those found on the CT scanner were obtained. The results of these measurements are tabularized in Table A-3.

Table A-3. Matching of CT and Diagnostic unit HVLs.

kVp	IN TUBE FILTRATION (mm Al)	ABSORBER (mm Al)	EXPOSURE (ROENTGENS)	NORMALIZED EXPOSURE
80	2 mm Al	0.00	6.09	1.00
80	2 mm Al	0.97	4.97	0.82
80	2 mm Al	1.95	4.11	0.67
80	2 mm Al	3.78	3.10	0.51
80	2 mm Al	3.99	2.94	0.48
80	2 mm Al	6.03	2.21	0.36
80	2 mm Al	8.07	1.69	0.28
80	2 mm Al	10.11	1.33	0.22
110	2 mm Al	0.00	6.58	1.00
110	2 mm Al	2.04	4.85	0.74
110	2 mm Al	4.08	3.79	0.58
110	2 mm Al	5.05	3.37	0.51
110	2 mm Al	8.12	3.05	0.46
110	2 mm Al	10.12	2.11	0.32
100	.1mmCu	0.00	4.73	1.00
100	.1mmCu	2.04	3.62	0.77
100	.1mmCu	4.08	2.88	0.61
100	.1mmCu	8.12	2.32	0.49
100	.1mmCu	10.12	1.55	0.33
100	.1mmCu	13.40	1.21	0.26
130	.1mmCu	0.00	4.15	1.00
130	.1mmCu	2.04	3.34	0.80
130	.1mmCu	4.08	2.75	0.66
130	.1mmCu	6.12	2.35	0.57
130	.1mmCu	8.18	1.96	0.47
130	.1mmCu	11.44	1.55	0.37

Graphically, the HVL determination for the diagnostic unit is shown in Figure A-5. With 2 mm of aluminum filtration, exposures at technique factors of 80 kVp and 110 kVp show HVLs of approximately 3.8 and 5.3 mm aluminum respectively. As indicated in Figure A-6, the HVLs are

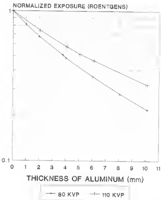

Figure A-5. Normalized diagnostic unit HVL determination at 80 and 110 kVp.

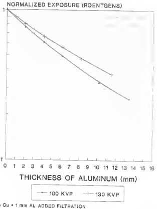

Figure A-6. Normalized diagnostic unit HVL determination at 100 and 130 kVp.

approximately 6 and 7.5 mm aluminum at 100 kVp and 130 kVp respectively.

A graphic comparison of isocentric HVLs of the CT scanner and the adjusted diagnostic unit are shown in Figure A-7. As indicated, the curves show excellent agreement in terms of HVLs. The HVL of the isocentrically measured CT beam at a setting of 80 kVp is virtually identical to that of the diagnostic unit at 80 kVp with 2 mm of added aluminum filtration. The HVL of the CT beam when operated at 120 kVp (4.8 mm of aluminum) also compares favorably with that of the adjusted diagnostic unit when operated at 110 kVp (5.3 mm of aluminum).

A comparison of the decentered CT beam HVLs with those of the diagnostic unit when operated with 0.1 mm Cu and 1 mm Al added filtration is shown in Figure A-8. The HVLs of the decentered CT beam at a technique of 80 kVp and the diagnostic unit operated at 100 kVp with 0.1 mm Cu and 1 mm of added aluminum filtration are identical at 5 mm of aluminum. The HVLs of the decentered CT beam with a tube potential of 120 kVp (8 mm of aluminum) and the diagnostic unit operated with a tube potential of 130 kVp with 0.1 mm Cu and 1 mm of added aluminum filtration (7.5 mm of aluminum) also shows good agreement.

The degree of difference in the HVLs of the CT beam at its isocentric position and the diagnostic unit operated at a tube potential of 80 kVp with 2 mm of added aluminum

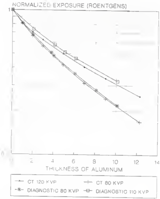

CT HVL MEASURED AT ISOCENTER

Figure A-7. Comparison of HVL of diagnostic unit and CT scanner measured at the isocenter.

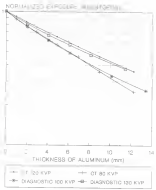

CT Measured at decentered location 14 cm from isocenter. 0.1 mm Cu + 1 mm aluminum added to diagnostic unit

Figure A-8. Comparison of HVL of diagnostic unit and CT scanner measured at the decentered location.

filtration and at 100 kVp with 0.1 mm Cu and 1 mm of aluminum added filtration are negligible. The difference between the CT beam HVLs measured at the decentered location and the diagnostic unit operated at 110 kVp with 2 mm of aluminum and at 130 kVp with 0.1 mm Cu and 1 mm aluminum added filtration are more pronounced. These differences range from 4.8 to 5.3 mm of aluminum for the 80 kVp CT beam and from 7.5 to 8.0 mm Al for the 120 kVp CT beam. In practical terms, these differences account for changes in effective energy of the CT and diagnostic beams of only about 2 keV. The change in TLD response over an energy range of 2 keV is insignificant.

Based on the above, it can be concluded that the calibration of TLD chips using the Philips diagnostic unit when appropriately matched to the HVLs of the CT scanner will not adversely affect the accuracy of the TLD measurements.

Having matched the HVL of the diagnostic unit with that of the CT scanner, it now becomes possible to use the wider beam of the diagnostic unit for sensitivity matching and calibration of TLD chips at the same beam energy encountered during CT scanning.

One hundred and forty TLD chips were matched for sensitivity following the procedure used by Properzio (1975). To accomplish this, the Philips diagnostic unit was used. The diagnostic unit was configured with 2 mm aluminum added filtration and operated at a tube potential of 80 kVp for 0.2 s (100 mAs). This configuration yielded a close approximation to the HVL of the CT scanner operated at 80 kVp and measured isocentrically (3.7 vs. 3.8 mm Al respectively).

The x-ray table was used to support a cardboard stand having a 20 x 20 cm section removed from the top to reduce backscatter. To support the TLD chips, a 0.5 mm thick layer of polyethylene was placed over the opening and secured. The base of the cardboard stand was left open. The top of the stand was 58 cm above the table top and 44 cm from the base of the x-ray tube housing. According to Johns (1983), a separation of approximately 50 cm between a diagnostic tube and the point of interest is sufficient to minimize scattering effects from the tube housing and external filtration.

The Capintec ion chamber was taped to the top-most surface of the stand so that its active volume extended to the midpoint of the 20 x 20 cm opening. The x-ray tube alignment light was used to center a 15 x 15 cm radiation field centered within the 20 x 20 cm stand opening. The room was darkened to minimize any non-radiation induced thermoluminescence (NRI-TL) that potentially could be caused by fluorescent lighting. All TLD chips were then placed in rows parallel to the ion chamber probe, beginning 5 cm from the left of the probe and extending 5 cm to the right of the probe. All chips were simultaneously exposed at a tube potential of 80 kVp for 0.2 sec (100 mAs) and the ion chamber exposure measurement was obtained.

After exposure, the chips were placed in numbered slots within lucite holders. These were sealed within light-tight bags and expeditiously preannealed. All chips were preannealed by placing them in vials suspended within a lucite grid partially submerged in boiling water for a period of 10 minutes. This allowed the preanneal temperature to be maintained at a constant 100°C.

All chips were then read on the Harshaw model 2000 TLD reader. The TLD reader was set to begin integrating the light output at 140°C and continue up to a maximum temperature of 250°C. The integration time was set for 30 s with a 5°C per second rate of temperature increase. The photomultiplier (PM) tube voltage was set at 700 volts. A 10 s purge time using N_2 gas at a flow rate of ten cubic feet per second (cfs) was utilized. These settings were maintained for all TLD readings made during the study.

All chips were individually read and their light output in nanocoulombs (nC) was recorded. After allowing the temperature in the TLD reader to cool below the 140°C beginning integration temperature, each chip was reread.

The purpose of the second reading was to insure full light output and to rezero the chip. Harshaw (1988) considers a chip whose second reading is ≤2% of the initial reading to be zeroed.

Due to the analog settings on the Philips diagnostic x-ray unit, the ion chamber readings for the two exposures showed some variation. The first exposure reading was 968 mR, while the second was 848 mR. The distribution of TLD values from readings one and two are shown in Table A-4 below:

Table A-4. TLD frequency distribution.

Statistic	Reading 1	Reading 2
Mean	58.45	91.65
Standard Deviation	±3.67	±3.38
Maximum	68.40	101.20
Minimum	49.40	78.20
Range	19.00	23.00
Number of TLDs	140.00	140.00

The frequency distribution of TLD readings for each of the two exposures is shown in Figure A-9. Both distributions shown are normally distributed with comparable ranges of 19 and 23 nC and standard deviations of 3.7 and 3.4 nC respectively.

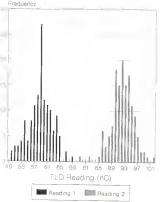

Figure A-9. Frequency distributions of TLD readings.

The frequency distribution of TLD readings shows a slightly decreased variability in the second exposure relative to the first. The F-statistic may be used to compare the variability between two distributions. The computed F-statistic for the two TLD distributions at the 95% confidence level is 1.18. With 139 degrees of freedom for both the numerator and denominator, and a confidence level of 95%, the critical value for the F-Statistic is 1.30. The apparent decrease in variability from the first to the second reading does not, therefore, represent a statistically significant difference in variability at the 95% confidence level.

Given the statistically non-significant difference in variability between the two distributions, as well as their normality, it was concluded that the TLDs were suitable for sensitivity pairing.

Since the mean exposure for each TLD run differed slightly, for the purpose of sensitivity pairing, the TLD readings from the two runs were considered as separate distributions. The TLD chip readings from each run were ranked according to Z-score for that run. The Z-statistic takes into account the measured value in relation to the mean of a particular distribution. Chips were then pooled and paired by Z-score to insure that the most and least sensitive chips were used together.

These matched sets of most and least sensitive chips were subsequently used together for all dosimetric measurements with the exception of those chips used to measure skin dose. Each of the two-chip pairs used for skin dose measurements were chosen from the middle of the Z-score distribution, with each chip having essentially the same Z-score. This was done for logistic reasons, the more extreme chip pairs having already been utilized.

TLD Response as a Function of Energy

LiF TLDs are often considered to be energy independent over a wide range of energies. This is only approximately correct. At energies ranging from approximately 200 keV through ten Mev, LiF has a flat energy response. From 10 through 200 keV, where the photoelectric process exerts a strong influence, LiF TLDs show increased sensitivity relative to soft tissue leading to a slight over-response. This is evident in Figure A-10.

Due to the presence of the bow-tie filter in the CT scanner, the TLD chips used in the dosimetric assessment of the QCT procedure would encounter varying beam energies depending on their location within scan field. Because of this, an assessment of LiF's response at various diagnostic energies was thought to be important.

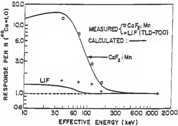

Figure A-10. Sensitivity of TL phosphors as a function of photon energy (courtesy of Charles C. Thomas, Publisher).

In order to assess TLD response, ten TLD chips were selected as five pairs matched for sensitivity and exposed using the Philips diagnostic x-ray unit. The same cardboard support used to sensitivity match TLDs was utilized to assess this energy dependence. The configuration used was also identical, using a 15 x 15 cm radiation field centered on the 20 x 20 cm opening. The Capintec ion chamber was positioned centrally within the radiation field. All pairs of chips were placed on each side and within 1 cm of the probe. The diagnostic x-ray unit was filtered and operated at a tube potential sufficient to approximate the 3.7 mm aluminum HVL measured isocentrically at a technique setting of 80 kVp on the CT scanner. All pairs of TLD chips were exposed at this HVL, preannealed, then read. The average response of the TLD chips was plotted against the Capintec reading obtained during the exposure.

The tube potential and filtration of the Philips diagnostic unit was readjusted to approximate the 6 mm aluminum HVL measured at the laterally decentered position on the CT scanner at a technique setting of 80 kVp, and the process was repeated. This same procedure was followed to expose the chips to HVLs (4.8 and 8 mm aluminum) measured on the CT scanner at 120 kVp.

The technique factors utilized with the diagnostic unit along with the measured TLD light output and exposure settings are tabularized below. A plot of the average TLD response as a function of HVL is shown in Figure A-11.

Table A-5. TLD response as a function of energy.

	HVL (mm Al)			
	3.8	5.3	6.0	7.6
Filtration	2mm Al	2mm Al	1mm Cu +1mm Al	1mm Cu +1mm Al
Technique				
kVp	80	110	100	130
mAs	100	50	64	45
Exposure (mR)	908	1031	834	979
Avg TLD output (nC)	94.7	102.7	82.3	94.4
TLD output/Exposure (nC/mR)	0.104	0.099	0.098	0.096

As indicated, the response is not perfectly linear but decreases slightly with increasing beam energy. Since the TLD response is the ratio of light output per unit exposure, the decrease in response is indicative of a decreasing light output with increasing beam energy. This is in consonance with the general trend shown previously in Figure A-10 (Cameron, 1968).

This change of 10% in TLD response as a function of energy over the range of interest was considered rather moderate. Since, however, the magnitude of effort involved

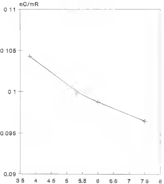

Figure A-11. TLD-100 response as a function of beam HVL.

in correcting the TLD readings according to energy response was minimal and accuracy in dose assessment would be improved, all TLD readings made during the dosimetry study were corrected for variations in light output as a function of energy.

Basic Checks on TLD Reader

Dark current measurements

The TLD reader used during this study was the Harshaw model 2000 system consisting of a thermoluminescent detector (model 2000-C, serial #1008) and an automatic integrating picoammeter (model 2000-B, serial #538). The serviceability of the Harshaw 2000 TLD system was undetermined. In order to establish its operating condition, several operational tests were performed. These included a test of system stability, signal to noise ratio, and "full readout" capability.

To evaluate the stability of the TLD reader, the unit was turned on and allowed to stabilize overnight. This allowed sufficient time for all electronics to warm up and for the photomultiplier tube to be cooled to operational temperatures. The voltage on the unit was set to 650 volts.

A general check of system stability was made by measuring the "dark" current. The dark current represents the inherent noise in the system and is obtained by measuring the output signal obtained without a light source (TLD chip) or reference light located beneath the photomultiplier tube.

With the empty TLD drawer fully inserted into the reader, the unit was configured for a 10 s integration time over a temperature range of 140 to 250°C with a heating rate of 5°C per second. The read cycle was initiated and the measured light output was recorded. This procedure was repeated 20 times with all settings held constant.

The results of the dark current measurements are tabulated in Table A-6. The maximum and minimum noise readings were 0.08 and 0.01 nC respectively for a range of 0.07 nC. The mean noise reading was 0.03 nC with a standard deviation of 0.02 nC.

Table A-6. Dark current readings at 650 volts.

Reading #	Dark Current (nC)
1	0.04
2	0.03
3	0.03
4	0.01
5	0.03
6	0.03
7	0.02
8	0.03
9	0.05
10	0.04
11	0.01
12	0.08
13	0.01
14	0.04
15	0.03
16	0.04
17	0.03
18	0.03
19	0.03
20	0.01

In addition to the magnitude of the dark current, it was important to determine whether these readings were random in nature or subject to some non-random influence in the instrumentation. In order to assess this, a runs test was performed on the data. A run is a succession of values all trending (increasing or decreasing) in the same direction. A runs test evaluates the sequence of the observations in order to determine if the observations are generated by a random process. If some form of non-random persistence is present, the sequence of observations will depart from the expected degree of randomness. The null hypothesis tested is that the sequence of observations is generated by a random process. The alternative hypothesis is that the sequence is generated by a non-random process.

To test this hypothesis the number of runs within the set of observations is counted. If persistence is present, the trends will either be in one direction and the number of runs will be small or will fluctuate periodically. The smallest number of runs possible is one, in such a case all of the values would show a trend in the same direction. The maximum number of runs is one less than the number of observations, in which case the values alternate from lower to higher with each successive observation. Clearly, either too low a number of runs or too high a number of runs would indicate a non-random process.

Performing a runs test on the data in Table A-6 found 11 runs out of a maximum possible 19 runs. The expected number of runs for this number of observations at the 95% confidence level is 13 ± 3.52 runs. Since the observed number of runs, 11, falls within the expected range of 9.5 to 16.5 runs, the null hypothesis that these observations are a result of small random fluctuations in the TLD reader electronics cannot be refuted.

The noise generated by the TLD reader appears then to be random in nature with small fluctuations about a mean value of 0.03 nC. The small size of the noise readings, their limited variability, and the random nature of their occurrence are all indicative of a properly functioning TLD system.

Light current measurements

To further check the functionality of the Harshaw 2000 TLD system, a light current test was performed. This test checks for proper functioning of the photomultiplier tube and associated electronics. The Harshaw model 2000-A TLD reader is equipped with a ^{14}C radioactive source imbedded in a NaI crystal located at the rear of the reader drawer. Since ^{14}C decays with an approximate half-life of 5,730 years, it provides a stable source of radiation within the NaI crystal and light within the TLD reader. When the drawer is pulled to its full forward position, the light source is positioned directly below the photomultiplier tube.

To test for tube stability using this reference light source, the TLD reader drawer was pulled forward to position the reference light source immediately below the PM tube. The system voltage was set to 650 volts with a heating rate of 5°C per second. The light output was integrated over a range of temperatures from 140°C to 250°C. This corresponds to the range of temperatures at which TLD-100 chips are normally read. The read cycle was initiated and the light output was recorded. This procedure was repeated until a total of 20 readings were obtained.

Table A-7. Light current readings at 650 volts.

Reading Number	Light Current (nC)
1	7.58
2	7.80
3	7.73
4	7.59
5	7.62
6	7.46
7	7.59
8	7.43
9	7.72
10	7.66
11	7.79
12	7.73
13	7.58
14	7.63
15	7.48
16	7.74
17	7.51
18	7.61
19	7.56
20	7.58

The maximal and minimal readings obtained were 7.80 and 7.43 nC respectively, yielding a range of 0.37 nC. The mean reading was 7.62 nC with a standard deviation of only 0.10 nC. All values obtained were within ±2% of the mean.

The results of the light current tests indicate a very consistent and stable light source reading. The fact that all values were within ±2% of the mean value implies that the PM tube and all associated electronics are functioning properly. The light current measurements provide increased confidence in the reliability of the TLD reader.

Signal to noise ratio

Normally, the TLD system would be operated at the voltage yielding the highest signal to noise ratio. To determine the signal to noise ratio over a range of voltages, a series of measurements of both light (signal) and dark current (noise) were made at potential settings ranging from 500 to 1,100 volts. Except for variations in voltage, all other parameters remained as described in the sections on dark and light current measurements.

The effect of changes in potential on the signal to noise ratio is tabulated in Table A-8. A graphic plot of this data is shown in Figure A-12.

Table A-8. Signal to noise ratio as a function of voltage.

POTENTIAL (VOLTS)	LIGHT CURRENT (nCOULOMB)	DARK CURRENT (nCOULOMB)	SIGNAL/NOISE RATIO
500	0.9	0.00	NA
600	4.3	0.011	392.27
700	12.9	0.023	560.87
800	34.3	0.067	511.94
900	84.7	0.163	519.63
1000	223.2	0.433	515.47
1100	818.4	1.729	473.34

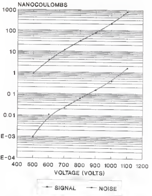

Signal = Light Current
Noise = Dark Current

Figure A-12. Harshaw 2000 TLD system reader signal to noise ratio as a function of PM tube potential.

As indicated, the signal to noise ratio varied from 392:1 at 600 volts to a maximum of 560:1 at 700 volts. The average signal to noise ratio over the entire range of voltages was 496:1. Based on this data, the anticipated operating voltage of 650 volts was not used. Instead, an operating voltage of 700 volts was chosen in order to maximize the signal to noise ratio to approximately 560:1. All subsequent TLD readings made during this study were made utilizing an operating voltage of 700 volts.

Full output of TLD reader

The system checks up to this point indicated a properly functioning TLD system. One further test was performed to determine appropriate functioning. This was the "full readout" test, which assesses the ability of the unit to provide uniform and appropriate heating of a TLD chip in order to obtain a full signal response during the first reading.

To do this, 12 chips were exposed to a ^{60}Co source for approximately ten minutes. Each exposed chip was placed in the TLD reader and read twice, the light output recorded for each reading. According to Harshaw (1988), if the TLD reader is functioning properly, the ratio of the second reading to the first reading should not be greater than 5%. The data collected is shown in Table A-8.

Table A-9. Output of TLD reader on first and second readings.

CHIP #	POTENTIAL (VOLTS)	READING 1 (nC)	READING 2 (nC)	Reading1/Reading2
1	650	4.28	0.26	6.17%
2	650	11.70	0.00	0.00%
3	650	7.94	0.21	2.61%
4	650	14.30	0.04	0.27%
5	650	5.18	0.02	0.35%
6	650	14.20	0.00	0.00%
7	650	0.74	0.00	0.00%
8	650	3.24	0.00	0.00%
9	650	5.45	0.00	0.00%
10	650	16.30	0.01	0.04%
11	650	5.77	0.00	0.00%
12	650	13.80	0.16	1.19%

The average ratio of the second to the first reading was 0.89% with a standard deviation of 1.76%. This is well within Harshaw's acceptable criteria of 5% and indicates that the TLD unit is able to produce a full value readout based on a single reading.

Linearity of TLD reader at one energy

The curve of TLD light output as a function of energy implies that the dose response at any one energy is linear over the range of doses encountered. In order to validate this assumption, ten sensitivity matched chips were used. Two chips served as background controls. The other chips were exposed to varying levels of radiation.

The same Philips diagnostic unit was used for this calibration as was used to match CT HVLs. A cardboard stand having a 20 x 20 opening on the top and the bottom removed to reduce scattering effects was used. The opening was covered by 0.5 mm polyethylene used to support the TLD chips. The cardboard support was placed on the x-ray table and directly below the tube head. A 15 x 15 cm light field was used to center the x-ray beam within the 20 x 20 support opening. The Capintec ion-chamber was placed within the center of a 15 x 15 x-ray field and secured in place.

The x-ray unit's filtration was set at 0.1 mm copper plus 1 mm aluminum. The tube potential was adjusted to 110 kVp. This combination of tube potential and filtration yields a beam with a HVL of approximately 6 mm of aluminum. This HVL was chosen since it represents a value midway between that of the CT unit operated at a tube potential of 80 kVp at isocenter (3.7 mm of aluminum) and at 120 kVp decentered (8 mm of aluminum). It was thus felt to be the most representative HVL for the CT energy range. The tube current on the diagnostic unit was varied to provide a range of exposures from 115 mR to 2,800 mR.

One matched pair of TLD chips was placed adjacent to the ion chamber and within 2 cm of it. The chip pair was then exposed and the exposure reading on the Capintec was noted. These chip pairs were replaced by a second matched pair set. The tube current was adjusted to yield a higher exposure, and a second exposure was obtained. This procedure was repeated until all chip pairs were irradiated at various levels of exposure. All chip pairs, to include those used for background, were preannealed at 100°C for 10 minutes by boiling using the apparatus previously described.

Table A-10. Linearity of TLD reader at one energy.

Chip pair number	Exposure (mR)	Average TLD Reading (nC)
1	0	0.0
2	115	11.5
3	564	57.6
4	1110	107.7
5	2800	284.9

The results of the linearity check of the TLD reader at one energy are shown in Table A-10. A graph of the calibration curve over this dose range (see Figure A-13) shows excellent linearity with a correlation coefficient of 0.999. This indicates that the light output from the TLD reader as a function of varying exposure at one energy is highly linear.

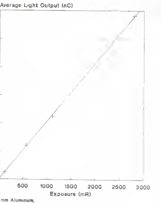

HVL = 6 mm Aluminum,
0.1 mm Cu + 1 mm Al filtration

Figure A-13 Harshaw 2000 system TLD reader calibration curve.

APPENDIX B

RESEARCH PROPOSAL

TITLE OF RESEARCH STUDY:

Determination of in-vivo Reproducibility by Quantitative Computed Tomography (QCT) of Spinal Bone Mineralization in Post-menopausal Women.

INTRODUCTION:

To determine loss of bone mineral in longitudinal studies of patients, sequential measurements are taken. The ability to detect a change in bone mineralization, with 95 percent confidence, is limited to approximately 2.8 times the standard deviation (reproducibility) of the technique.[1] The reproducibility of Quantitative Computed Tomography (QCT) in the determination of spinal bone mineralization varies from institution to institution and is a function of hardware, software, and operator induced variabilities.

---

[1] Zamenhof R. Optimization of Spinal Bone Density Measurement Using Computerized Tomography. Osteoporosis Update 1987. Radiology Research and Education Foundation, University of California Printing Services, 1987.

The reproducibility of our spinal bone mineral QCT technique is important in determining the minimal change in bone mineralization that can be confidently detected. This information will enable a better determinion of the frequency at which studies should be repeated based on expected maximum rates of bone loss. This potentially could save patients radiation exposure from procedures which are unlikely to produce statistically significant measures.

The principal investigator for this study will be Thurman Gillespy, III, MD. The principal co-investigator for this study will be James Davis, MS

SPECIFIC AIMS.

1. This study will determine the reproducibility of our spinal bone mineral QCT technique enabling a better determination of the frequency at which studies should be repeated.

2. It will also allow us to evaluate the reproducibility of a new QCT software analysis package with no additional patient radiation exposure or risk.

3. A comparison of the new QCT software analysis package with our currently used QCT software program will enable a determination of the relative merits of each. Such

information will be of value in making future purchasing decisions and in providing the best available patient care.

EXPERIMENTAL PROTOCOL:

Twenty-five volunteer postmenopausal women will be selected from the community. Each will be scanned using normal, established procedures for QCT spinal bone mineral determination. Each subject will have a lateral scout image made encompassing the region of the torso from vertebra T-12 through S-1. Areas for axial scans will be determined and a total of four axial scans will be taken on vertebra T-12 through L-4. Radiographic technique factors for these scans include 80 KVP, 40 mA, 2 second scan time. The published dose figures from this procedure are normally cited as 100-300mrem, although some references cite doses as high as 1 rem[1]. (Even though the figure of 1 rem will be used in later "worst case" calculations it should be noted that the dose from our CT scanner dose for this procedure is actually only 20 to 30 percent of this value.)

Upon completion of the examination, the patient will remove themselves from the scanning table. After a few moments the patient will then return to the scanning table. The scan will then be repeated, using the same procedure as indicated above. (This will simulate a longitudinal study over time).

---

[1] Genant H, Block J, Steiger P, Claus-Christian G: Quantitative Computed Tomography in the Assessment of Osteoporosis Osteoporosis Update 1987. Radiology Research and Education Foundation, University of California Printing Services, 1987.

Data will be analyzed using two different spinal bone mineral analysis software programs. The reproducibility of the QCT procedure will be compared for each software package.

Volunteers will be informed of their bone mineral status as determined from the above procedure. Medical counseling by the principal investigator will be provided upon request to those whose bone mineralization is found to be abnormal .

RISKS:

Risk estimates from whole-body low level radiation are cited in the literature as 1.4×10^{-6} excess cancer deaths per person per rad per year[2]. It should be noted that this value is for an exposure to the entire body and therefor includes risk to several radio-sensitive organs (thyroid and breasts) which are not directly irradiated during a QCT procedure. It therefor represents an overestimate of the risk, since the radiation from QCT is more localized and primary irradiation does not include the thyroid or breasts.

---

[2] Shleien B, Pharm D, Terpilak MS The Health Physics and Radiological Health Handbook, Nucleon Lectern Associates, pp 195-197,1986.

We can, however, use this value (1.4×10^{-6} excess cancer deaths per person per rad per year) along with the highest published value for the QCT procedure (1 rem) as a "worst case" estimate of the radiation risk from this study. If we assume a remaining lifetime of 30 years among these post-menopausal women, we find the number of excess cancer deaths to be:

Excess cancers deaths = (1.4×10^{-6} excess cancer deaths/(person x rem x year) x (25 persons) x (1 rem/study) x (2 studies) x (30 years) = 0.0021 excess cancer deaths.

The American Cancer Society has reported that approximately one out of five (20 percent) deaths in the U.S. are attributable to cancer[3]. Out of this group of 25 individuals, that would imply that approximately 5 individuals will die of cancer. The radiation from the proposed QCT study would increase the expected number of cancer deaths in this group from 5 to 5.0021. This represents an increase of 0 042 percent to this group.

The risk of a cancer induction can be similarly derived using the value of 450×10^{-6} excess cancers per million persons per lifetime after exposure to 1 rem of radiation[4]. Using this figure as in the calculation above (and omitting the 30 years, since this value represents a lifetime risk) yields an estimate of .0225 excess cancers induced. Using the published data from the American Cancer Society that 30 percent of the American population will develop cancer in their lifetime[5], this increases the expected cancer incidence in this group from 7.5 to 7.5225 cancers. This represents an increased risk of cancer induction in this group of 0.3 percent.

---

[3] Cancer Facts and Figures - 1987, American Cancer Society, 1987

Even though the increased risk of cancer induction is extremely small, it should be emphasized that it represents a gross over-estimate of the risks involved since:

1. It utilizes the highest reported dose for the QCT procedure. More typical doses are reported to be only 20 to 30 percent of that used in the calculations.

2. The risk figures assume a uniform whole body exposure which would include several radiosensitive organs. These organs are spared direct radiation exposure using the QCT procedure. Further, the primary radiation from the eight axial scans that will be performed on each patient

---

[4] Shleien B, Phare D, Terpilek M, 1986.

[5] Cancer Facts and Figures - 1987, American Cancer Society, 1987.

are confined to a very narrow (5-10 mm slice thickness) so that only a small area of the body is subject to primary radiation.

3. The risk figure for cancer induction assumes a lifetime risk. For a post-menopausal woman with a remaining life expectancy of approximately 30 years, the risk would be substantially reduced.

4. The risk figure used for cancer induction is the highest in the published range of 160-450 additional cancers in one million people after exposure to 1 rem of radiation.[6]

Finally, it should be noted that there are no adverse genetic risks to this post-menopausal population.

POTENTIAL BENEFITS:

Each volunteer will benefit directly from the assessment of her bone mineralization. Results will be provided to each participant both in terms of amount of bone mineralization and normative ratings. Women who are below normal for their age and who are believed to be at risk for fracture would be provided with medical counseling from the project director upon request.

---

[6] Shleien B, Pharm D, Terpilak M, 1986.

The institution will benefit from the study through the determination of the reproducibility of the QCT procedure utilizing the equipment at this institution. Such a finding will allow a determination of the minimal amount of bone loss that can be determined by any two sequential QCT measurements. This will allow us to better judge the frequency with which such scans should be done and prevent the unnecessary scanning of patients whose bone loss is unlikely to produce statistically significant measures.

The Institution will also benefit from determining which of the two bone mineral software analysis programs provides the highest reproducibility, thus insuring "state of the art" medical treatment

INFORMED CONSENT:

See Attached.

INFORMED CONSENT TO PARTICIPATE IN RESEARCH

J. HILLIS MILLER HEALTH CENTER
UNIVERSITY OF FLORIDA
GAINESVILLE, FLORIDA 32610

You are being asked to volunteer as a participant in a research study. This form is designed to provide you with information about this study and to answer any of your questions.

TITLE OF RESEARCH STUDY:

Determination of in-vivo Reproducibility of Quantitative Computed Tomography (QCT) in the Determination of Spinal Bone Mineralization in Post-menopausal Women.

PROJECT DIRECTOR:

Name: Thurman Gillespy, III, MD

Telephone Number: 395-2275

PURPOSE OF RESEARCH:

The purpose of this research is to determine the in-vivo reproducibility of spinal bone mineral determination using Quantitative Computed Tomography (QCT) on the GE 8800 CT scanner.

PROCEDURES FOR THIS RESEARCH.

Each individual will be scanned using normal, well established procedures for QCT spinal bone mineral determination. Each person will have an x-ray made encompassing the region of the torso from just below the lungs to the top of the hips (vertebra T-12 through S-1). Areas for further x-rays (axial scans) will be determined and a total of four axial x-ray scans will be taken, one for each vertebra in the small of the back (T-12 through L-4). Radiographic technique factors for these scans are designed to minimize radiation exposure (80 KVP, 40 mA, 2 second scan time). The published dose figures from this procedure are normally cited as 100-300mrem; although some references cite doses as high as 1 rem. (Even though the figure of 1 rem has been used in these "worst case" calculations, it should be noted that the dose from our CT scanner dose for this procedure is actually only 10 to 30 percent of this value.)

Upon completion of the examination, you will be asked to get off the scanning table. After a few moments you will return to the scanning table. The scan will then be repeated, using the same procedure as indicated above. (This will simulate a longitudinal study over time)

POTENTIAL RISKS OR DISCOMFORTS:

As with any procedure involving radiation, some risk exists. The risk involved from this study is considered to be minimal. Based on an estimate from the American Cancer Society, each individual has a 30 percent (0.30) chance of developing cancer in their lifetime. Calculated risks of cancer induction using "worst case" estimates from this procedure will increase your risk of developing cancer from 0.30 to 0.3009 (approximately one third of one percent).

The American Cancer Society estimates that each of us has a 20 percent (0.20) chance of dying from cancer. Calculations indicate that this procedure will increase your risk of developing a fatal cancer from 0.20 to 0.200084 (approximately four hundredths of one percent).

There should be absolutely no pain or discomfort experienced during this procedure.

If you wish to discuss these risks or any discomforts you may experience, you may call the Project Director listed in #2 of this form.

POTENTIAL BENEFITS TO YOU OR OTHERS.

Each person will benefit directly from the assessment of her bone mineralization. Results will be provided to each person both in terms of amount of bone mineralization and normative ratings. Women who are below normal for their age and who are believed to be at risk for fracture would be provided with medical counseling from the project director upon request.

This hospital will benefit from the study through the determination of the reproducibility of the QCT procedure utilizing the equipment at this institution. Such a finding will allow a determination of the minimal amount of bone loss that can be determined by any two sequential QCT measurements This will allow us to better judge the frequency with which such scans should be done and prevent the unnecessary scanning of patients whose bone loss is unlikely to have exceeded amount which is minimally detectable.

ALTERNATIVE TREATMENT OR PROCEDURES, IF APPLICABLE.

Bone mineral assessment may also be obtained through a procedures known as single photon and dual photon absorptiometry. These techniques generally do not provide as high a degree of accuracy as QCT but do result in less radiation exposure.

REFERENCES

Alderson Research Laboratories, 1969, Alderson Rando Phantom Systems for Radiotherapy, Technical bulletin 43. Stamford, CT.

American Cancer Society, 1987, Cancer Facts and Figures-- 1987. Atlanta, GA: American Cancer Society.

Armstrong, D., 1987, Selection and Calibration of Thermoluminescent Dosimeters for Attenuation Studies on Pulsed Beam Driven High Power Microwave Generators. Thesis, Univ. of Florida.

Cann, C., 1987, Quantitative Computed Tomography for Bone Mineral Analysis:Technical Considerations. Osteoporosis Update. San Francisco, CA: University of California Printing Services, pp 138-139.

Cann, C., 1988, Quantitative CT for Determination of Bone Mineral Density. A Review. Radiology. 166: 509-522.

Cohn, S., 1981, Non-Invasive Measurements of Bone Mass and their Clinical Application. Boca Raton, FL: CRC Press.

Constantinou, C., Attix, F., and Bhudatt, R., 1982, A Solid Water Phantom Material for Radiotherapy X-ray and Gamma-ray Beam Calibrations. Medical Physics, 9(3), 436-440

Cummings, S., 1987a, Epidemiology of Osteoporotic Fractures, Osteoporosis Update 1987, San Francisco, CA: University of California Printing Svcs, p. 7.

Cummings, S., 1987b, Use of Bone Density Measurements Osteoporosis Update 1987, San Francisco, CA: University of California Printing Svcs, p. 115.

Cummings, S. and Black, D., 1986, Should Peri-menopausal Women be Screened for Osteoporosis? Ann Intern Med. 104: 817-823.

Genant, H., Block, J., Steiger, P., and Gluer, C., 1987, Quantitative Computed Tomography in the Assessment of Osteoporosis. Osteoporosis Update, p. 49.

Hall, E., 1978, Radiology for the Radiologist. 2nd ed, Philadelphia, PA: Harper and Row, p. 414.

Hall, E., 1988, Radiobiology for the Radiologist. 3rd ed. Philadelphia: J. B. Lippincott, p. 469.

Harshaw/Filtrol Partnership, 1977, Harshaw 2000C Thermoluminescent Analyzer--Users Manual. Cleveland, OH: Harshaw/Filtrol Partnership.

The Image Analyis handbook, 1987, Irvine, CA: Image Analysis Corp. p. 22.

Internation Commission on Radiological Protection (ICRP), 1975, Report of the Task Group on Reference Man: publication 23. Oxford, Pergammon Press, p 91.

Internation Commission on Radiological Protection (ICRP), 1977, Recommendations of the International Commission on Radiological Protection; publication 26. Oxford, Pergammon Press, p 10.

Internation Commission on Radiological Protection (ICRP), 1968, Publication 11. Oxford, Pergammon Press.

Johns, H.E. and Cunningham, J.R., 1983, The Physics of Radiology, Fourth Ed. Springfield, IL. Charles C. Thomas.

Kimmel, P., 1984, Radiologic Methods to Evaluate Bone Mineral Content. Annals of Internal Medicine, 100, pp 908-911.

King, S. D. and Spiers, F. W., 1985, Photoelectron Enhancement of the Absorbed Dose from X-rays to Human Bone Marrow: Experimental and theoretical studies. British Journal of Radiology, 58, pp 345-356.

Mazess, R., 1987, Bone Up '87, New Answers to Old Questions. Madison, WI: Lunar Radiation Corp., pg 2.

Navy Clothing and Textile Research Center, 1979, Analysis of Body Size Measurements for U.S. Navy Women's Clothing and Pattern Design. Technical Report 138. Natick, MA: Navy Clothing and Textile Research Facility.

Notelovitz, M. and Ware, M., 1982, Stand Tall! The Informed Woman's Guide to Preventing Osteoporosis. Gainesville, FL: Triad Publishing Company.

Peck, W., Riggs, B., Bell, N., 1987, Physicians Resource Manual on Osteoporosis - A Decision Making Guide. Washington, DC: National Osteoporosis Foundation, pp 15-16.

Properzio, W., 1975, The Radiological Health Significance of Cardiovascular Special Procedures. Gainesville: Department of Nuclear Engineering, University of Florida.

Shleien, B., and Terpilak M., 1986, The Health Physics and Radiological Health Handbook, Olney, MD. Nucleon Lectern Associates, pp 195-197.

Tortora, G., and Anagnostakos N., 1984, Principles of Anatomy and Physiology, 4 Ed, New York: Harper and Row.

Wall, B., Harrison, R., and Spiers, F., 1988, Patient Dosimetry Technique in Diagnostic Radiology. Lodon: The Institute of Physical Sciences in Medicine, Bocardo Press Limited.

Weiss, N.S., Ure, C.L., Ballard J.H., Williams A.R., Daling J.R., 1980, Decreased risk of fractures of the hip and forearm with postmenopausal use of estrogen. N Engl J Med 303, 1195.

World Almanac and Book of Facts, 1987, New York: Newspaper Enterprise Association, pp 533-536

Zamenhoff, R., 1987, Optimization of Spinal Bone Density Measurement Using Computerized Tomography. Osteoporosis Update, San Francisco, CA: University of California Printing Svcs, p. 49.

BIOGRAPHICAL SKETCH

James Stephen Davis was born January 2, 1949 in St. Petersburg, Florida. He is married to the former Carolee Yaxley of DeLand, Florida. They have two children, Amanda and Christopher. As the son of a career military officer, he has grown up in many areas of the world to include the Philipines and Alaska. He graduated from St. Petersburg Senior High School in 1967 and received his bachelor of science degree in biology from Stetson University in 1971

Following graduation he taught high school for a year at Ribault Senior High School in Jacksonville, Florida. In 1972, he began a military service obligation as a commissioned officer in the United States Army. His military service took him to many areas of the country to include Georgia, Texas, Missouri, California, Washington, and Florida. He has served tours of duty as the company commander of a fixed hospital as well as an 400 bed evacuation hospital.

While serving on active duty in Missouri, he received a dual masters degree in human relations and counselling services from Websters College. In 1982 he received a masters of science degree in environmental engineering from the University of Florida in Gainesville, Florida. After receiving this degree he was assigned to the United States

Nuclear and Chemical Agency in Washington, D.C., where he served as a Nuclear Medical Science officer. In 1985 he received the rank of major, a rank he still holds. Since 1985 he has been assigned to the University of Florida for advanced schooling.

I certify that I have read this study and that in my opinion it conforms to acceptable standards of scholarly presentation and is fully adequate, in scope and quality, as a dissertation for the degree of Doctor of Philosophy.

W. Emmett Bolch

William Emmett Bolch, Chairman
Professor of Environmental
Engineering Sciences

I certify that I have read this study and that in my opinion it conforms to acceptable standards of scholarly presentation and is fully adequate, in scope and quality, as a dissertation for the degree of Doctor of Philosophy.

Lawrence Fitzgerald

Lawrence Fitzgerald,
Associate Professor of Nuclear
Engineering Sciences

I certify that I have read this study and that in my opinion it conforms to acceptable standards of scholarly presentation and is fully adequate, in scope and quality, as a dissertation for the degree of Doctor of Philosophy.

Thurman Gillespy, III, MD
Associate Professor of Radiology

I certify that I have read this study and that in my opinion it conforms to acceptable standards of scholarly presentation and is fully adequate, in scope and quality, as a dissertation for the degree of Doctor of Philosophy.

Walter Mauderli

Walter Mauderli,
Professor of Nuclear Engineering Sciences

I certify that I have read this study and that in my opinion it conforms to acceptable standards of scholarly presentation and is fully adequate, in scope and quality, as a dissertation for the degree of Doctor of Philosophy.

William Properzio

William Properzio
Associate Professor of Nuclear Engineering
Sciences and Environmental Engineering
Sciences

I certify that I have read this study and that in my opinion it conforms to acceptable standards of scholarly presentation and is fully adequate, in scope and quality, as a dissertation for the degree of Doctor of Philosophy.

Genevieve S Roessler

Genevieve Roessler,
Associate Professor of Nuclear
Engineering Sciences.

This dissertation was submitted to the Graduate Faculty of the College of Engineering and to the Graduate School and was accepted as partial fulfillment of the requirements for the degree of Doctor of Philosophy.

December 1988

Hubert A. Bevis

Dean, College of Engineering

Dean, Graduate School